

BUCKLING DRIVEN DELAMINATION OF ORTHOTROPIC
FUNCTIONALLY GRADED MATERIALS

A THESIS SUBMITTED TO
THE GRADUATE SCHOOL OF NATURAL AND APPLIED SCIENCES
OF
MIDDLE EAST TECHNICAL UNIVERSITY

BY

SUPHİ YILMAZ

IN PARTIAL FULFILLMENT OF THE REQUIREMENTS
FOR
THE DEGREE OF MASTER OF SCIENCE
IN
MECHANICAL ENGINEERING

NOVEMBER 2006

Approval of the Graduate School of Natural and Applied Sciences

Prof. Dr. Canan ÖZGEN
Director

I certify that this thesis satisfies all the requirements as a thesis for the degree of Master of Science.

Prof. Dr. S. Kemal İDER
Head of Department

This is to certify that we have read this thesis and that in our opinion it is fully adequate, in scope and quality, as a thesis for the degree of Master of Science.

Asst. Prof. Dr. Serkan DAĞ
Co-Supervisor

Assoc. Prof. Dr. Suat KADIOĞLU
Supervisor

Examining Committee Members

Prof. Dr. Metin AKKÖK	(METU, ME)	_____
Assoc. Prof. Dr. Suat KADIOĞLU	(METU, ME)	_____
Asst. Prof. Dr. Serkan DAĞ	(METU, ME)	_____
Assoc. Prof. Dr. Bora YILDIRIM	(Hacettepe Univ.)	_____
Prof. Dr. Bülent DOYUM	(METU, ME)	_____

I hereby declare that all information in this document has been obtained and presented in accordance with academic rules and ethical conduct. I also declare that, as required by these rules and conduct, I have fully cited and referenced all material and results that are not original to this work.

Name, Last name : Suphi YILMAZ

Signature :

ABSTRACT

BUCKLING DRIVEN DELAMINATION OF ORTHOTROPIC FUNCTIONALLY GRADED MATERIALS

YILMAZ, Suphi

M.S. Department of Mechanical Engineering

Supervisor: Assoc. Prof. Dr. Suat Kadiođlu

Co-Supervisor: Asst. Prof Dr. Serkan Dađ

November 2006, 98 pages

In today's technology severe working conditions increase demands on structural materials. A class of materials which are developed to meet these increased demands is Functionally Graded Materials (FGMs). These are inhomogeneous structural materials which are able to withstand large temperature gradients and corrosive environment. Application areas of FGMs are in aerospace industry, nuclear reactors, chemical plants and turbine systems. FGMs have gradual compositional variation from metal to ceramic which give them mechanical strength, toughness and heat resistance. However under high temperature gradients, cracking problems may arise due to thermal stresses. In layered structures the final stage of failure may be delamination due to crack extension.

The objective of this study is to model a particular type of crack problem in a layered structure consisting of a substrate, a bond coat and an orthotropic FGM coating. There is an internal crack in the orthotropic layer and it is perpendicular to material gradation of coating. The position of the crack inside the coating is kept as a variable. The steady-state temperature distribution between the substrate and the coating causes a buckled shape along crack face. The critical temperature change,

temperature distribution, mixed mode stress intensity values and energy release rates are calculated by using Displacement Correlation Technique. Results of this study present the effects of geometric parameters such as crack length, crack position, etc as well as the effects of the type of gradation on buckling behavior and mixed mode stress intensity factors.

Keywords: Fracture Mechanics, Interface Crack, Stress Intensity Factor, Displacement Correlation Technique, Buckling

ÖZ

ORTOTROPİK FONKSİYONEL DERECELENDİRİLMİŞ MALZEMELERİN BURKULMAYA BAĞLI DELAMİNASYONU

YILMAZ, Suphi

Yüksek Lisans, Makina Mühendisliği Bölümü

Tez Yöneticisi: Doç. Dr. Suat Kadioğlu

Ortak Tez Yöneticisi: Yar. Doç. Dr. Serkan Dağ

Kasım 2006, 98 Sayfa

Günümüz teknolojisinde ağır çalışma koşulları yapısal malzemeler üzerindeki talebi artırmıştır. Bu artan talepleri karşılamak için geliştirilen bir malzeme sınıfı da fonksiyonel derecelendirilmiş malzemeler (FDM) dir. Bunlar, yüksek sıcaklık farkına ve aşınmaya dirençli homojen olmayan yapısal malzemelerdir. FDM'lerin uygulama alanları havacılık endüstrisi, nükleer reaktörler, kimyasal fabrikalar ve türbin sistemleridir. FDM'ler, mekanik dayanım, tokluk ve sıcaklığa karşı direnç sağlayan, bileşimleri metalden seramiğe aşamalı olarak değişen malzemelerdir. Bununla beraber bu tür yapılarda da yüksek sıcaklık farklılıklarından dolayı, ısıl gerilmelere bağlı olarak çatlama ortaya çıkabilir. Tabakalı yapılarda, sorunun son aşaması çatlakların büyümesine bağlı olarak delaminasyon olabilmektedir.

Bu tez çalışmasının amacı, taban tabaka, bağlayıcı katman ve ortotropik FDM kaplamadan oluşan tabakalı yapılarda belirli bir çatlama probleminin modellenmesidir. Ortotropik katmanda bir iç çatlak bulunmaktadır ve bu çatlak kaplamanın malzeme değişimine diktir. Çatlağın yeri problemin değişkenlerinden biridir. Taban tabaka, bağlayıcı katman ve kaplama sistemi, çatlama yüzeyinde burkulmaya sebep olan sıcaklık dağılımı sebebiyle yüklenmektedir. Burkulmaya

sebep olan kritik sıcaklık deęiřimi ve karıřık mod gerilme řiddeti deęerleri Yerdeęiřtirme Korelasyon Teknięi kullanılarak hesaplanmaktadır. Bu alıřma sonucu, atlak uzunluęu, atlak yeri vb. geometrik parametrelerle malzeme zelliklerinin deęiřim profillerinin burkulma davranıřı ve karıřık mod gerilme řiddeti faktrlerine etkileri incelenmiřtir.

Anahtar Kelimeler: Kırılma Mekaniki, Arayzey atlaęı, Gerilme řiddeti Faktr, Yerdeęiřtirme Korelasyon Teknięi, Burkulma

To My Dear Wife

ACKNOWLEDGMENTS

I would like to thank my supervisors Assoc. Prof. Dr. Suat Kadiođlu and Asst. Prof. Dr. Serkan Dađ for their help and guidance throughout the study.

I also wish to express my thanks to Asst. Prof. Dr. Bora Yıldırım for his guidance and valuable contributions in finite element modeling.

I am thankful to my company ASELSAN Inc. for letting and supporting of my thesis.

I want to thank my family for their continuous encouragement.

I am especially thankful to my wife, Aysun, for her help, support, patience and encouragement to complete this study.

TABLE OF CONTENTS

PLAGIARISM	iii
ABSTRACT	iv
ÖZ	vi
ACKNOWLEDGMENTS	ix
TABLE OF CONTENTS	x
LIST OF TABLES	xii
LIST OF FIGURES	xiii
CHAPTER	
1 INTRODUCTION.....	1
1.1 Introduction.....	1
1.2 Literature Survey.....	3
1.3 Scope of the Study	9
2 PROBLEM DEFINITION	11
2.1 Fracture Mechanics	11
2.2 The Displacement Correlation Technique	12
2.3 Crack Tip Fields in Orthotropic FGMs.....	14
2.3.1 Calculation of Mode I Stress Intensity Factor.....	19
2.3.2 Calculation of Mode II Stress Intensity Factor	21
2.3.3 Calculation of Energy Release Rate.....	23
3 FINITE ELEMENT ANALYSIS OF ORTHOTROPIC FGM COATING ON A SUBSTRATE	25
3.1 Introduction.....	25
3.2 Nonlinear Bucking Analysis	26
3.2.1 Nonlinearities	26
3.2.2 Buckling Analysis	27
3.2.3 Finite Element Analysis of Buckling Problems.....	28
3.3 Modeling of Fracture Problem for orthotropic materials.....	28

3.3.1 Fracture Mechanics Issues in ANSYS	29
3.3.2 Basic Information about Nonlinear Analysis in ANSYS.....	30
3.3.3 Basic Information about Buckling Analysis in ANSYS	31
3.3.3.1 Eigenvalue (Linear) Buckling Analysis	31
3.3.3.2 Nonlinear Buckling Analysis	32
3.4 The Finite Element Model	32
4 VERIFICATION of FINITE ELEMENT PROCEDURES	34
4.1 Introduction	34
4.2 Slanted Crack Problem.....	34
4.2.1 Homogeneous orthotropic plate with a slanted crack	36
4.3 The Interface Crack Problem	38
4.4 The Plane Strain Problem.....	41
5 RESULTS and DISCUSSION	46
5.1 Introduction	46
5.2 The Interface Crack Problem	46
5.2.1 Geometry of the Problem	46
5.2.2 Boundary Conditions	47
5.2.3 Material Properties	48
5.3 The Internal Crack Problem	53
5.4 Steady State Temperature Distribution	54
5.5 Figures.....	57
5.6 Discussion of Results and Conclusion	81
REFERENCES.....	84
APPENDICES	
A. SAMPLE APDL CODE.....	88

LIST OF TABLES

TABLES

Table 1.1 Material properties of FGM coating- substrate system.....	1
Table 4.1 SIF values for homogeneous orthotropic plate.	36
Table 4.2 Mixed mode stress intensity factors for isotropic interface crack problem, solution with 6966 elements.	40
Table 4.3 Mixed mode stress intensity factors for isotropic interface crack problem, solution with 53283 elements.	40
Table 4.4 Mixed mode stress intensity factors for orthotropic interface crack problem, solution with 58073 elements.	41
Table 4.5 Material properties of the zirconia coating and Rene-41 substrate.....	42
Table 4.6 Displacement and SIF values for changing crack length and temperature gradient.....	43
Table 4.7 Displacement and SIF values for FGM and homogeneous coatings.	44
Table 5.1 Constants of material variation in orthotropic FGM.....	50

LIST OF FIGURES

FIGURES

Figure 1.1 Buckling of FGM coating under thermal load.....	3
Figure 1.2 The geometry of the internal crack problem.....	9
Figure 2.1 Singular elements at the crack tip and nodes used in calculation of SIFs.	13
Figure 2.2 Definitions of isotropic and anisotropic materials.....	14
Figure 2.3 Crack tip coordinates.	16
Figure 2.4 Nodal displacements in x_2 -direction near the crack tip.	19
Figure 2.5 Nodal displacements in x_1 -direction near the crack tip.	21
Figure 3.1 Curves of in-plane load (F) versus transverse displacement (u).	27
Figure 3.2 Examples of 2-D singular elements. PLANE2 and PLANE82.	29
Figure 3.3 Node locations of PLANE82 element.	30
Figure 3.4 Newton-Rapson iterative method (4 iterations are shown)	31
Figure 3.5 Thermal buckling problem of orthotropic FGM coating bonded to homogeneous substrate.	33
Figure 4.1 Geometry and boundary conditions of plate with a slanted crack.....	35
Figure 4.2 Homogeneous orthotropic material, finite element mesh configuration. .	37
Figure 4.3 Homogeneous orthotropic material, deformed shape at the crack.	37
Figure 4.4 An interface crack between a graded orthotropic coating and homogeneous orthotropic substrate.....	38
Figure 4.5 Finite element mesh used in the solution of interface crack problem.	39
Figure 4.6 Geometry of the plane strain thermal buckling problem.	42
Figure 4.7 Crack opening displacement at the center of the crack vs. temperature drop in FGM and homogeneous coatings, $T_0=100K$, (Chiu (1999)).	45
Figure 4.8 Normalized stress intensity factors for FGM coating as a function of temperature drop, $T_0=100K$, (Chiu (1999)).	45
Figure 5.1 The geometry of interface crack the problem.....	47

Figure 5.2 Deformed shape of the FGM, bond coat and substrate system due to temperature distribution, $a/h_I=10$ and <i>CRI</i> material.	51
Figure 5.3 Buckled shape of the FGM layer above the crack, $a/h_I=10$ and <i>CRI</i> material.....	52
Figure 5.4 Plane2 singular elements at the crack tip.....	52
Figure 5.5 The geometry of the internal crack problem.....	54
Figure 5.6 Distribution of temperature between upper surface of crack and lower surface of crack.	55
Figure 5.7 Variation of temperature at the end of the specimen, $x_I=L$	56
Figure 5.8 Normalized mode I stress intensity factors for crack at the bond coat – FGM interface, $a/h_I=1$	57
Figure 5.9 Normalized mode II stress intensity factors for crack at the bond coat – FGM interface, $a/h_I=1$	57
Figure 5.10 Normalized energy release rate values for crack at the bond coat – FGM interface, $a/h_I=1$	58
Figure 5.11 Normalized mode I stress intensity factors for crack at the bond coat – FGM interface, $a/h_I=5$	58
Figure 5.12 Normalized mode II stress intensity factors for crack at the bond coat – FGM interface, $a/h_I=5$	59
Figure 5.13 Normalized energy release rate values for crack at the bond coat – FGM interface, $a/h_I=5$	59
Figure 5.14 Normalized mode I stress intensity factors for crack at the bond coat – FGM interface, $a/h_I=10$	60
Figure 5.15 Normalized mode II stress intensity factors for crack at the bond coat – FGM interface, $a/h_I=10$	60
Figure 5.16 Normalized energy release rate values for crack at the bond coat – FGM interface, $a/h_I=10$	61
Figure 5.17 Normalized mode I stress intensity factors for crack at the bond coat – FGM interface, $a/h_I=15$	61
Figure 5.18 Normalized mode II stress intensity factors for crack at the bond coat – FGM interface, $a/h_I=15$	62

Figure 5.19 Normalized energy release rate values for crack at the bond coat – FGM interface, $a/h_I=15$	62
Figure 5.20 Normalized mode I stress intensity factors for crack at the bond coat – FGM interface, $a/h_I=20$	63
Figure 5.21 Normalized mode II stress intensity factors for crack at the bond coat – FGM interface, $a/h_I=20$	63
Figure 5.22 Normalized energy release rate values for crack at the bond coat – FGM interface, $a/h_I=20$	64
Figure 5.23 Normalized mode I stress intensity factors for crack at the bond coat – FGM interface, $a/h_I=25$	64
Figure 5.24 Normalized mode II stress intensity factors for crack at the bond coat – FGM interface, $a/h_I=25$	65
Figure 5.25 Normalized energy release rate values for crack at the bond coat – FGM interface, $a/h_I=25$	65
Figure 5.26 Normalized mode I stress intensity factors for crack at the bond coat – FGM interface, <i>CR1</i> material properties for FGM.....	66
Figure 5.27 Normalized mode II stress intensity factors for crack at the bond coat – FGM interface, <i>CR1</i> material properties for FGM.....	66
Figure 5.28 Normalized energy release rate values for crack at the bond coat – FGM interface, <i>CR1</i> material properties for FGM	67
Figure 5.29 Normalized mode I stress intensity factors for crack at the bond coat – FGM interface, <i>CR2</i> material properties for FGM.....	67
Figure 5.30 Normalized mode II stress intensity factors for crack at the bond coat – FGM interface, <i>CR2</i> material properties for FGM.....	68
Figure 5.31 Normalized energy release rate values for crack at the bond coat – FGM interface, <i>CR2</i> material properties for FGM	68
Figure 5.32 Normalized mode I stress intensity factors for crack at the bond coat – FGM interface, <i>MRI</i> material properties for FGM.....	69
Figure 5.33 Normalized mode II stress intensity factors for crack at the bond coat – FGM interface, <i>MRI</i> material properties for FGM.....	69
Figure 5.34 Normalized energy release rate values for crack at the bond coat – FGM interface, <i>MRI</i> material properties for FGM.....	70

Figure 5.35 Normalized mode I stress intensity factors for crack at the bond coat – FGM interface, <i>MR2</i> material properties for FGM.....	70
Figure 5.36 Normalized mode II stress intensity factors for crack at the bond coat – FGM interface, <i>MR2</i> material properties for FGM.....	71
Figure 5.37 Normalized energy release rate values for crack at the bond coat – FGM interface, <i>MR2</i> material properties for FGM.....	71
Figure 5.38 Normalized mode I stress intensity factors for changing crack heights, $a/h_I=20$ and <i>CR1</i> material properties	72
Figure 5.39 Normalized mode II stress intensity factors for changing crack heights, $a/h_I=20$ and <i>CR1</i> material properties	72
Figure 5.40 Normalized energy release rate values for changing crack heights, $a/h_I=20$ and <i>CR1</i> material properties	73
Figure 5.41 Normalized mode I stress intensity factors for changing crack heights, $a/h_I=20$ and <i>CR2</i> material properties	73
Figure 5.42 Normalized mode II stress intensity factors for changing crack heights, $a/h_I=20$ and <i>CR2</i> material properties	74
Figure 5.43 Normalized energy release rate values for changing crack heights, $a/h_I=20$ and <i>CR2</i> material properties	74
Figure 5.44 Normalized mode I stress intensity factors for changing crack heights, $a/h_I=20$ and <i>MR1</i> material properties	75
Figure 5.45 Normalized mode II stress intensity factors for changing crack heights, $a/h_I=20$ and <i>MR1</i> material properties	75
Figure 5.46 Normalized energy release rate values for changing crack heights, $a/h_I=20$ and <i>MR1</i> material properties	76
Figure 5.47 Normalized mode I stress intensity factors for changing crack heights, $a/h_I=20$ and <i>MR2</i> material properties	76
Figure 5.48 Normalized mode II stress intensity factors for changing crack heights, $a/h_I=20$ and <i>MR2</i> material properties	77
Figure 5.49 Normalized energy release rate values for changing crack heights, $a/h_I=20$ and <i>MR2</i> material properties	77
Figure 5.50 Steady-state temperature distribution on the crack surfaces for changing crack lengths, <i>CR1</i> material properties.	78

Figure 5.51 Steady-state temperature distribution on the crack surfaces for changing material properties, $a/h_I=15$	78
Figure 5.52 Steady-state temperature distribution on line $x_I=L$, $a/h_I=5$ and CRI material properties are chosen.....	79
Figure 5.53 Steady-state temperature distribution on line $x_I=0$, $a/h_I=5$ and CRI material properties are chosen.....	79
Figure 5.54 Steady-state temperature distribution by changing position of internal crack, $a/h_I=20$ and CRI material properties are chosen.	80
Figure 5.55 Comparison of mode I and mode II stress intensity factors for changing crack lengths, CRI material properties.	82

CHAPTER 1

INTRODUCTION

1.1 Introduction

With the rapid development in the technology, performance requirements on components subjected to severe working conditions are increased. Some examples of such technological applications are combustion chambers, aerospace structures, fusion reactors, heat engine components, thermo electric generators etc. In these severe environments, demands on structural materials are increased to a level at which homogeneous materials can not satisfy all of requirements. The required material properties can be listed as, high heat corrosion resistance, low heat conduction, high toughness, stiffness and wear resistance. By using a composite coating consisting of a ceramic layer on a metal substrate, advantages of constituents can be combined and protection from temperature and corrosion can be obtained. However using a ceramic coating on a metallic component, means bonding dissimilar homogeneous materials, which causes some problems. The major shortcomings are poor interfacial bonding strength, low toughness, high thermal stresses and as a result tendency to cracking which brings failure. Table 1.1 shows the material properties of a typical homogenous ceramic coating- metal substrate system, where the constituents are isotropic

Table 1.1 Material properties of FGM coating- substrate system

	Material	E (GPa)	ν	α ($\times 10^{-6} \text{C}^{\circ}$)
Substrate	Ni-based Superalloy	175.8	0.25	13.91
Bond Coat	NiCrAlZr	137.9	0.27	15.16
Ceramics	ZrO ₂ -8wt%Y ₂ O ₃	27.6	0.25	10.01

To overcome these shortcomings coatings with graded composition can be used. In such coatings thermo-mechanical material properties vary in thickness direction. These composites, combining heat and corrosion resistance of ceramics with mechanical strength and toughness of metals, are called functionally graded materials (FGM). By using graded materials, smoother stress distributions and higher bonding strengths are obtained between substrate and coating, Chiu (1999).

The processing techniques of FGMs are plasma spraying, chemical and physical vapor deposition, combustion sintering, centrifugal casting and electrophoretic deposition, Chiu (1999). These manufacturing methods usually determine material properties. For example, FGMs produced by plasma spray technique have lamellar structure, while physical vapor deposition technique leads to a columnar structure. Due to the nature of processing techniques the graded materials lose their isotropy. Thus, mechanics of FGMs need to be studied using the model of orthotropic elastic continuum.

In order to employ new generation protective coatings in high temperature environments, the failure mechanisms and structural reliability of them must be determined. One major mode of failure is cracking which leads to delamination in substrate coating system. The difference between the thermal expansion coefficients of metal and FGM coating causes residual stresses under temperature gradients. In case of an internal crack in FGM coating-substrate system, while cooling down from an elevated temperature, these residual stresses can cause buckling along the crack face which leads to crack propagation and delamination of coating layer. Figure 1.1 shows change in the shape of coating bonded to substrate in case of a given temperature difference $\Delta T = T_2 - T_1$.

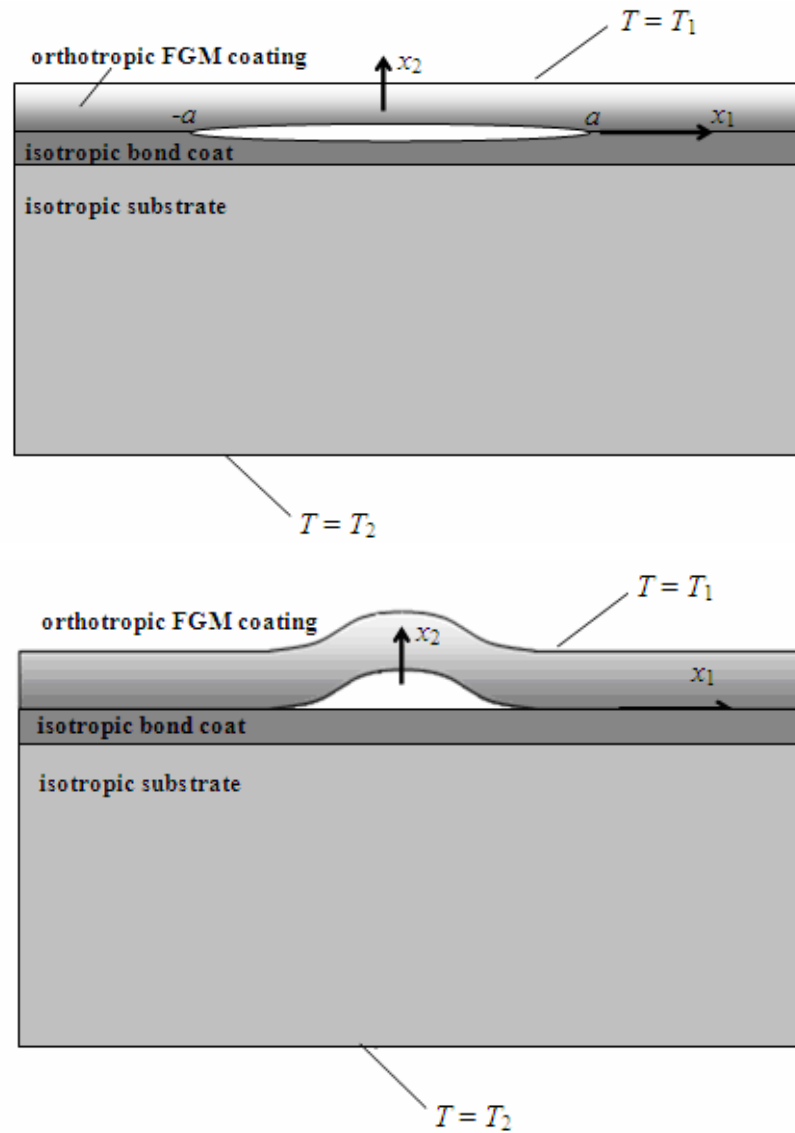


Figure 1.1 Buckling of FGM coating under thermal load.

The delamination behavior of the crack will be investigated in this study by determining fracture mechanics parameters for an FGM coating bonded to homogeneous substrate.

1.2 Literature Survey

For functionally graded materials, analytical solutions to crack problems are limited to relatively simple geometries and loading conditions. As a result, application of

numerical methods such as the finite element method becomes necessary to analyze crack problems and obtain fracture mechanics parameters.

A review of the recent literature, relevant to the problem under consideration is given below. Crack problems in orthotropic FGMs are investigated by analytical techniques in various studies. Gu and Asaro (1996) solved mixed mode stress intensity factors analytically for a semi infinite crack of an isotropic and FGM strip. They determined the effects of material gradients on the mode I and mode II stress intensity factors and the phase angle. By using orthotropy rescaling, the analytical solution was extended to orthotropic solution. The relation between driving force, the energy release rate and toughness of the material were studied with respect to crack propagation. Depending on the type of material nonhomogeneity these factors determined the direction of crack propagation.

The symmetric crack problem of graded material is examined by Ozturk and Erdogan (1997). The properties of the medium was assumed to vary in one direction and symmetric in other direction. In the formulation of inhomogeneous orthotropic medium four independent engineering constants, E_{11} , E_{22} , G_{12} and ν_{12} are used. For mode I case the effect of all these parameters were investigated. The results of this study can be summarized as follows. The Poisson's Ratio has negligible influence on SIFs, shear parameter κ may be significant for $\kappa < -0.5$, modulus of elasticity E and stiffness ratio δ have no influence on SIF, the effect of material inhomogeneity parameter on SIF and displacements is quite significant.

In addition to the analytical solutions to calculate fracture mechanics parameters numerical techniques are also employed. First studies on this subject were the calculation of fracture mechanics parameters by numerical methods. Araújo et al. (2000) described the numerical procedures to estimate fracture parameters both in linear elastic and elastic plastic analysis. The techniques used in numerical estimation are Displacement Correlation Technique (DCT), Modified Crack Closure (MCC) method and J-Integral evaluation accomplished by means of equivalent domain integrals. To calculate fracture mechanics parameters quarter point triangular

elements are employed at the crack tip region. Comparison of results obtained by rosettes of elements with angles 30° , 40° and 45° have been done. Results from each numerical technique are compared with analytical and other available numerical results. While solving the problem, depending on the type of the problem such as linear elastic or elastic plastic, rosettes of elements with different angles are used around the crack tip.

In the study of Gray et al. (2003) improved quarter point crack tip element is presented in the solution of two dimensional fracture mechanics problems. During calculation of stresses intensity factors they employed displacement correlation technique, which produces highly accurate results. Results from standard singular elements are compared with improved quarter point elements.

By the following studies comparison of various numerical techniques are given in case of homogeneous and nonhomogeneous orthotropic material properties. In these studies different crack geometries are investigated under different loading conditions and also verification of analytical results with numerical results are also given. Kaya and Nied (1993) investigated interface cracking between bonded ceramic and metal layers. In this study “enriched” finite crack tip elements are specifically developed for the analysis of interface cracking between dissimilar orthotropic layers. Equations of energy release rate (G) and stress intensity factors (K_I , K_{II}) for the bonded system are given analytically. They investigated the effect of material anisotropy on energy release rates and stress intensity factors and compared to the isotropic case.

In the paper by J.H. Kim and G.H. Paulino (2002) fracture analysis of orthotropic functionally graded materials which are oriented with respect to the principal axes of material orthotropy are considered. They used numerical techniques (DCT and MCC) to evaluate stress intensity factors for mode I and mixed mode two dimensional problems. The orthotropic material properties are defined as functions of finite elements. By comparing numerical results with available results in the literature they investigated the effects of boundary conditions, material properties and crack tip mesh generation on the results. They concluded that the DCT and MCC

provide accurate SIFs for mixed mode problems. In addition Poisson's ratio and boundary conditions were found to have significant effect on energy release rate and SIF values in mixed mode problems.

The axisymmetric crack problem for thermal barrier coatings (TBC) under a uniform temperature change is studied by Yıldırım and Erdoğan (2004). The nickel based super alloy substrate, bond coat and FGM coating system is studied to determine the effect of temperature dependence of the material properties. Also the position of edge crack in FGM coating and the effect of material inhomogeneity constant on fracture mechanics parameters such as stress intensity factor and energy release rate were investigated by using finite element method. Temperature dependent energy release rate values are compared to constant material property ones which provides useful insight into how type of coating affect interfacial bond strength.

In the study by Dağ et al. (2004) the interface crack problem between a graded orthotropic coating and a homogenous substrate is solved by employing both analytical and finite element methods. The effects of material gradation on fracture mechanics parameters for cracks lying along the interface is examined. The isotropic and orthotropic interface crack problem, periodic interface cracking and the four point bending test are modeled for orthotropic materials. For each problem the axes of orthotropy are assumed to be parallel and perpendicular to the crack plane. The main results this study are the effect of nonhomogeneity on Mode I and mode II stress intensity factors and energy release rate values for each problem.

Three dimensional surface crack problems in FGMs subjected to mechanical and transient thermal loads were examined by Yıldırım et al. (2005). In the solution of the problem they employed finite element method and calculated SIF values by using DCT. These SIF values were for four different types of coating which showed that maximum SIFs computed during thermal loading for FGMs are lower than homogeneous ceramic coatings.

L. Banks-Sills et al. (2005) investigated the problem of a crack by using FEM in an anisotropic material under linear elastic fracture mechanics conditions. They derived stress intensity factors for various problems by employing Displacement Extrapolation, M-Integral and J-Integral methods. Although all of these methods were presented for isotropic materials, the first two are extended for orthotropic and monoclinic materials. L. Banks-Sills et al. obtained solutions for several problems in the literature by comparing results of these three methods. They discussed the effect of material anisotropy E_{11}/E_{22} and mesh refinement on the accuracy of the results.

In addition to studies on calculation of fracture mechanics parameters by analytical and numerical techniques, various studies on thermal buckling of FGM plates have been performed. The problem of thermal buckling of circular plates was discussed by Najafizadeh and Eslami (2002) for different type of thermal loads. They derived analytical solutions to nonlinear equilibrium and linear stability equations. In another study by Javaheri and Eslami (2002a), (2002b) thermal buckling problem of functionally graded rectangular plate was studied. The solutions are obtained for several types of thermal loads using the classical and the higher order shear deformation theories of plates.

Su and Kim (2003) performed study on three dimensional thermal buckling of FGMs. In this problem material properties were assumed temperature dependent and varied in thickness direction. Thermal buckling behavior of rectangular plate under uniform, linear and sinusoidal temperature change across the thickness was analyzed. They defined the effect of material inhomogeneity on critical temperature under these temperature change cases.

Ma and Wang (2003) investigated the axisymmetric large deflection bending of a functionally graded circular plate under mechanical, thermal and combined loading conditions. Thermal postbuckling of functionally graded circular plate is also investigated. The mechanical and thermal properties of FGM are assumed to vary in thickness direction. They discussed effect of material inhomogeneity constant,

boundary conditions, nonlinear bending, critical buckling temperature and thermal postbuckling behavior of the FGM plate in details.

Using the first order shear deformation theory Lanhe (2004) obtained equilibrium and stability equations for a simply supported rectangular functionally graded plate under thermal loading. He investigated buckling of graded plate under two different types of temperature changes. Critical buckling temperatures for homogeneous and graded plates and changing inhomogeneity parameters are determined.

Up to now the studies can be grouped as “calculation of fracture mechanics parameters for FGM layers having a crack” and “thermal buckling of FGM plates”. The study by Chiu (1999) is an example where both cases are considered. By using continuum elasticity Chiu developed a solution to the buckling instability problem. The effect of material inhomogeneity in graded coatings on the instability, postbuckling behavior and fracture mechanics parameters such as the stress intensity factor and strain energy release rate are investigated. He simplified the plane strain problem of graded coating bonded to a homogeneous substrate containing an interface crack to an eigenvalue problem and calculated instability load analytically. Examination of postbuckling behavior and calculation of stress intensity factors and strain energy release rates are done by using nonlinear finite element solution. In the solution of the problem enriched crack tip elements are employed. Plane strain and axisymmetric interface crack problem is examined for homogeneous and graded coatings under uniform temperature drop. Comparison of the results coming from plate theories with the numerical results shows that the former one predicts lower energy release rate values. In addition graded coating gives lower strain energy release rates due to lower thermal residual stresses and higher bending stiffness. Also results of mode I and mode II stress intensity values indicates dominant mode, direction of crack growth and gives an idea about delamination behavior of coating substrate system.

Although various studies on thermal or mechanical loading of FGMs have been performed, very limited studies have been done on the delamination problem driven

by thermal buckling. The study by Chiu gives the spallation mechanism for the cracks lying at substrate-coating interface for isotropic materials. He employed enriched elements in the solution, but in this study a different finite element technique and fracture mechanics parameter calculation method will be employed in the analysis of the fracture model. Furthermore orthotropy of the coating and material gradation will be taken into account.

1.3 Scope of the Study

The main objective of this study is to model a particular type of crack problem in a layered structure consisting of a substrate (Nickel-based Superalloy), a bond coat (NiCrAlZr) and an orthotropic FGM coating.

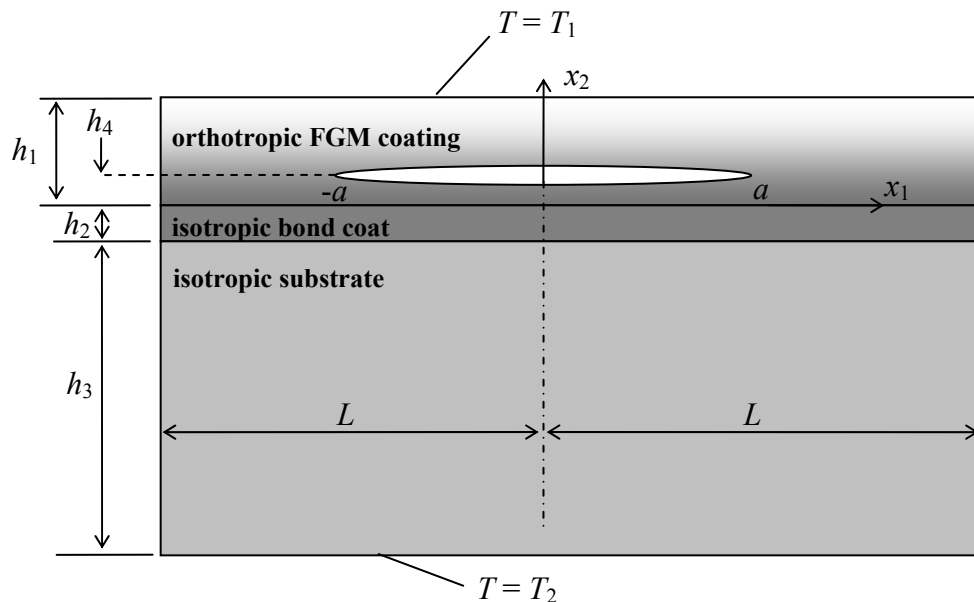


Figure 1.2 The geometry of the internal crack problem.

The crack is perpendicular to material gradation of coating and position of the crack changes in gradation direction. The surfaces of substrate and coating have different temperatures and the lateral surfaces of the system are insulated. The substrate, bond coat and coating system is loaded with a steady-state heat flow which causes a buckled shape along crack face. A two-dimensional finite element model of an

internal crack in the orthotropic layer or an interface crack is modeled using the ANSYS finite element software. In the finite element model of the problem, singular elements are used around the crack tip. In calculation of mode I and II stress intensity factors and energy release rate, displacement correlation technique is employed. Since the available functions to calculate SIF given by ANSYS can not be used for orthotropic materials, ANSYS Parametric Design Language (APDL) subroutines are developed to model the whole problem and calculate SIFs from nodal displacements. This study presents the effects of geometric parameters such as crack length, crack position, etc as well as the effects of type of gradation on buckling behavior and mixed mode stress intensity factors. The consistency of results and accuracy of the model is verified by solving example problems and comparing the results with those given by Kim and Paulino (2002), Dağ et al. (2004) and Chiu (1999).

Having given brief information about recent literature and the scope of this study, information about two dimensional fracture analysis and displacement correlation technique will be given in the next chapter. In Chapter 3 details of finite element model will be given. Chapter 4 includes sample results for some previously solved problems and comparison of these results with the available results in the literature. Hence the validity of the finite element procedures is established. Chapter 5 includes the original results and their discussion, pertaining to the problem considered in this study.

CHAPTER 2

PROBLEM DEFINITION

2.1 Fracture Mechanics

Linear Elastic Fracture Mechanics is an engineering discipline defined within the context of linear theory of elasticity. It has a wide range of application areas including, analysis of brittle fracture of low toughness materials and crack growth analysis. Since over 80 percent of brittle fractures occur in case of crack growths, these applications on analysis of nature of fracture gain importance. In fracture mechanics, to predict state of stress near the tip of a crack, stress intensity factor is used. Depending on the state of stress near the crack tip, growth of crack starts when crack driving force reaches a critical value. Under different loading conditions stress intensity factor is a measure of loading at the crack tip. Stress intensity factors can be considered as a function of size and position of the crack, applied stress and geometry of the workpiece. Depending on the loading condition and displacement of crack surfaces there are three modes of SIF values. Mode I is opening or tensile mode where crack surfaces move directly apart. Mode II is sliding mode where crack surfaces slide over one other. Mode III is tearing mode where crack surfaces move relative to one another. Depending on the loading conditions mixed modes are also possible. Crack propagation and unstable fracture occurs when the stress intensity factor reaches a critical value.

To investigate and determine stress intensity factors several techniques are employed. In the two dimensional thermal buckling problem considered here, stress intensity factors will be determined by employing Displacement Correlation Technique. The subject below gives detailed information about this technique and the derivation of equations used in the calculations.

2.2 The Displacement Correlation Technique

In the calculation of Fracture Mechanics parameters associated with FGM coating substrate structures, analytical approaches can be employed only for some relatively simple problems. However for more complicated cases where large deformations and anisotropic material properties, are involved, analytical methods are not appropriate to find fracture mechanics parameters. Finite Element Analysis is one of the numerical solution methods that can be used in the solution of Linear Elastic Fracture Mechanics (LEFM) and Elastic-Plastic Fracture Mechanics problems. While using this method special care must be taken in modeling of the crack tip (refined meshes, element types) and in the formulation required to calculate Fracture Mechanics parameters such as Stress Intensity Factor (SIF) and Energy Release Rate.

In this study the problem of a crack in an orthotropic functionally graded material under LEFM condition is presented. The stress, strain and displacement fields around crack region are governed by Stress Intensity Factors. Using the displacement field obtained by numerical analysis, SIF values can be calculated easily. The methods presented in the literature are;

- Displacement Correlation Technique (DCT)
- Virtual Crack Extension
- Modified Crack Closure Method (MCC Method)
- J-Integral Method

These techniques can be grouped in two categories according to Milne et al. (2003). First one is “Direct Approaches” which finds stress intensity factors using displacement values from finite element solution. Second one is “Energy Approaches”. Although energy approaches are more accurate, direct approaches which are relatively simple have been widely employed in SIF calculations. DCT, which is utilized in this study, is in the first group and the remainders are in second group.

The displacement field of FGM coating–substrate system will be found by using ANSYS finite element software and SIF values will be calculated using the displacement values at the crack tip by DCT.

Chan (1970) introduced displacement correlation which is one of the first techniques to find SIF values. In this method, one substitutes the displacement results from the finite element analysis into the analytical expressions defined near the crack. In the model of the crack region, crack faces should be coincident and the elements around the crack tip should be quadratic. Midside nodes of the element are placed at the quarter points. Detailed information about singular elements is given in Chapter3. Nodes used in the DCT are shown in Figure 2.1.

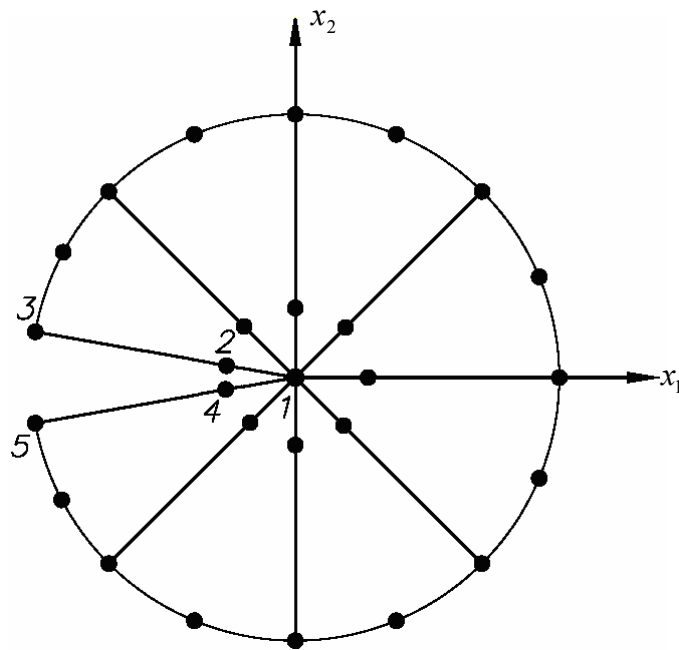


Figure 2.1 Singular elements at the crack tip and nodes used in calculation of SIFs.

In the case of an orthotropic FGM coating on a homogeneous substrate with a crack at or near the interface (lying parallel to the interface) formulation used in the calculation of SIFs must be valid for orthotropic materials. The forthcoming section presents crack tip fields in orthotropic functionally graded material.

2.3 Crack Tip Fields in Orthotropic FGMs

A material is isotropic if all its material properties at a point are independent of direction. On the other hand a material is said to be anisotropic if it has directionally dependent material properties. If m is defined as material property with respect to the selected coordinate system, $m=m'$ for isotropic materials and $m \neq m'$ for an anisotropic material. Figure 2.2 shows coordinate system orientations for a material.

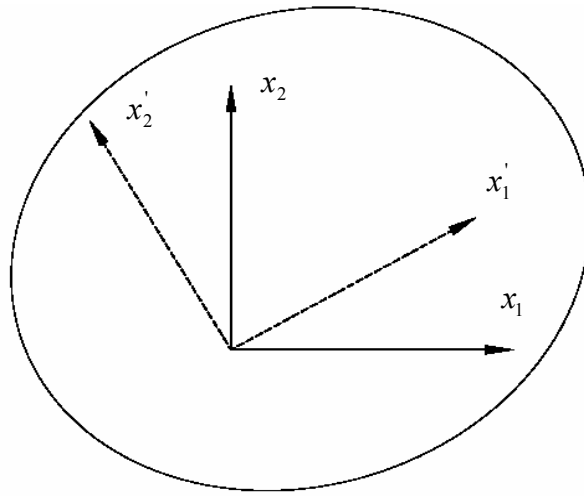


Figure 2.2 Definitions of isotropic and anisotropic materials.

For an anisotropic material, stress-strain relations are given as,

$$\varepsilon_{ij} = C_{ijkl} \cdot \sigma_{kl} , \quad (2.1)$$

Where ε_{ij} is the strain tensor, σ_{ij} is the stress tensor and C_{ijkl} is the fourth order compliance tensor. Although compliance tensor has 81 components, using symmetry of σ_{ij} and ε_{ij} the number of independent components can be reduced to 36. Then one can write

$$\varepsilon_i = C_{ij} \cdot \sigma_j , \quad (i, j = 1, 2, \dots, 6) \quad (2.2)$$

By using strain energy density function U_0 , number of independent parameters is reduced to 21.

$$\begin{pmatrix} \varepsilon_1 \\ \varepsilon_2 \\ \varepsilon_3 \\ \varepsilon_4 \\ \varepsilon_5 \\ \varepsilon_6 \end{pmatrix} = \begin{pmatrix} C_{11} & C_{12} & C_{13} & C_{14} & C_{15} & C_{16} \\ & C_{22} & C_{23} & C_{24} & C_{25} & C_{26} \\ & & C_{33} & C_{34} & C_{35} & C_{36} \\ & & & C_{44} & C_{45} & C_{46} \\ & & & & C_{55} & C_{56} \\ & \text{sym} & & & & C_{66} \end{pmatrix} \begin{pmatrix} \sigma_1 \\ \sigma_2 \\ \sigma_3 \\ \sigma_4 \\ \sigma_5 \\ \sigma_6 \end{pmatrix}, \quad (2.3)$$

where

$$\sigma_1 = \sigma_{11}, \quad \sigma_2 = \sigma_{22}, \quad \sigma_3 = \sigma_{33}, \quad \sigma_4 = \sigma_{23}, \quad \sigma_5 = \sigma_{13}, \quad \sigma_6 = \sigma_{12}. \quad (2.4)$$

$$\varepsilon_1 = \varepsilon_{11}, \quad \varepsilon_2 = \varepsilon_{22}, \quad \varepsilon_3 = \varepsilon_{33}, \quad \varepsilon_4 = 2\varepsilon_{23}, \quad \varepsilon_5 = 2\varepsilon_{13}, \quad \varepsilon_6 = 2\varepsilon_{12}. \quad (2.5)$$

This is the general stress-strain relation for anisotropic materials. However some anisotropic materials have material symmetries which give them fewer independent components in stiffness tensor. This symmetry condition is called as plane of elastic symmetry. This term is defined by Ochoa and Reddy (1992) as follows; “The elastic coefficients at a point have the same values for every pair of coordinate systems which are mirror images of each other in a certain plane, that plane is called a plane of elastic symmetry for the material at that point.” An orthotropic material has three mutually perpendicular planes of elastic symmetry. In this case generalized Hooke’s law for stress and strain in x,y,z coordinates are given by Lekhnitskii (1968)

$$\varepsilon_x = C_{11} \cdot \sigma_x + C_{12} \cdot \sigma_y + C_{13} \cdot \sigma_z, \quad (2.6a)$$

$$\varepsilon_y = C_{12} \cdot \sigma_x + C_{22} \cdot \sigma_y + C_{23} \cdot \sigma_z, \quad (2.6b)$$

$$\varepsilon_z = C_{13} \cdot \sigma_x + C_{23} \cdot \sigma_y + C_{33} \cdot \sigma_z, \quad (2.6c)$$

$$\gamma_{yz} = C_{44} \cdot \tau_{yz}, \quad (2.7a)$$

$$\gamma_{xz} = C_{55} \cdot \tau_{xz}, \quad (2.7b)$$

$$\gamma_{xy} = C_{66} \cdot \tau_{xy}, \quad (2.7c)$$

The number of independent parameters is reduced to 9 in the case of orthotropy,

$$\begin{pmatrix} \varepsilon_1 \\ \varepsilon_2 \\ \varepsilon_3 \\ \varepsilon_4 \\ \varepsilon_5 \\ \varepsilon_6 \end{pmatrix} = \begin{pmatrix} C_{11} & C_{12} & C_{13} & 0 & 0 & 0 \\ & C_{22} & C_{23} & 0 & 0 & 0 \\ & & C_{33} & 0 & 0 & 0 \\ & & & C_{44} & 0 & 0 \\ & & & & C_{55} & 0 \\ & \text{sym} & & & & C_{66} \end{pmatrix} \begin{pmatrix} \sigma_1 \\ \sigma_2 \\ \sigma_3 \\ \sigma_4 \\ \sigma_5 \\ \sigma_6 \end{pmatrix}. \quad (2.8)$$

In the solution of two dimensional crack problem of orthotropic medium, the crack is assumed to be in x_1 direction as shown in Figure 2.3.

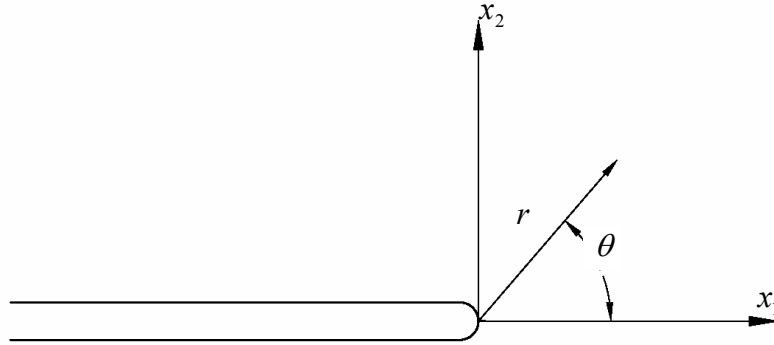


Figure 2.3 Crack tip coordinates.

The stress determination in a plate with an elliptic inclusion is defined by Lekhnitskii (1968). Using these definitions Hoenig derived stress and displacement field equations near crack region for an orthotropic material. These equations can be found in the study by Banks-Sills et al. (2005)

$$\sigma_{xx} = \frac{1}{\sqrt{2\pi r}} \cdot \operatorname{Re} \left(\sum_{i=1}^2 \frac{p_i^2 \cdot B_i}{Q_i} \right), \quad (2.9a)$$

$$\sigma_{yy} = \frac{1}{\sqrt{2\pi r}} \cdot \operatorname{Re} \left(\sum_{i=1}^2 \frac{B_i}{Q_i} \right), \quad (2.9b)$$

$$\sigma_{xy} = \frac{-1}{\sqrt{2\pi r}} \cdot \operatorname{Re} \left(\sum_{i=1}^2 \frac{p_i \cdot B_i}{Q_i} \right), \quad (2.9c)$$

$$\sigma_{zx} = \frac{1}{\sqrt{2\pi r}} \cdot \operatorname{Re} \left(\frac{p_3 \cdot B_3}{Q_3} \right), \quad (2.9d)$$

$$\sigma_{zy} = \frac{-1}{\sqrt{2\pi r}} \cdot \operatorname{Re} \left(\frac{B_3}{Q_3} \right), \quad (2.9e)$$

$$u_i = \sqrt{\frac{2r}{\pi}} \cdot \operatorname{Re} \left(\sum_{j=1}^3 m_{ij} \cdot B_j \cdot Q_j \right), \quad (2.10)$$

The Re term defines the real part of the equation. p_i , $i=1,2,3$ are found from the sixth order polynomial equation given by Banks-Sills et al. (2005). Solution of (2.11) leads to three pairs of complex conjugate roots. The three with positive imaginary part are used in Equations (2.9)-(2.10).

$$l_4(p) \cdot l_2(p) = 0, \quad (2.11)$$

where

$$l_2(p) = S_{55} \cdot p^2 + S_{44}, \quad (2.12a)$$

$$l_4(p) = S_{11} \cdot p^4 + (2 \cdot S_{12} + S_{66}) \cdot p^2 + S_{22}. \quad (2.12b)$$

Here, the S_{ij} terms are derived from compliance parameters for plane strain case

$$S_{ij} = C_{ij} - \frac{C_{i3} \cdot C_{3j}}{C_{33}}. \quad (2.13)$$

The B_j and Q_i parameters are

$$\begin{pmatrix} B_1 \\ B_2 \\ B_3 \end{pmatrix} = \frac{1}{p_2 - p_1} \cdot \begin{pmatrix} p_2 & 1 & 0 \\ -p_1 - 1 & -1 & 0 \\ 0 & 0 & p_1 - p_2 \end{pmatrix} \cdot \begin{pmatrix} K_I \\ K_{II} \\ K_{III} \end{pmatrix}, \quad (2.14)$$

$$Q_i = \sqrt{\cos(\theta) + p_i \cdot \sin(\theta)}. \quad (2.15)$$

The parameters K_j are the stress intensity factors K_I , K_{II} and K_{III} . The parameters m_{ij} are given by

$$m_{1i} = S_{11} \cdot p_i^2 + S_{12}, \quad (2.16a)$$

$$m_{2i} = S_{21} \cdot p_i + \frac{S_{22}}{p_i}, \quad (2.16b)$$

for $i=1,2$

$$m_{13} = m_{23} = 0, \quad (2.17a)$$

$$m_{33} = \frac{-S_{44}}{p_3}. \quad (2.17b)$$

In the calculation of SIF, the displacement equation given at Equation (2.10) will be used. For three planes of elastic symmetry Banks-Sills (2005) defines the expressions for SIF values as

$$K_I = \frac{\sqrt{2\pi}}{4} \cdot \frac{1}{\sqrt{S_{22}} \cdot D_0} \cdot \frac{\Delta u_2}{\sqrt{r}}, \quad (2.18)$$

$$K_{II} = \frac{\sqrt{2\pi}}{4} \cdot \frac{1}{\sqrt{S_{11}} \cdot D_0} \cdot \frac{\Delta u_1}{\sqrt{r}}, \quad (2.19)$$

$$K_{III} = \frac{1}{4 \cdot \sqrt{S_{44} \cdot S_{55} - S_{45}}} \cdot \sqrt{\frac{2\pi}{r}} \cdot \Delta u_3. \quad (2.20)$$

where the term D_o is defined as

$$D_o = \left[2 \cdot \sqrt{S_{11} \cdot S_{22}} + 2S_{12} + S_{66} \right]^{\frac{1}{2}} \quad (2.21)$$

2.3.1 Calculation of Mode I Stress Intensity Factor

For the crack opening model given in Figure 2.4 displacement values of nodes near crack tip are put in the analytical solution.

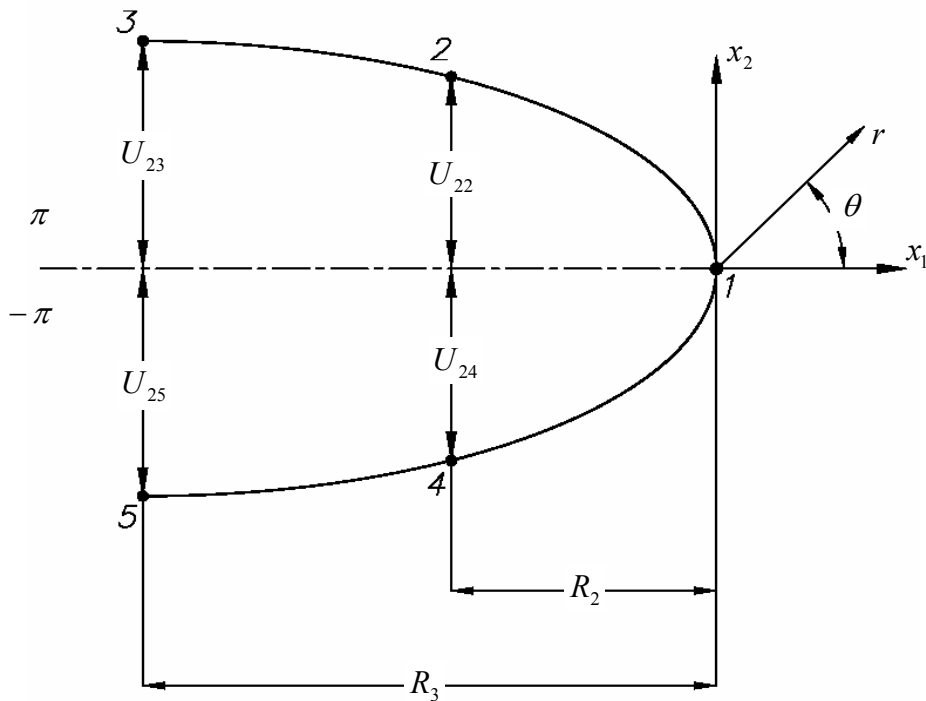


Figure 2.4 Nodal displacements in x_2 -direction near the crack tip.

Nodes near the crack tip are given at a distance R and depending on the side of the crack face they are placed at angle θ and $-\theta$. In the calculation of K_I displacements in x_2 -direction are used. Substituting the values of these displacements obtained from the finite element solution in to Equations (2.18)-(2.20), SIF value can be found.

Defining upper side of the crack face $\theta=\pi$ and lower side as $\theta=-\pi$ Equation (2.18) can be rewritten

$$K_I = \frac{\sqrt{2\pi}}{4} \cdot \frac{1}{\sqrt{S_{22}} \cdot D_o} \cdot \left(\lim_{r \rightarrow 0} \frac{U_2(r, \pi) - U_2(r, -\pi)}{\sqrt{r}} \right). \quad (2.22)$$

Assuming the part of equation whose limit is being taken is linear in r , one can write

$$\frac{U_2(r, \pi) - U_2(r, -\pi)}{\sqrt{r}} = Ar + B. \quad (2.23)$$

Then

$$r = R_2 \rightarrow \frac{U_2(R_2, \pi) - U_2(R_2, -\pi)}{\sqrt{R_2}} = \frac{U_{22} - U_{24}}{\sqrt{R_2}} = AR_2 + B, \quad (2.24a)$$

$$r = R_3 \rightarrow \frac{U_2(R_3, \pi) - U_2(R_3, -\pi)}{\sqrt{R_3}} = \frac{U_{23} - U_{25}}{\sqrt{R_3}} = AR_3 + B. \quad (2.24b)$$

As “ r ” goes to zero, then Equation (2.23) is equal to “ B ”. From Equation (2.24a) and (2.24b) B can be calculated as

$$B = \frac{(U_{22} - U_{24}) \cdot R_3^{\frac{3}{2}} - (U_{23} - U_{25}) \cdot R_2^{\frac{3}{2}}}{\sqrt{R_2} \cdot R_3 \cdot (R_3 - R_2)}. \quad (2.25)$$

The elements at the crack tip are modeled such that, $R_3=4R_2$. Using this relation and then combining Equations (2.22) and (2.25) K_I is written in terms of nodal displacements.

$$K_I = \frac{\sqrt{2\pi}}{4} \cdot \frac{1}{\sqrt{S_{22}} \cdot D_o} \cdot B, \quad (2.26)$$

$$K_I = \frac{\sqrt{2\pi}}{24} \cdot \frac{1}{\sqrt{S_{22}} \cdot D_0} \cdot \left[\frac{8 \cdot (U_{22} - U_{24}) - (U_{23} - U_{25})}{\sqrt{R_2}} \right]. \quad (2.27)$$

Up to this point the mode I stress intensity factor formulation is given for an orthotropic material. If the displacement field of the problem is solved for any type of loading by finite element methods K_I can be calculated using this formula.

Having defined the formulation for mode I case, similar derivations can be done for mode II cases well.

2.3.2 Calculation of Mode II Stress Intensity Factor

The analytical expression for K_{II} is given in Equation(2.19). Applying a procedure similar to the one used for K_I , the mode II stress intensity factor formulation will be done by employing displacements in x_1 -direction. Displacements in x_1 - direction can be seen from Figure 2.5.

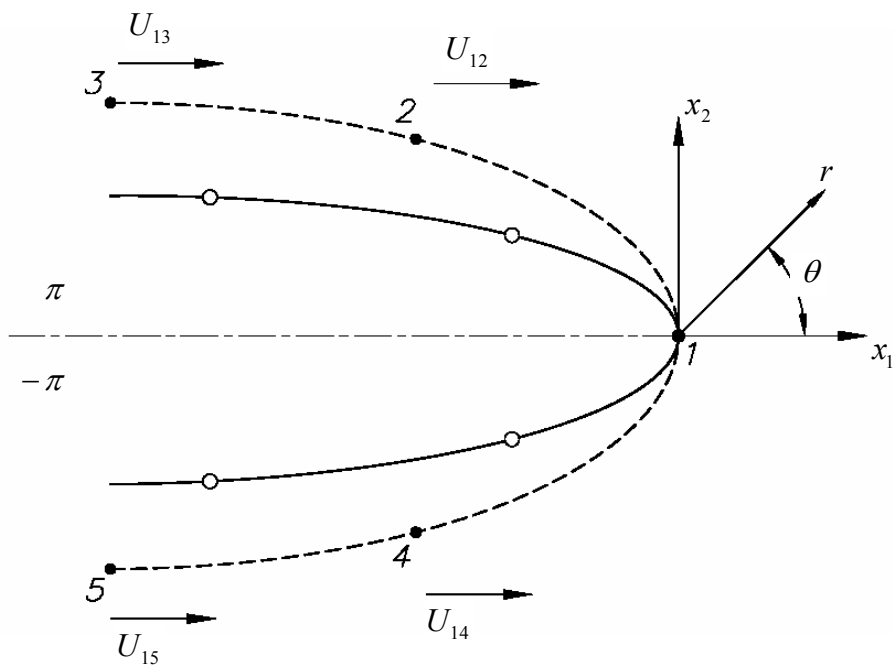


Figure 2.5 Nodal displacements in x_1 -direction near the crack tip.

Again defining upper side of the crack face $\theta=\pi$ and lower side as $\theta=-\pi$ Equation (2.19) can be rewritten

$$K_{II} = \frac{\sqrt{2\pi}}{4} \cdot \frac{1}{\sqrt{S_{11}} \cdot D_0} \cdot \left(\lim_{r \rightarrow 0} \frac{U_1(r, \pi) - U_1(r, -\pi)}{\sqrt{r}} \right). \quad (2.28)$$

Considering the part of equation in limit is linear, boundary conditions applied at points 2,3,4 and 5 on the crack face.

$$\frac{U_1(r, \pi) - U_1(r, -\pi)}{\sqrt{r}} = Ar + B. \quad (2.29)$$

Then

$$r = R_2 \rightarrow \frac{U_1(R_2, \pi) - U_1(R_2, -\pi)}{\sqrt{R_2}} = \frac{U_{12} - U_{14}}{\sqrt{R_2}} = AR_2 + B, \quad (2.30a)$$

$$r = R_3 \rightarrow \frac{U_1(R_3, \pi) - U_1(R_3, -\pi)}{\sqrt{R_3}} = \frac{U_{13} - U_{15}}{\sqrt{R_3}} = AR_3 + B. \quad (2.30b)$$

As “ r ” goes to zero, then the Equation (2.29) is equal to “ B ”. From Equation (2.30a) and (2.30b) B can be calculated as

$$B = \frac{(U_{12} - U_{14}) \cdot R_3^{\frac{3}{2}} - (U_{13} - U_{15}) \cdot R_2^{\frac{3}{2}}}{\sqrt{R_2} \cdot R_3 \cdot (R_3 - R_2)}. \quad (2.31)$$

The elements at the crack tip are modeled such that, $R_3=4R_2$. Using this relation and then combining Equations (2.28) and (2.31) K_{II} is written in terms of nodal displacements.

$$K_{II} = \frac{\sqrt{2 \cdot \pi}}{24} \cdot \frac{1}{\sqrt{S_{11}} \cdot D_o} \cdot B, \quad (2.32)$$

$$K_{II} = \frac{\sqrt{2 \cdot \pi}}{24} \cdot \frac{1}{\sqrt{S_{11}} \cdot D_o} \cdot \left[\frac{8 \cdot (U_{12} - U_{14}) - (U_{13} - U_{15})}{\sqrt{R_2}} \right]. \quad (2.33)$$

2.3.3 Calculation of Energy Release Rate

The strain energy release rate for cracks between dissimilar orthotropic materials is given by Kaya and Nied (1993) as

$$G = \frac{H_{11} \left(\frac{H_{22}}{H_{11}} K_I^2 + K_{II}^2 \right)}{4 \cosh^2 \pi \varepsilon}, \quad (2.34)$$

For a crack at bimaterial interface between two dissimilar materials, bimaterial constant ε is defined as

$$\varepsilon = \frac{1}{2\pi} \ln \left(\frac{1 - \beta}{1 + \beta} \right), \quad (2.35)$$

where

$$\beta = \frac{\left[\sqrt{S_{11} S_{22}} + S_{12} \right]_2 - \left[\sqrt{S_{11} S_{22}} + S_{12} \right]_1}{\sqrt{H_{11} H_{22}}}, \quad (2.36)$$

H_{11} and H_{22} terms are given as

$$H_{11} = \left[2n\lambda^{\frac{1}{4}} \sqrt{S_{11} S_{22}} \right]_1 + \left[2n\lambda^{\frac{1}{4}} \sqrt{S_{11} S_{22}} \right]_2, \quad (2.37a)$$

$$H_{22} = \left[2n\lambda^{-\frac{1}{4}} \sqrt{S_{11}S_{22}} \right]_1 + \left[2n\lambda^{-\frac{1}{4}} \sqrt{S_{11}S_{22}} \right]_2, \quad (2.37a)$$

with n and λ given by

$$n = \sqrt{(1 + \rho)/2}, \quad (2.38)$$

$$\lambda = \frac{S_{11}}{S_{22}}, \quad (2.39)$$

where

$$\rho = \frac{2S_{12} + S_{66}}{2\sqrt{S_{11}S_{22}}}, \quad (2.40)$$

Since in our problem at the interface of FGM coating and bond coat layer material properties are the same, β term is equal to zero and ε is also equal to zero. As a result energy release rate equation can be rewritten simply

$$G = H_{22}K_I^2 + H_{11}K_{II}^2 \quad (2.41)$$

After calculating mode I and mode II stress intensity factors by using nodal displacements near the crack zone, energy release rate can be found by putting these results in equation (2.41).

CHAPTER 3

FINITE ELEMENT ANALYSIS OF ORTHOTROPIC FGM COATING ON A SUBSTRATE

3.1 Introduction

Finite Element Analysis is a structural problem solving method which is developed during academic and industrial researches between 1950s and 1960s. It is a tool which simulates and shows the results of the models under different loading conditions. Previously destructive testing methods are applied to structures to understand their mechanical properties and possible failure modes. An alternative to these tests can be numerical analyses. In today's technology with the developments in computers and software used in finite element analyses, numerical simulations can be done easily which gives the designer cost and time saving.

In these simulations deformation, stress and strains are calculated for the selected problem. These calculations are used in understanding structural response and failure characteristics. To get accurate results, modeling the problem in a proper way has great importance. While preparing the finite element model, the characteristics of the problem specifies the analysis method and the tools to be used during analysis. These characteristics can be listed such as; type of the analysis applied (i.e. structural static analysis, nonlinear analysis, buckling analysis, modal analysis), material properties, loading conditions (i.e. pressure, displacement and temperature gradient) etc.

There are examples of analytical solutions to buckling problems or some fracture problems. However for the problem of FGM coating bonded to homogeneous substrate containing an interface crack under compressive loads can only be solved by employing nonlinear buckling analysis. This will be done by using finite element

method. The full displacement field of the problem is investigated by ANSYS finite element program. In case of buckling large deformation occurs on the FGM coating layer. As a result, while preparing finite element model special attention must be paid on nonlinear buckling analysis and modeling of FGM for fracture mechanics solution. The following topic will give information about nonlinearities and nonlinear analysis. Afterwards some details will be given on modeling and numerical solution.

3.2 Nonlinear Bucking Analysis

3.2.1 Nonlinearities

A solid material will deform when a force is applied on it. The relation between the applied load and the deformation can be defined by linear equations known as Hooke's Law. Using this linear equation, structure can be analyzed by finite element software. However in most cases the relationship between force and displacement is not linear. In such structures loading causes considerable change in stiffness which makes that structure nonlinear. Different from linear structures, the numerical solution of nonlinear structures can be done by iterative series of linear solutions. Causes of this nonlinear behavior are

- Material Nonlinearities
- Geometric Nonlinearities
- Changing Status

The first case is a result of nonlinear stress-strain relationship of the material. Environmental effects such as temperature, load history of the material and time of the load applied are causes of the stress- strain nonlinearities.

The second case happens when the structure experiences large deformations which cause that structure to behave nonlinearly. Types of geometric nonlinearities are

large strains, large deflections and stiffness changes due to initial stresses on structure.

Finally the status dependent behavior of structures is a cause of geometric instability. An example to this can be sudden changes in stiffness due to contact, tension or external causes.

3.2.2 Buckling Analysis

Plate buckling happens when a plate is compressively loaded in its plane. In the problem of a layered structure consisting of a substrate, a bond coat and an orthotropic FGM coating, due differences in thermal expansion coefficients, under large thermal gradients compressive residual stresses can occur in the structure. In case of an internal crack in the layered structure, these stresses cause a buckled shape along crack face. The relation between the load and the displacement given by the classical buckling theory is shown in Figure 3.1, (Turvey and Marshall (1995)).

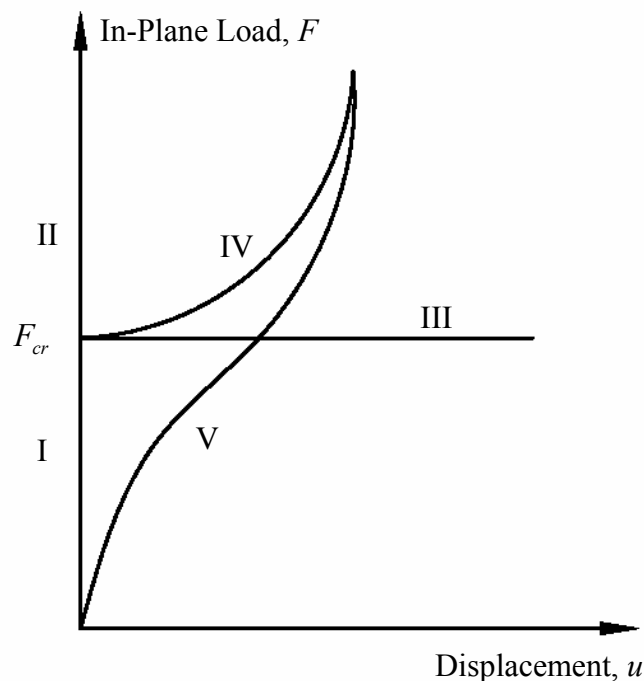


Figure 3.1 Curves of in-plane load (F) versus transverse displacement (u).

According to classical buckling theory the bifurcation behavior can be seen in branches I,II and III. With increasing load F , the displacement curve follows the ordinate I without transverse displacement. The Bifurcation point is a point on load-displacement curve (F_{cr}) where two solutions are possible. Either the structure deforms only in the plane of F and follow curve II or deforms out of plane and follow buckling path III. If one considers nonlinear behavior of the material, the displacement curve follows ordinate IV, called postbuckling curve. However in most cases due to imperfections in the structure or in the loading it is expected that curve would follow ordinate V.

3.2.3 Finite Element Analysis of Buckling Problems

There are analytical solution methods for plate problems. According to Ochoa and Reddy (1992) examples of these solutions are Navier solutions, Lévy solutions, Rayleigh-Ritz and Galerkin methods. However these methods are limited to simple geometries because of the difficulty in constructing the approximation functions for complicated geometries. At this point numerical solutions techniques give us solution of geometrically complicated problems. Among these techniques the finite element method is most powerful and flexible solution method. By using a computer wide range of problems can be solved where input data such as physical properties and initial conditions are changing.

3.3 Modeling of Fracture Problem for orthotropic materials

Today many software packages and different modeling techniques are used to solve models of the problems. The numerical solutions of this study will be obtained by ANSYS finite element software. In the solution of the interface crack in substrate-FGM coating system a nonlinear analysis is performed under buckling loads and fracture mechanics parameters will be calculated using nodal displacements near crack tip.

3.3.1 Fracture Mechanics Issues in ANSYS

In order to calculate fracture parameters, region around the crack tip must be modeled carefully. The recommended element type used in fracture mechanics problems are PLANE2 and PLANE82. PLANE2 is a 6-node triangular element, and PLANE82 is a quadrilateral element which has 8-nodes. Figure 3.2 shows PLANE2 and PLANE82 elements as used in the modeling of crack tip region. The important point is singularity of elements around the crack region. Here mid-side nodes are placed at quarter points of the element and crack faces are modeled coincident. In ANSYS there is a special command KSCON which defines a concentration about a point about which an area mesh will be defined. In fracture mechanics problem this command is used to create crack tip elements around crack tip. 2D singular element, PLANE82 can be seen from Figure 3.3. By using KSCON command 8 node element collapsed to a 6 node singular element.

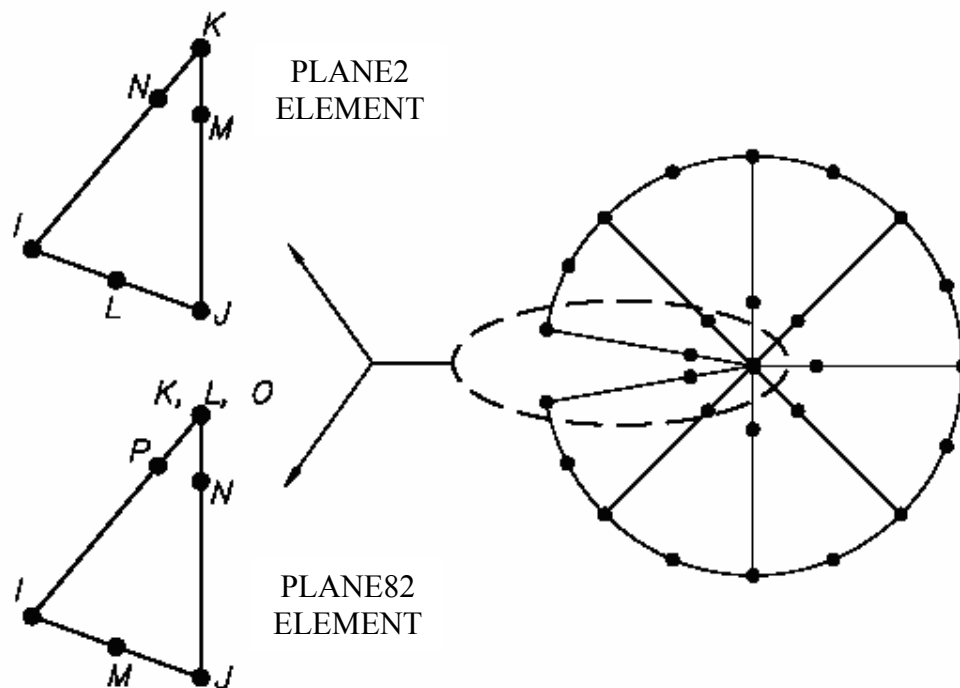


Figure 3.2 Examples of 2-D singular elements. PLANE2 and PLANE82.

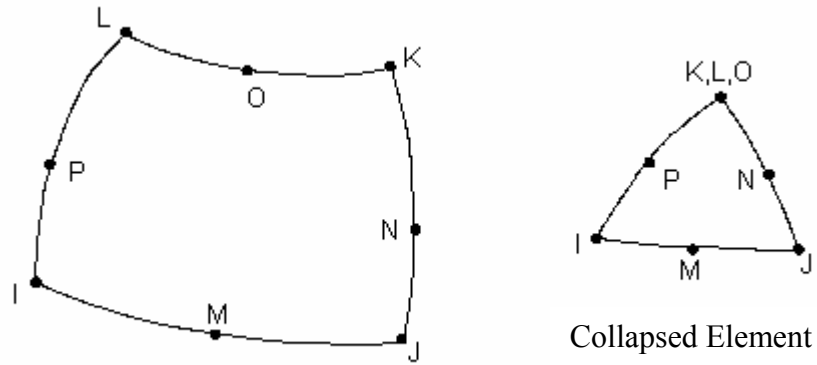


Figure 3.3 Node locations of PLANE82 element.

3.3.2 Basic Information about Nonlinear Analysis in ANSYS

As mentioned before the nonlinear analysis of structure can be done using iterative series of linear solutions. In ANSYS Newton-Rapson Method solves nonlinear problems by dividing the load into a series of load increments. The iteration is done according to Equation (3.1)

$$[K^T] \cdot \{\Delta u\} = \{F^{ext}\} - \{F^{nr}\} \quad (3.1)$$

where

$[K^T]$ =Tangent Stiffness Matrix

$\{\Delta u\}$ =Displacement Increment

$\{F^{ext}\}$ =External Load Vector

$\{F^{nr}\}$ =Internal Force Vector

At each solution step the tangent stiffness matrix and difference between external load and internal load is updated. Solution converges when the difference between to loads is in an admissible tolerance. A graph showing the iterations done by Newton-Rapson method is given in Figure 3.4.

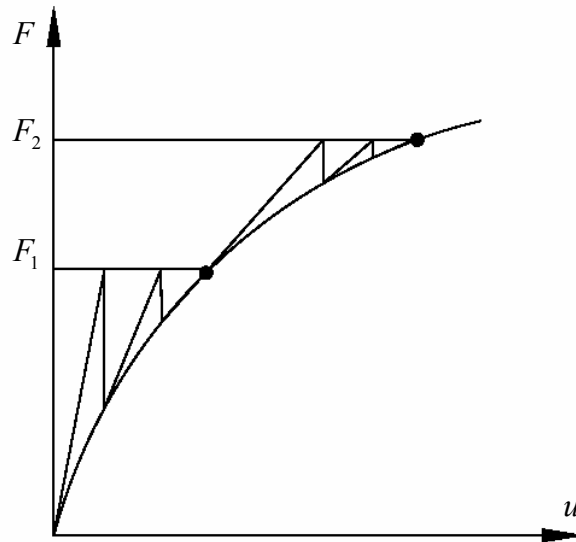


Figure 3.4 Newton-Rapson iterative method (4 iterations are shown)

3.3.3 Basic Information about Bucking Analysis in ANSYS

By solving buckling problems in ANSYS buckling loads, displacements and buckled mode shapes can be found. This analysis can be done by Eigenvalue (linear) buckling analysis or by nonlinear buckling analysis.

3.3.3.1 Eigenvalue (Linear) Buckling Analysis

The first one is mostly employed to determine critical buckling load called bifurcation point. Usually this critical load is used in determination of load defined in nonlinear analysis. Eigenvalue analysis is also used in determination of buckled mode shapes. The advantages of this analysis technique are

- Critical load and modal shapes are solved very quickly.
- Buckled shapes can be used as geometric imperfection in nonlinear analysis.

Nevertheless, nonlinear behavior of structures makes the results of eigenvalue buckling analysis inconsistent. Since the load of our problem is temperature drop, there is no need to employ structural analysis. The critical temperature gradient at which buckling starts can be seen from displacement versus time plots. As a result a nonlinear analysis must be employed to calculate real response of the structure.

3.3.3.2 Nonlinear Buckling Analysis

By using nonlinear analysis in ANSYS large deformations are included in the solution of the buckling problem. The solution is done by employing a nonlinear static analysis with gradually increasing loads. This load increments designates the load level at which a structure becomes unstable. Since this analysis is more accurate than linear analyses, it is used in design and evaluation of the structures.

3.4 The Finite Element Model

The model of the problem shown in Figure 3.5 is modeled using ANSYS finite element software. Since the object of this study is investigating position and length of the crack in the FGM coating same problem must be solved for different values of crack height and crack length. In order to model the problem each time, APDL is used to model and solve the problem. APDL is a scripting language that one can use to automate common tasks and build its own model in terms of parameters. (See Appendix I for a sample APDL code.) Especially definition of graded orthotropic material properties can only be performed with APDL. The variation of the material properties such as modulus of elasticity, shear modulus and Poisson's Ratio is incorporated into the model by defining material properties at the centroid of each element.

In finite element models up to 100,000 elements are used depending on position and length of the crack and accuracy of the result. To model material orthotropy and increase number of elements PLANE2 elements are preferred. Details of PLANE2

element can be seen in Figure 3.2. The elements used near the crack tip are singular elements. The radius of singular elements is $a/1000$ and 24 elements are used around the crack tip. The steps of APDL program can be listed as below

- Definition of analysis type, Static
- Definition of element type, PLANE2
- Input initial temperature, T_i
- Enter constants used in the program
- Model the geometry, lines and areas
- Define line divisions before meshing
- Mesh the geometry
- Define material properties at centroid of each element
- Define nonlinear solution options
- Enter boundary conditions, symmetry
- Load the geometry to final temperature, T_f
- Solve
- Read displacement values in the fully crack model
- Compute SIFs by employing DCT
- Compute energy release rate from SIF results

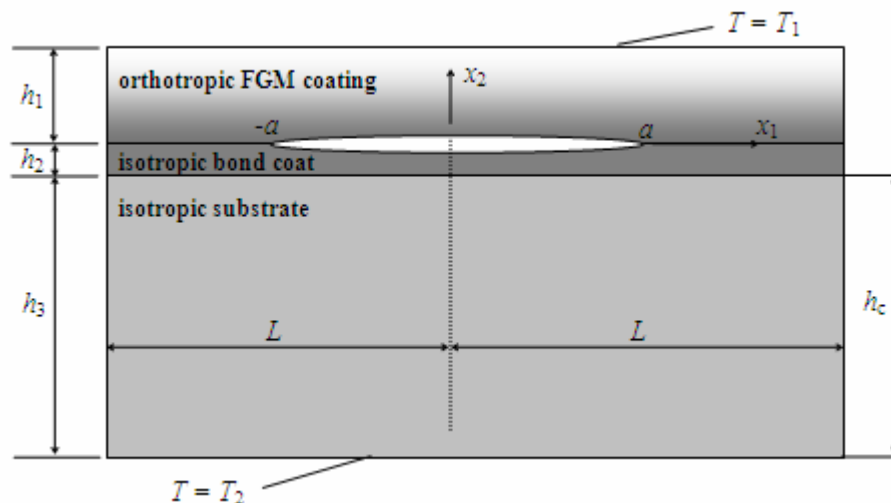


Figure 3.5 Thermal buckling problem of orthotropic FGM coating bonded to homogeneous substrate.

CHAPTER 4

VERIFICATION of FINITE ELEMENT PROCEDURES

4.1 Introduction

To make sure that results of fracture analyses, obtained from the models prepared in ANSYS are correct, sample crack problems in the literature are modeled and SIF values from these problems are compared with the results calculated by DCT. First “Plate with Slanted Crack Problem” by Kim and Paulino (2002) is modeled. Then, the interface crack problem given by Dağ et al. is modeled and solved for isotropic and orthotropic case. Finally the Plain Strain Problem of Chiu is modeled and the SIF values are compared under thermal buckling load.

After verifying the accuracy of finite element model, the FGM coating bonded to homogeneous substrate with an interface crack problem is modeled and solved in the next chapter.

4.2 Slanted Crack Problem

The slanted crack problem with a crack length $2a$ located in a finite two-dimensional plate under tension is given in Figure 4.1. The dimensions of problem and orthotropic material properties are given below

$$\begin{aligned} 2a &= 2\sqrt{2}, \quad L/W = 2, \\ E_{11}(x_1) &= E_{11}^0 e^{\alpha x_1}, \quad E_{22}(x_1) = E_{22}^0 e^{\beta x_1}, \quad G_{12}(x_1) = G_{12}^0 e^{\gamma x_1} \\ E_{11}^0 &= 3.5 \times 10^6, \quad E_{22}^0 = 12 \times 10^6, \quad G_{12}^0 = 3 \times 10^6, \quad \nu_{12} = 0.204. \end{aligned} \quad (4.1)$$

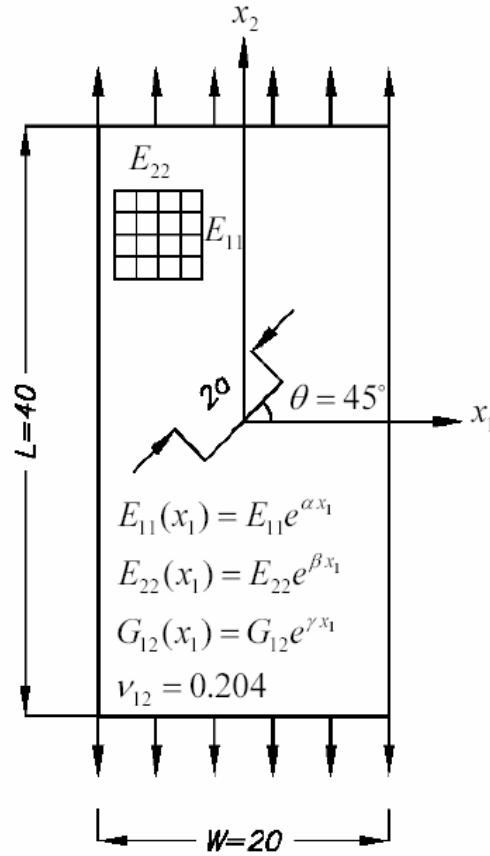


Figure 4.1 Geometry and boundary conditions of plate with a slanted crack.

Kim and Paulino obtained solutions with I_FRANC2D code with assumption of generalized plane stress. Solutions are given for different material variations,

- i. Homogeneous orthotropic plate with a slanted crack: $(\alpha, \beta, \gamma) = (0, 0, 0)$
- ii. FGM proportional plate with a slanted crack: $(\alpha, \beta, \gamma) = (0.2, 0.2, 0.2)$
- iii. FGM non-proportional crack with a slanted crack: $(\alpha, \beta, \gamma) = (0.5, 0.4, 0.3)$

While giving these results solutions are compared with those available in the literature. For problem (i) there are analytical and numerical results in the literature. However for problem (ii) and (iii) there are no other solutions except the results given by Kim and Paulino.

4.2.1 Homogeneous orthotropic plate with a slanted crack

For the homogeneous orthotropic material the constants in the material variation are given as: $(\alpha, \beta, \gamma) = (0, 0, 0)$. The solutions to this problem are given by Sih et al. (complex variable approach), Atluri et al. (FEM hybrid displacement model), Wang et al. (FEM-M integral) and Kim and Paulino (MCC and DCT methods). In the solution of the problem ANSYS Parametric Design Language (APDL) is used and the equations Equation (2.24) and Equation (2.30) derived for the calculation of stress intensity factors in orthotropic materials is employed for the homogeneous crack problem. Table 4.1 shows the SIFs using the DCT in comparison with the reference solutions given by previous studies.

Table 4.1 SIF values for homogeneous orthotropic plate.

MATERIAL	METHOD	K_I	K_{II}	% Error K_I	% Error K_{II}
HOMOGENEOUS $(\alpha, \beta, \gamma) = (0, 0, 0)$	Sih et al.	1,0539	1,0539	0,00	0,00
	Atluri et al	1,0195	1,0795	3,26	-2,43
	Wang et al	1,0230	1,0490	2,93	0,46
	Kim and Paulino (MCC)	1,0670	1,0440	-1,24	0,94
	Kim and Paulino (DCT)	1,0770	1,0350	-2,19	1,79
	ANSYS (1650 elements)	1,0715	1,0508	-1,67	0,30
	ANSYS (2186 elements)	1,0529	1,0509	0,09	0,28
	ANSYS (12644 elements)	1,0572	1,0543	-0,32	-0,04

The results show that calculation of stress intensity factor by using nodal displacements around crack tip gives consistent results and gives outputs with an error less than 1%. Also increasing number of elements in model makes results of DCT closer to analytical SIF values. Figure 4.2 and 4.3 show finite element mesh configuration and deformed shape at the crack tip.

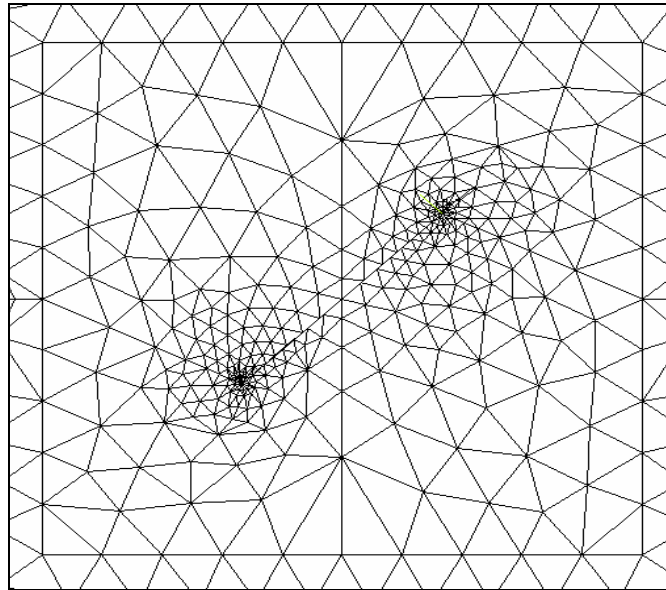


Figure 4.2 Homogeneous orthotropic material, finite element mesh configuration.

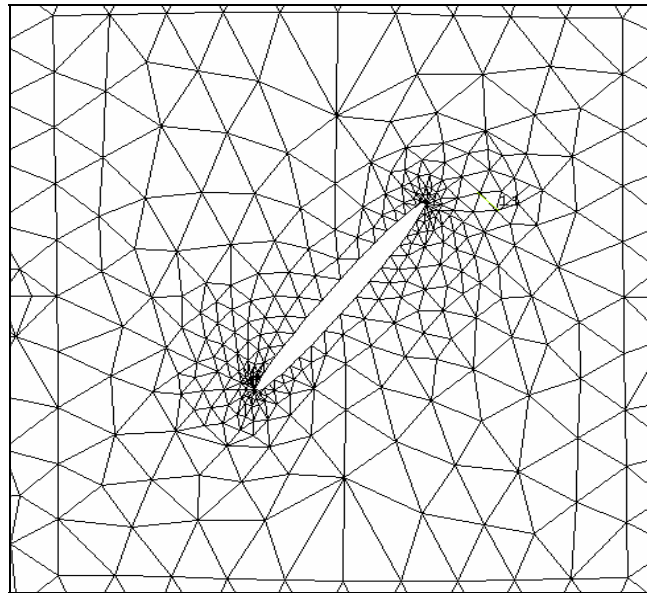


Figure 4.3 Homogeneous orthotropic material, deformed shape at the crack.

4.3 The Interface Crack Problem

The interface crack problem between graded orthotropic coating and homogeneous substrate is shown in Figure 4.4. Thickness of coating and substrate is given as h_1 and h_2 , respectively, the axes of orthotropy are defined as x_1 and x_2 . Both materials have infinite length and pressure is applied to the crack surfaces.

The problem is formulated using averaged constants of plane orthotropic elasticity introduced by Krenk (1979). These constants are called effective stiffness E , shear parameter κ , stiffness ratio δ and stiffness ratio ν . For plane stress problem relations between stress and strain parameters can be expressed as

$$E = \sqrt{E_{11}E_{22}}, \quad \nu = \sqrt{\nu_{12}\nu_{21}}, \quad \delta^4 = \frac{E_{11}}{E_{22}} = \frac{\nu_{12}}{\nu_{21}}, \quad \kappa = \frac{E}{2G_{12}} - \nu. \quad (4.2)$$

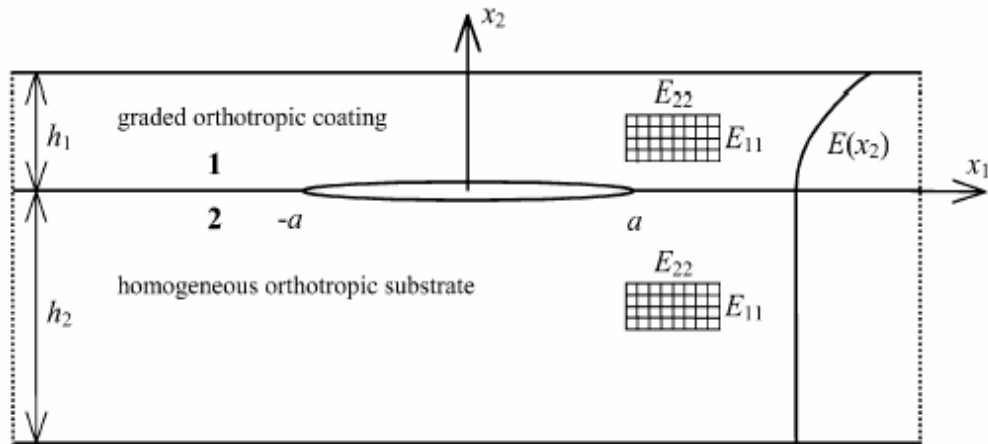


Figure 4.4 An interface crack between a graded orthotropic coating and homogeneous orthotropic substrate.

The interface crack problem is solved for two cases. First one is isotropic case with constants of elasticity $\delta_0^4=1$ and $\kappa_0 = 1$. The results from DCT are compared with the results found by Chen and Erdogan (1990) and Dağ et al. (2004). Second one is

orthotropic case with constants of elasticity $\delta_0^4 = 2$ and $\kappa_0 = 2$. The results found in ANSYS are compared with the analytical and numerical results given by Dağ et al. (2004).

Since the problem is symmetric about x_2 axis half of the problem is modeled in ANSYS. Figure 4.5 shows the finite element mesh used in the model and deformed shape of the crack region. To check the accuracy of the results number of elements is increased in a second solution. Since the materials are graded, increasing number of elements gives more accurate SIF values. The analytical and finite element results for isotropic and orthotropic cases are provided in Tables 4.2 through Table 4.4

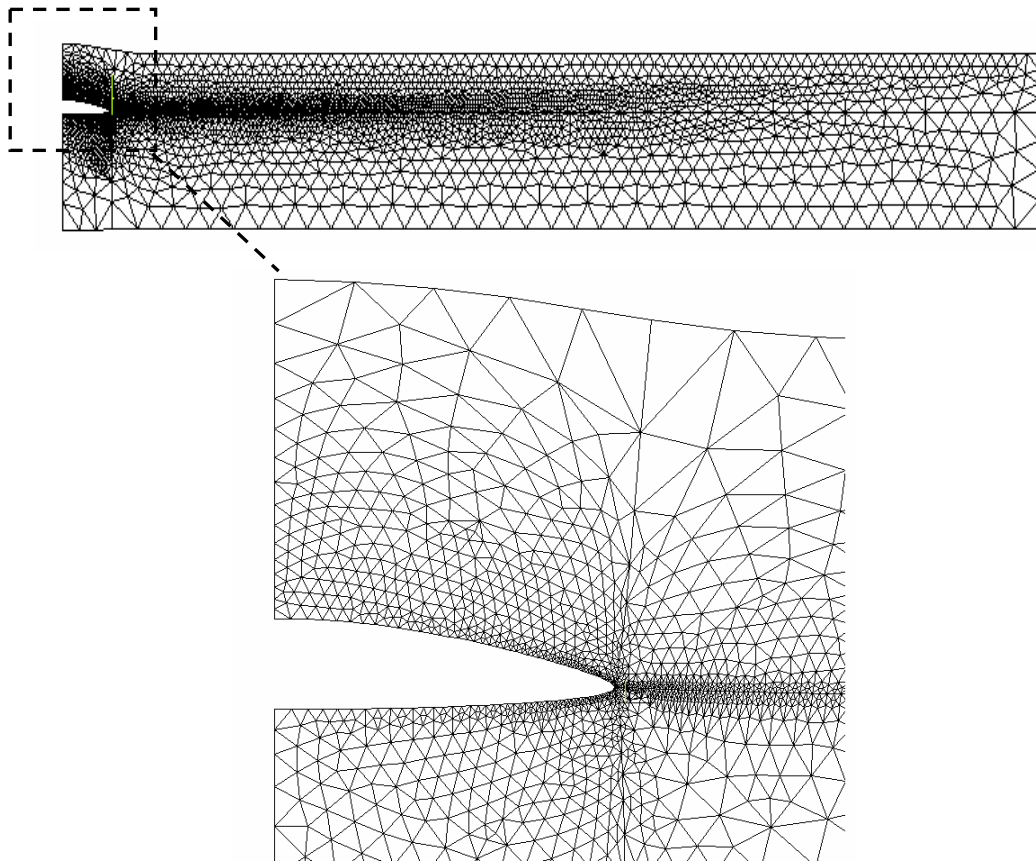


Figure 4.5 Finite element mesh used in the solution of interface crack problem.

Table 4.2 Mixed mode stress intensity factors for isotropic interface crack problem, solution with 6966 elements.

βa	Chen and Erdoğan		Analytical		Enriched Elements		DCT (ANSYS)		% Error (DCT)	
	K_I	K_{II}	K_I	K_{II}	K_I	K_{II}	K_I	K_{II}	K_I	K_{II}
-2.00	2.087	-0.471	2.087	-0.471	2.089	-0.472	2.090	-0.468	-0.156	0.673
-1.00	1.799	-0.296	1.799	-0.296	1.800	-0.297	1.800	-0.293	-0.045	0.847
-0.50	1.675	-0.221	1.675	-0.221	1.677	-0.222	1.675	-0.219	-0.019	0.719
-0.25	1.618	-0.187	1.618	-0.187	1.620	-0.188	1.618	-0.185	-0.008	0.831
-0.01	1.566	-0.156	1.566	-0.156	1.568	-0.157	1.566	-0.155	-0.019	0.842
0.25	1.514	-0.125	1.514	-0.125	1.516	-0.125	1.513	-0.123	0.037	1.339
0.50	1.466	-0.096	1.466	-0.096	1.468	-0.097	1.466	-0.095	0.016	1.024
1.00	1.380	-0.044	1.380	-0.044	1.382	-0.044	1.379	-0.044	0.065	1.136
2.00	1.237	0.042	1.237	0.042	1.239	0.042	1.237	0.041	0.015	1.442

Table 4.3 Mixed mode stress intensity factors for isotropic interface crack problem, solution with 53283 elements.

βa	Chen and Erdoğan		Analytical		Enriched Finite Elements		DCT (ANSYS)		% Error (DCT)	
	K_I	K_{II}	K_I	K_{II}	K_I	K_{II}	K_I	K_{II}	K_I	K_{II}
-2.00	2.087	-0.471	2.087	-0.471	2.089	-0.472	2.090	-0.472	-0.131	-0.266
-1.00	1.799	-0.296	1.799	-0.296	1.800	-0.297	1.800	-0.297	-0.054	-0.222
-0.50	1.675	-0.221	1.675	-0.221	1.677	-0.222	1.676	-0.222	-0.039	-0.425
-0.25	1.618	-0.187	1.618	-0.187	1.620	-0.188	1.619	-0.188	-0.031	-0.353
-0.01	1.566	-0.156	1.566	-0.156	1.568	-0.157	1.567	-0.157	-0.043	-0.385
0.25	1.514	-0.125	1.514	-0.125	1.516	-0.125	1.514	-0.125	0.013	0.065
0.50	1.466	-0.096	1.466	-0.096	1.468	-0.097	1.466	-0.096	-0.003	-0.320
1.00	1.380	-0.044	1.380	-0.044	1.382	-0.044	1.379	-0.044	0.061	-0.474
2.00	1.237	0.042	1.237	0.042	1.239	0.042	1.236	0.042	0.076	0.697

Table 4.4 Mixed mode stress intensity factors for orthotropic interface crack problem, solution with 58073 elements.

	βa	Analytical		Enriched Finite Elements		DCT (ANSYS)		% Error (DCT)	
		K_I	K_{II}	K_I	K_{II}	K_I	K_{II}	K_I	K_{II}
$h_1/a = h_2/a = 10$	-2.00	1.711	-0.357	1.711	-0.358	1.714	-0.358	-0.20	-0.21
	-1.00	1.357	-0.158	1.357	-0.158	1.359	-0.158	-0.13	0.04
	-0.50	1.180	-0.072	1.180	-0.072	1.181	-0.072	-0.10	0.13
	0.00	1.010	0.000	1.011	0.000	1.011	0.000	-0.07	0.00
	0.50	0.893	0.051	0.893	0.051	0.893	0.051	0.03	-0.57
	1.00	0.834	0.085	0.834	0.085	0.833	0.085	0.08	-0.22
	2.00	0.779	0.128	0.779	0.128	0.778	0.127	0.18	0.48
$h_1/a = 1, h_2/a = 10$	-2.00	1.885	-0.449	1.887	-0.449	1.888	-0.449	-0.13	-0.08
	-1.00	1.631	-0.285	1.633	-0.285	1.633	-0.285	-0.11	0.13
	-0.50	1.520	-0.214	1.522	-0.214	1.520	-0.214	-0.03	-0.10
	0.00	1.418	-0.152	1.420	-0.151	1.418	-0.151	-0.01	0.35
	0.50	1.326	-0.096	1.328	-0.096	1.326	-0.096	0.00	0.01
	1.00	1.244	-0.047	1.246	-0.047	1.243	-0.047	0.04	-0.71
	2.00	1.107	0.032	1.109	0.032	1.106	0.032	0.12	0.59
$h_1/a = 0.5, h_2/a = 10$	-2.00	2.493	-0.848	2.496	-0.848	2.496	-0.849	-0.14	-0.12
	-1.00	2.283	-0.694	2.286	-0.695	2.285	-0.694	-0.08	-0.05
	-0.50	2.187	-0.624	2.190	-0.625	2.188	-0.624	-0.02	0.03
	0.00	2.095	-0.558	2.099	-0.559	2.096	-0.558	-0.03	0.08
	0.50	2.009	-0.496	2.013	-0.496	2.009	-0.495	0.00	0.13
	1.00	1.928	-0.438	1.932	-0.438	1.927	-0.437	0.03	0.22
	2.00	1.780	-0.332	1.784	-0.332	1.778	-0.331	0.10	0.25

4.4 The Plane Strain Problem

The interface crack problem of zirconia coating - Rene-41 substrate system, subjected to uniform temperature drop, is investigated by Chiu (1999). The geometry of the problem can be seen in Figure 4.6. Coating thickness, substrate thickness and length of specimens are given as $h_c=2\text{mm}$, $h_s=12.5\text{mm}$ and $l=100\text{mm}$. The variations

of mechanical properties are given below and material properties of the plane strain specimen are given in Table 4.5.

$$E_y(y) = \begin{cases} E_c + (E_s - E_c)\left(\frac{h_s + h_c - y}{h_c}\right), & h_s < y < h_s + h_c, \\ E_s, & 0 < y < h_s \end{cases}, \quad (4.3)$$

$$\alpha_y(y) = \begin{cases} \alpha_c + (\alpha_s - \alpha_c)\left(\frac{h_s + h_c - y}{h_c}\right), & h_s < y < h_s + h_c, \\ \alpha_s, & 0 < y < h_s \end{cases}. \quad (4.3)$$

Table 4.5 Material properties of the zirconia coating and Rene-41 substrate.

	Material	E (GPa)	ν	α (10^{-6}C^{-1})
Substrate	Rene-41	219.7	0.3	16.7
Ceramics	Zirconia	151	0.3	10.0

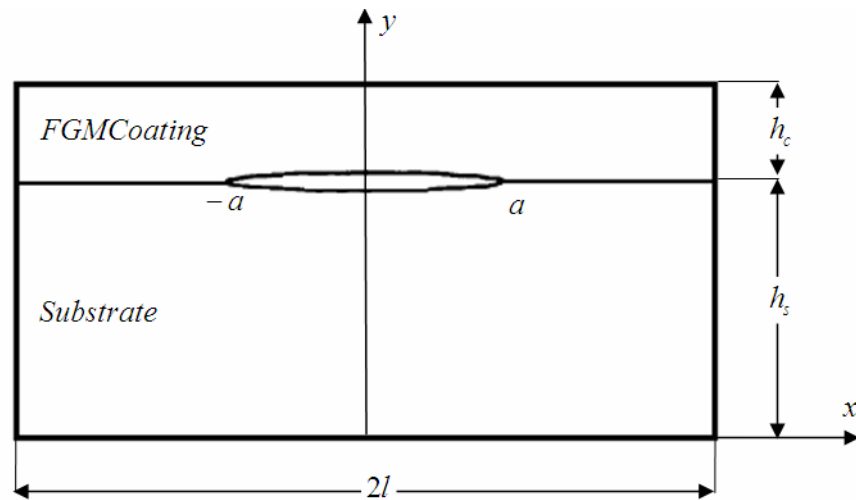


Figure 4.6 Geometry of the plane strain thermal buckling problem.

The plane strain problem covers calculation of SIF values for different a/h_c ratios under uniform temperature change (i.e. Bulk temperature change). Table 4.8-4.9 show the results of the thermal buckling analysis of FGM coating and substrate system. It is observed from COD plot in Figure 4.7 displacement values of FGM are smaller than that of homogeneous coating. This result can be concluded to decrease

in thermal stresses in FGM due to transition in material properties. From these displacement values the critical temperature at which buckling starts can be seen also. The change in crack length has influence on the buckling temperature and SIF values. From these results is seen that mode II is the dominant mode and minus sign of K_{II} shows that crack initiation will be into the coating. To make comparisons, this problem is modeled in ANSYS environment and the results are given in Tables 4.6 and 4.7.

The results given by Chiu (1999) are presented as plots of crack opening displacements and SIFs versus temperature change in Figures 4.7-4.8. If these graphical results are compared with Tables 4.6 and 4.7 it is observed that SIFs and energy release rate values have the same characteristics and results are consistent.

Table 4.6 Displacement and SIF values for changing crack length and temperature gradient.

	$\Delta T/T$	COD	δ/h_c	K_I	K_{II}
$a/h_c = 15$	0	0.0000	0.0000	0.000	0.000
	2	-0.0001	-0.0266	0.002	-0.001
	4	-0.0001	-0.0498	0.010	-0.006
	6	-0.0001	-0.0672	0.025	-0.017
	8	-0.0001	-0.0737	0.054	-0.039
	10	-0.0001	-0.0563	0.109	-0.086
	12	0.0000	0.0171	0.219	-0.193
	14	0.0003	0.1676	0.393	-0.397
	16	0.0007	0.3316	0.559	-0.643
$a/h_c = 20$	0	0.0000	0.0000	0.000	0.000
	2	-0.0001	-0.0251	0.004	-0.002
	4	-0.0001	-0.0350	0.020	-0.013
	6	0.0000	0.0077	0.070	-0.056
	8	0.0005	0.2438	0.223	-0.226
	10	0.0010	0.5038	0.379	-0.480
	12	0.0016	0.7766	0.477	-0.713
	14	0.0019	0.9588	0.543	-0.926
	16	0.0022	1.1109	0.589	-1.125

Table 4.6 (Continued) Displacement and SIF values for changing crack length and temperature gradient.

$a/h_c = 25$	0	0.0000	0.0000	0.000	0.000
	2	0.0000	-0.0199	0.006	-0.004
	4	0.0001	0.0431	0.049	-0.040
	6	0.0010	0.4937	0.214	-0.254
	8	0.0018	0.8817	0.317	-0.494
	10	0.0023	1.1607	0.371	-0.704
	12	0.0028	1.3835	0.402	-0.898
	14	0.0031	1.5711	0.418	-1.081
	16	0.0035	1.7343	0.424	-1.256

Table 4.7 Displacement and SIF values for FGM and homogeneous coatings.

	$\Delta T/T$	<i>COD</i>	δ/h_c	K_I	K_{II}
$a/h_c = 20$ (FGM)	0	0.0000	0.0000	0.000	0.000
	2	-0.0001	-0.0251	0.004	-0.002
	4	-0.0001	-0.0350	0.020	-0.013
	6	0.0000	0.0077	0.070	-0.056
	8	0.0005	0.2438	0.223	-0.226
	10	0.0010	0.5038	0.379	-0.480
	12	0.0016	0.7766	0.477	-0.713
	14	0.0019	0.9588	0.543	-0.926
	16	0.0022	1.1109	0.589	-1.125
$a/h_c = 20$ (Homogeneous)	0	0.0000	0.0000	0.0000	0.0000
	2	0.0000	0.0044	0.0244	-0.0224
	4	0.0010	0.5095	0.2854	-0.4076
	6	0.0021	1.0552	0.4477	-0.9550
	8	0.0028	1.4195	0.4937	-1.4156
	10	0.0034	1.7045	0.4925	-1.8357
	12	0.0039	1.9427	0.4646	-2.2311
	14	0.0043	2.1495	0.4193	-2.6094
	16	0.0047	2.3324	0.3620	-2.9747

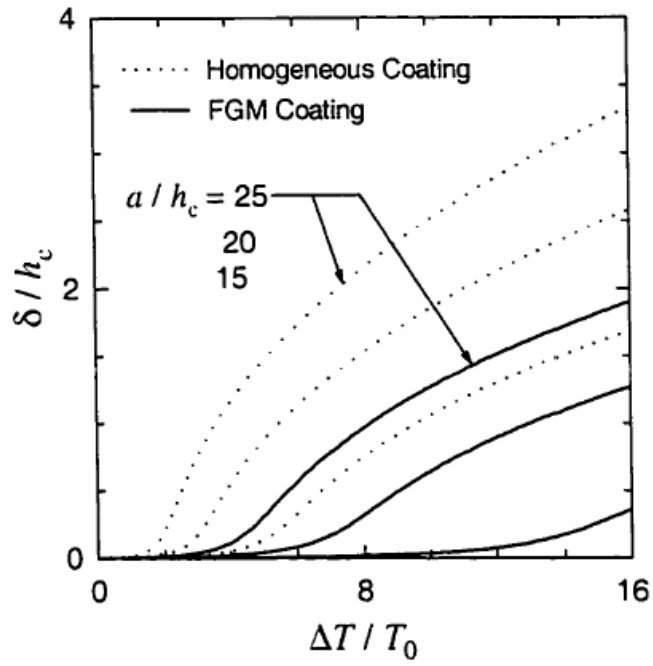


Figure 4.7 Crack opening displacement at the center of the crack vs. temperature drop in FGM and homogeneous coatings, $T_0=100\text{K}$, (Chiu (1999)).

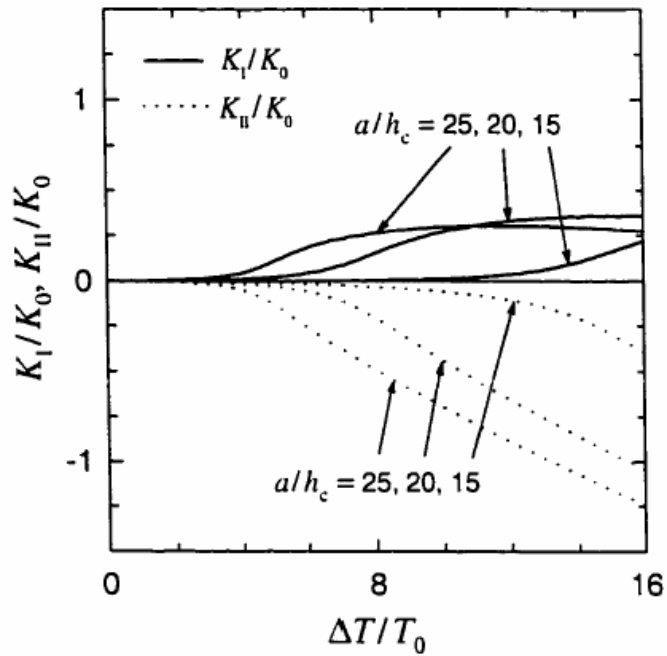


Figure 4.8 Normalized stress intensity factors for FGM coating as a function of temperature drop, $T_0=100\text{K}$, (Chiu (1999)).

CHAPTER 5

RESULTS and DISCUSSION

5.1 Introduction

This chapter examines the solution of the nonlinear buckling problem and determination of SIF and energy release rate values by displacement correlation technique. Details of numerical procedure used in the calculation of fracture mechanics parameters are given in Chapter 2. The results of interest are steady state temperature distribution, mode I and II stress intensity factors and energy release rate. The effect of geometric parameters and material properties on fracture mechanics parameters will be given in sections 5.2 and 5.3. In the first problem, crack is at the bond coat FGM coating interface and the variables are crack length and material properties. In the second case position of the crack is changing in FGM coating for a given crack length. The geometry of the problems and results are given in the following sections.

5.2 The Interface Crack Problem

5.2.1 Geometry of the Problem

The geometry of the orthotropic FGM coating bonded to isotropic substrate containing an interface crack is shown in Figure 5.1. The thickness of the orthotropic FGM coating, bond coat layer and isotropic substrate are taken as h_1 , h_2 , h_3 . The crack lying at the coating and bond coat interface has a length of $2a$. the length of the specimen is $2L$ and crack lies at the center of the specimen. Relation between these dimensions are given as

$$h_1/h_2 = 2, \quad h_3/h_2 = 10, \quad L = 8a. \quad (5.1)$$

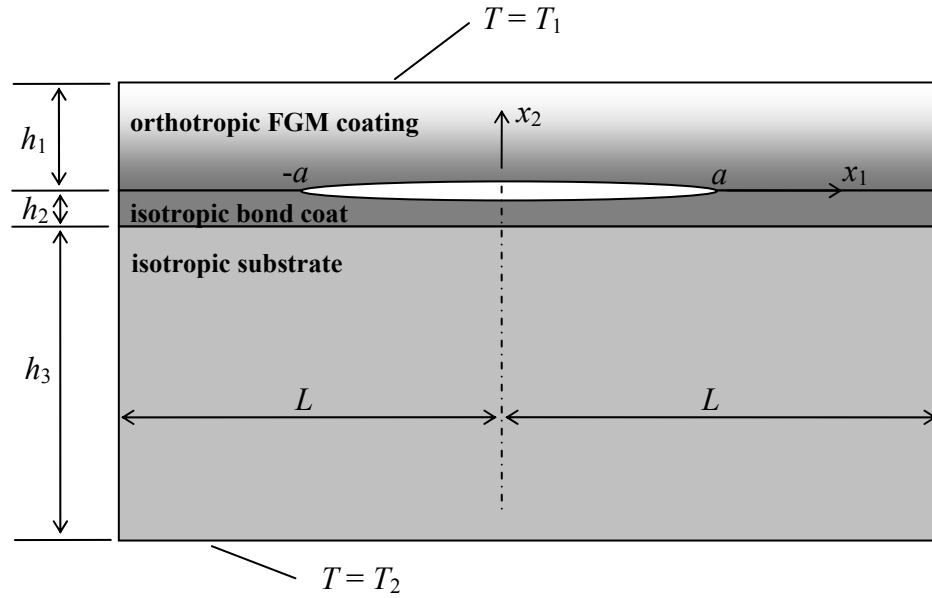


Figure 5.1 The geometry of interface crack the problem.

5.2.2 Boundary Conditions

In interface crack problem buckling occurs in case of thermal gradient. The upper surface of the coating, $x_2 = h_1$ is at temperature T_1 and the lower surface of the substrate, $x_2 = -(h_2 + h_3)$ is at T_2 . A reference temperature introduced, T_0 and it is set as temperature of substrate, T_2 . For a given temperature difference ΔT between the top and bottom surfaces, heat conduction occurs between coating and substrate surfaces. The relation between these temperatures are given as

$$T_{\text{reference}} = T_0 = 293 \text{ K},$$

$$T_2 = T_0,$$

$$T_1 = 1273 \text{ K},$$

$$\Delta T_{\text{max}} = T_1 - T_2 = 980 \text{ K}, \quad (5.2)$$

The solution is done by nonlinear analysis with gradually increasing loads. For thermal solution these load increments can be considered as changes in temperature difference between the top and bottom surfaces. In finite element model 250 time

steps are defined and plots of stress intensity factors and energy release rate are generated by using results calculated at each time step.

Since the problem is symmetric about the x_2 axis, half of the problem is modeled in finite element model. The x_2 axis is symmetry axis and the lateral surfaces are taken as thermally insulated.

5.2.3 Material Properties

For an orthotropic material compliance tensor has 9 independent parameters which determine the stress-strain relation for a given material. The material properties, modulus of elasticity, Poisson's ratio and shear modulus, used in the calculation of these parameters are given for the orthotropic ceramic coating. In addition to these structural properties thermal properties are also given for ceramic, bond coat and substrate materials. Since there is heat transfer from substrate to ceramic layer, conductivity and thermal expansion coefficients are included in the model.

Material properties are given below for orthotropic coating, bond coat and isotropic substrate. The superscripts cr , bc and s stands for the ceramic, bond coat and substrate. Since the problem is 2D, material properties in z direction are not given. Although these parameters have no effect on finite element results, in APDL program they are set equal to the material properties given in x direction.

- FGM Coating

$$\begin{aligned}
 E_1(x_2) &= E^{bc} + (E_1^{cr} - E^{bc})(x_2/h_1)^{\gamma_1}, \\
 E_2(x_2) &= E^{bc} + (E_2^{cr} - E^{bc})(x_2/h_1)^{\gamma_2}, \\
 \nu_{21}(x_2) &= \nu^{bc} + (\nu_{21}^{cr} - \nu^{bc})(x_2/h_1)^{\beta_{21}}, \\
 \nu_{23}(x_2) &= \nu^{bc} + (\nu_{23}^{cr} - \nu^{bc})(x_2/h_1)^{\beta_{23}}, \\
 \nu_{32}(x_2) &= \nu^{bc} + (\nu_{32}^{cr} - \nu^{bc})(x_2/h_1)^{\beta_{32}}, \\
 \nu_{31}(x_2) &= \nu^{bc} + (\nu_{31}^{cr} - \nu^{bc})(x_2/h_1)^{\beta_{31}}, \\
 G_{12}(x_2) &= G^{bc} + (G_{12}^{cr} - G^{bc})(x_2/h_1)^{\gamma_{12}},
 \end{aligned}$$

$$\begin{aligned}
\alpha_1(x_2) &= \alpha^{bc} + (\alpha_1^{cr} - \alpha^{bc})(x_2/h_1)^{\delta_1}, \\
\alpha_2(x_2) &= \alpha^{bc} + (\alpha_2^{cr} - \alpha^{bc})(x_2/h_1)^{\delta_2}, \\
\alpha_3(x_2) &= \alpha^{bc} + (\alpha_3^{cr} - \alpha^{bc})(x_2/h_1)^{\delta_3}, \\
k_1(x_2) &= k^{bc} + (k_1^{cr} - k^{bc})(x_2/h_1)^{\omega_1}, \\
k_2(x_2) &= k^{bc} + (k_2^{cr} - k^{bc})(x_2/h_1)^{\omega_2}.
\end{aligned} \tag{5.3}$$

Material property variations related to the position are given above and are assumed to be function of x_2 . The variation in FGM is an exponential variation and exponents γ , β , δ and ω are changing in this problem. By changing these values metal rich, (*MR*) and ceramic rich, (*CR*) compositions in FGM layer can be obtained.

The constant terms in these formulations are given as

$$\begin{aligned}
E_1^{cr} &= 90.43 \text{ GPa}, \quad E_2^{cr} = 116.36 \text{ GPa}, \quad G_{12}^{cr} = 38.21 \text{ GPa} \\
\nu_{21}^{cr} &= 0.28, \quad \nu_{23}^{cr} = 0.27, \quad \nu_{32}^{cr} = 0.21, \quad \nu_{31}^{cr} = 0.14 \\
k_1^{cr} &= 21.25 \text{ W/(mK)}, \quad k_2^{cr} = 29.82 \text{ W/(mK)} \\
\alpha_1^{cr} &= 8(10)^{-6} (\text{ }^\circ\text{C})^{-1}, \quad \alpha_2^{cr} = 7.5(10)^{-6} (\text{ }^\circ\text{C})^{-1}, \quad \alpha_3^{cr} = 9(10)^{-6} (\text{ }^\circ\text{C})^{-1}.
\end{aligned} \tag{5.4}$$

- **Bond coat**

$$\begin{aligned}
E &= E^{bc} = 137.9 \text{ GPa}, \\
\nu &= \nu^{bc} = 0.27, \\
G &= G^{bc} = E^{bc} / (2(1 + \nu^{bc})), \\
\alpha &= \alpha^{bc} = 15.16(10)^{-6} (\text{ }^\circ\text{C})^{-1}, \\
k &= k^{bc} = 25 \text{ W/(mK)}.
\end{aligned} \tag{5.5}$$

- **Substrate**

$$\begin{aligned}
E &= E^s = 175.8 \text{ GPa}, \\
\nu &= \nu^s = 0.25,
\end{aligned}$$

$$\begin{aligned}
G &= G^s = E^s / (2(1 + \nu^s)), \\
\alpha &= \alpha^s = 13.91(10)^{-6} (\text{°C})^{-1}, \\
k &= k^s = 7 \text{ W/(mK)}.
\end{aligned}
\tag{5.6}$$

In the finite element model material properties are defined for each element by using an APDL code. This code is developed to specify the structural and thermal properties at the centroid of each element. In the analyses, both steady state thermal problem and mechanical problem will be solved. First steady state temperature distribution between top and bottom surfaces is obtained. Then the result of thermal solution is used in the nonlinear solution. The interface crack problem is modeled for changing crack lengths and changing material properties. These variables can be listed as below

- Changing crack length, $a/h_1 = 25, 20, 15, 10, 5, 1$
- Material gradation, $CR1, CR2, MR1, MR2$

For the second case parameters of material variation are given for $CR1, CR2, MR1, MR2$ in Table 5.1

Table 5.1 Constants of material variation in orthotropic FGM.

	γ_1	γ_2	γ_{12}	β_{21}	β_{23}	β_{32}	β_{31}	δ_1	δ_2	δ_3	ω_1	ω_2
Ceramic-Rich FGM ($CR1$)	2.5	2.5	2.5	2	2	2	2	1.5	1.5	1.5	1.5	1.5
Ceramic-Rich FGM ($CR2$)	2.5	2.5	2.5	2.5	2.5	2.5	2.5	2.5	2.5	2.5	2.5	2.5
Metal-Rich FGM ($MR1$)	0.4	0.4	0.4	0.5	0.5	0.5	0.5	0.6	0.6	0.6	0.6	0.6
Metal-Rich FGM ($MR2$)	0.4	0.4	0.4	0.4	0.4	0.4	0.4	0.4	0.4	0.4	0.4	0.4

For the results which are given in Section 5.5, the normalization on temperature, K_I, K_{II} and G values will be done. The constants used in the normalization are

Normalized temperature:

$$\hat{T} = T/T_0$$

Normalized stress intensity factors:

$$\hat{K}_I = K_I/K_0, \quad \hat{K}_{II} = K_{II}/K_0, \quad \text{where } K_0 = E^s \alpha^s T_0 \sqrt{\pi h_3}$$

Normalized energy release rate:

$$\hat{G} = G/G_0, \quad \text{where } G_0 = (1-\nu_s^2)K_0^2/E_s$$

To get the whole results of this problem 24 different cases are considered and solved in ANSYS finite element software. For each problem using nodal displacement near crack zone mode I and II stress intensity factors and energy release rate values are calculated. Finite element results showing buckled crack surfaces and elements used in the crack region are given in Figures 5.2, 5.3 and 5.4. First figure shows the colored plot of FGM, bond coat and substrate system for a given crack length and material type. Dimensionless color scale shows deformation of specimen under buckling load. Variation in thermal properties causes buckling in case of temperature distribution between upper and lower surfaces. In Figure 5.3 and 5.4 deformed shape of crack region and meshes of finite element model can be seen. At the tip of the crack 48 elements are used. To increase the accuracy of the results number of elements is kept as much as possible in thickness direction.

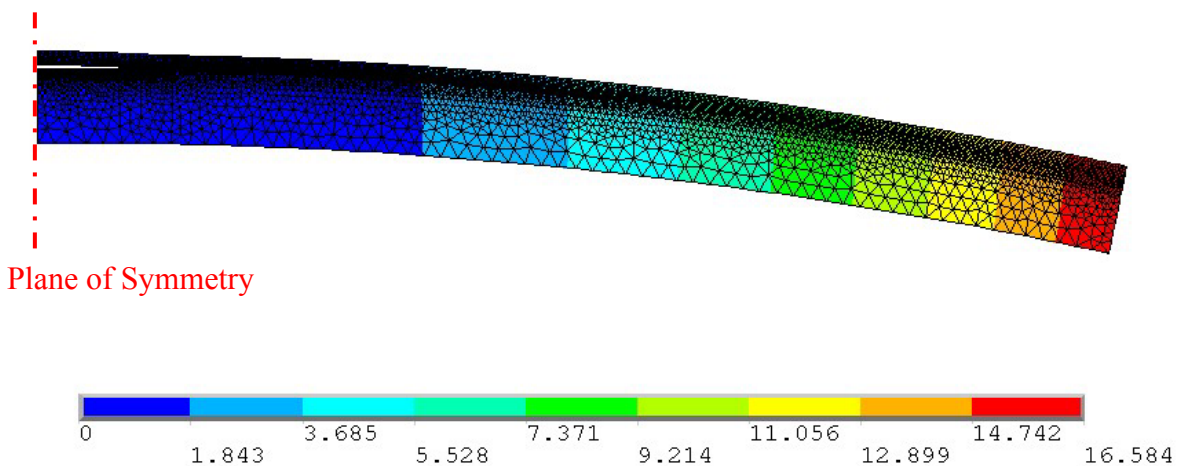


Figure 5.2 Deformed shape of the FGM, bond coat and substrate system due to temperature distribution, $a/h_1=10$ and *CR1* material.

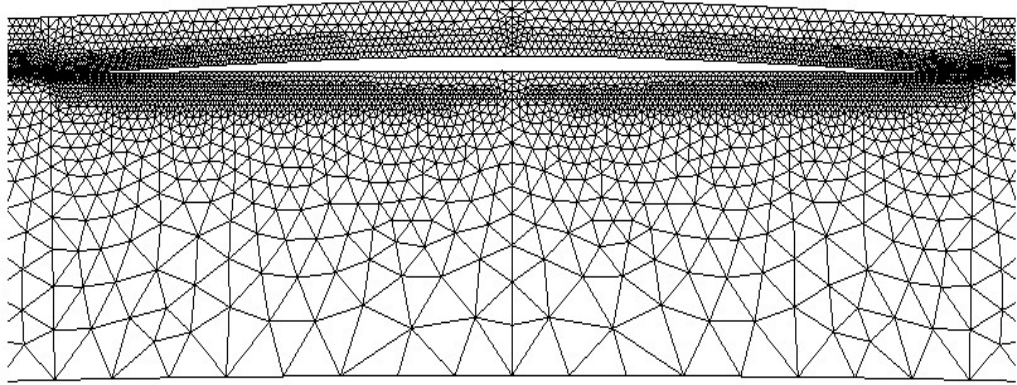


Figure 5.3 Buckled shape of the FGM layer above the crack, $a/h_1=10$ and *CR1* material.

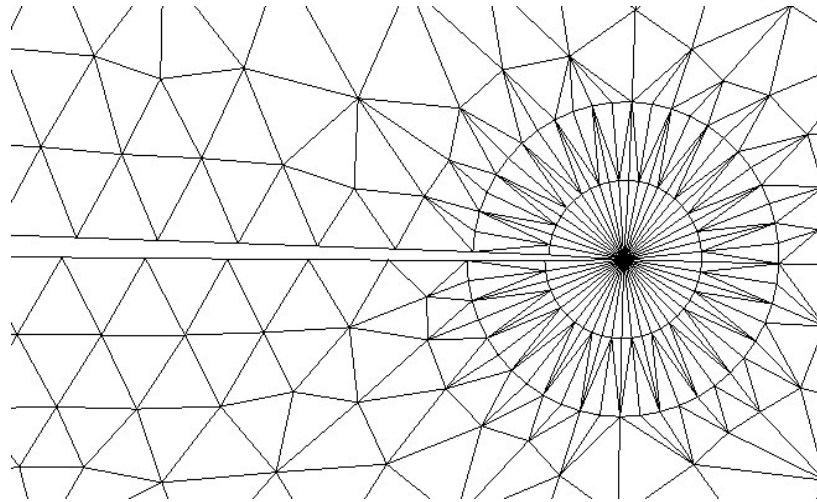


Figure 5.4 Plane2 singular elements at the crack tip.

Figures 5.8, 5.11, 5.14, 5.17, 5.20, 5.23 give the normalized mode I stress intensity factor, K_I/K_0 as a function of applied temperature difference, $\Delta T/T$ for several values of crack length a/h_1 . Normalized mode I curves of *CR1*, *CR2*, *MR1* and *MR2* material properties are shown on the same plot to see the effect of changing material properties on fracture mechanics parameters. Similarly results of normalized mode II stress intensity factors and normalized energy release rate values are given in Figures 5.9, 5.12, 5.15, 5.18, 5.21, 5.24 and 5.10, 5.13, 5.16, 5.19, 5.22, 5.25.

Second variable considered in interface crack problem is change in material properties from metal to ceramic in FGM coating layer. The normalized mode I and II stress intensity factors and energy release rate values are computed for the ceramic rich (*CR1* and *CR2*) and metal rich (*MR1* and *MR2*) coatings for various crack dimensions. In the solution of the problem same boundary conditions are considered. Figures 5.26, 5.29, 5.32, 5.35 give the normalized mode I stress intensity factor, K_I/K_0 for changing material properties. In these plots results of different crack lengths are shown on the same plot to make comparison of effect of crack length on buckling. Result of normalized mode II stress intensity factors and normalized energy release rate values are given in Figures 5.27, 5.30, 5.33, 5.36 and 5.28, 5.31, 5.34, 5.37.

5.3 The Internal Crack Problem

The problem considered here is the change in the position of the crack in FGM coating layer and effect of this change on fracture mechanics parameters. The height of internal crack is defined as h_4 . Similar to the previous problem same geometry is used. The thickness of the orthotropic FGM coating, bond coat layer and isotropic substrate are taken as h_1, h_2, h_3 . The relations between these dimensions are given as

$$h_1/h_2 = 2, \quad h_3/h_2 = 10, \quad 0 \leq h_4 \leq h_1, \quad L = 8a. \quad (5.7)$$

Same boundary conditions are applied as in the interface crack problem. The upper surface is at a temperature T_1 and lower surface of the substrate is at T_2 . Lateral surfaces are taken thermally insulated. Under these boundary conditions buckling occurs as a result of thermal gradient. The material properties, modulus of elasticity, Poisson's ratio, shear modulus, coefficient of thermal expansion and conductivity are the same as previous cases for substrate, bond coat and FGM coating.

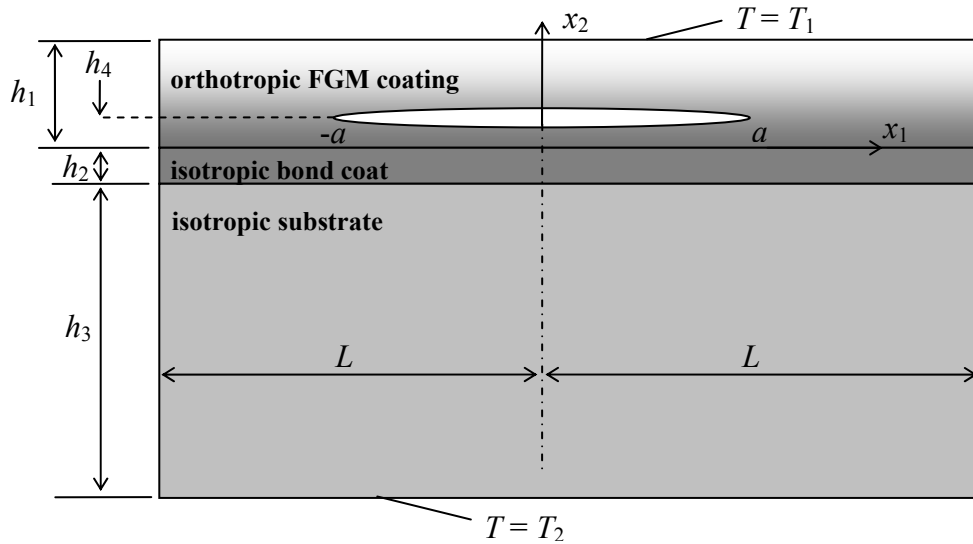


Figure 5.5 The geometry of the internal crack problem.

In the solution of the problem crack length is chosen constant, $a/h_1=20$. The variables of the problem are changing material properties and height of the crack. 5 different crack positions are considered in the solution. These are $h_4/h_1=0.00, 0.10, 0.25, 0.50$ and 0.75 . Figures 5.38, 5.41, 5.44, 5.47 give the normalized mode I stress intensity factors as a function of changing temperature, $\Delta T/T$ for changing crack heights. Similarly the results of normalized mode II stress intensity factors, K_{II}/K_0 and normalized energy release rate values, G/G_0 are given in Figures 5.39, 5.42, 5.45, 5.48 and 5.40, 5.43, 5.46, 5.49. ($\Delta T/T = 3.34$)

5.4 Steady State Temperature Distribution

In this section the distribution of temperature between upper surface and lower surface of the specimen is investigated. The upper surface of the system has a temperature $T_1=1273\text{K}$ and lower surface has a temperature $T_2=293\text{K}$.

The existence of crack between FGM coating and bond coat layer disturbs the one dimensional temperature distribution in the specimen and the problem becomes one of two dimensional heat conduction in graded FGM layer. The thermal conductivities of FGM layer are changing exponentially in thickness direction and bond coat and

substrate layer have constant thermal conductivities. The crack surfaces are taken as insulated. With the help of increased number of elements in thickness direction, the thermal conductivity variation is modeled in finite element software and 2D thermal conduction problem is solved. The variation of temperature between two surfaces near crack region is given in Figure 5.6. The temperature distribution near the ends ($x_1 = \pm L$) is shown in Figure 5.7

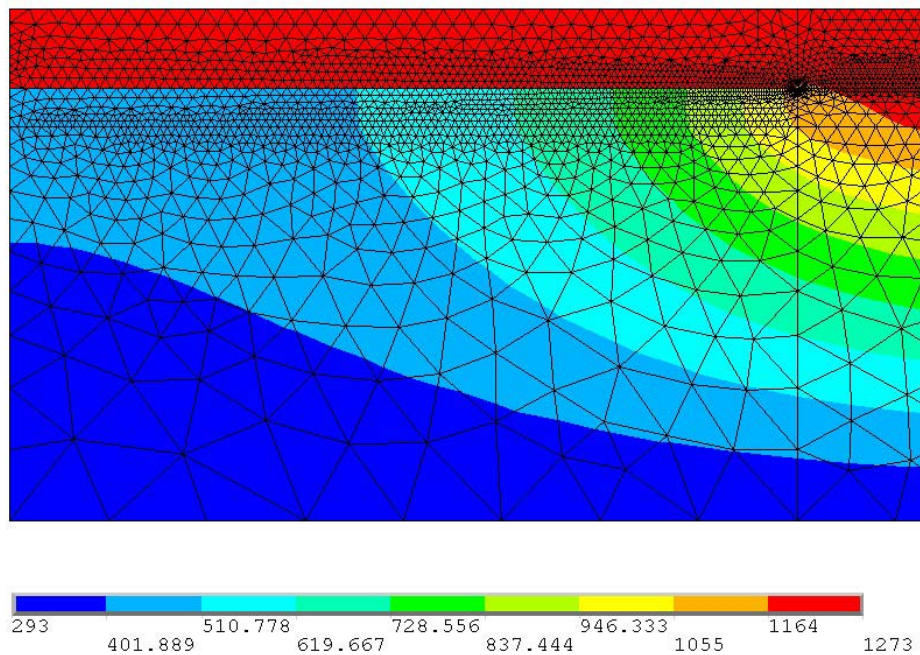


Figure 5.6 Distribution of temperature between upper surface of crack and lower surface of crack.

The temperature variations on the upper and lower crack surfaces are given in Figures 5.50-5.54. In all of these figures the curves that are concave downward are the temperatures of upper surfaces of crack and the figures concave upward are the temperatures of the lower crack surface. In Figure 5.50 the effect of material nonhomogeneity on crack surface temperature as a function of position, x_1/a for changing crack lengths are given. In this plot the curves of upper surface temperature merges with lower surface temperature curve at a point on $x_1=a$ line. For the upper surface of crack temperature is same for all crack lengths. However for the lower

surface of the crack, as the length of crack increases, the temperature difference between crack surfaces are increasing. A similar plot for changing material properties are given in Figure 5.51. It is seen that, all the curves overlap and the change in thermal conductivities given in this problem has practically no effect on crack surface temperatures.

In interface crack problem and internal crack problems the cause of buckling is the difference of temperatures on upper and lower surfaces. The temperature variations across the thickness at $x_1=L$ and at $x_1=0$ are shown in Figures 5.52 and 5.53, respectively. In these plots, continuous variation of temperature at $x_1=L$ and sudden change in temperature at the crack along the line $x_1=0$ can be seen.

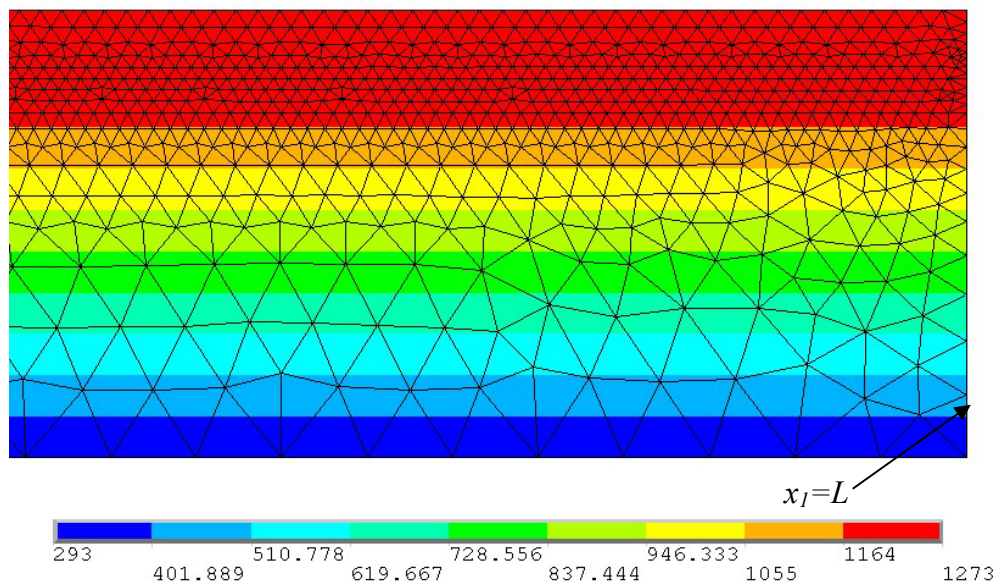


Figure 5.7 Variation of temperature at the end of the specimen, $x_1=L$.

In internal crack problem different locations of cracks are considered such as, $h_4/h_1=0.00, 0.10, 0.25, 0.50$ and 0.75 . The effect of crack location on temperature distribution with respect to position, x_1/a is given in Figure 5.54. It is found that, as crack location gets closer to the upper surface, (h_4/h_1 increases) temperatures of lower surface are increasing.

5.5 Figures

Results of mode I and mode II stress intensity factors and energy release rate will be given in Figures 5.8-5.25 for changing crack lengths.

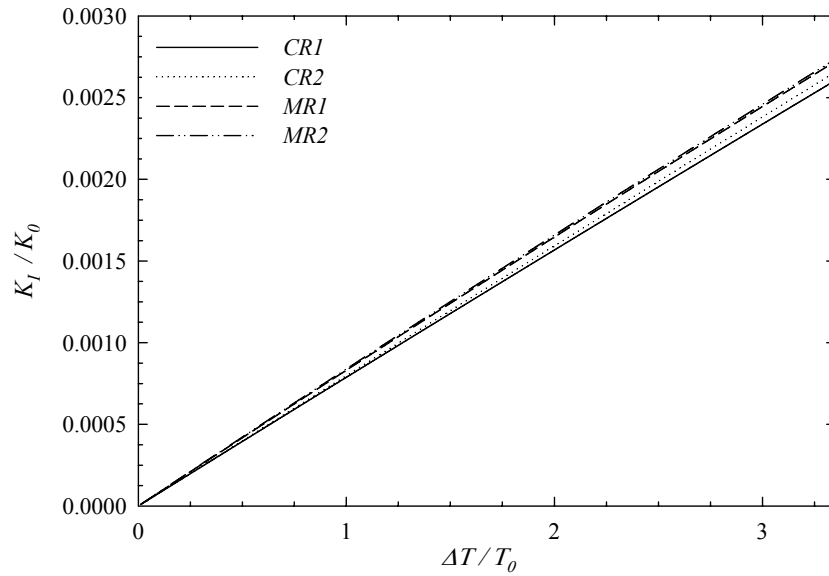


Figure 5.8 Normalized mode I stress intensity factors for crack at the bond coat – FGM interface, $a/h_I=1$

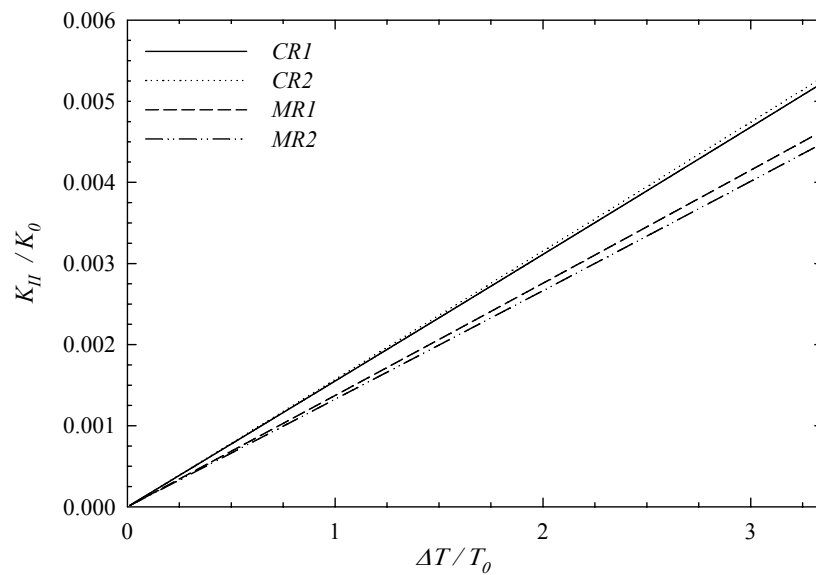


Figure 5.9 Normalized mode II stress intensity factors for crack at the bond coat – FGM interface, $a/h_I=1$

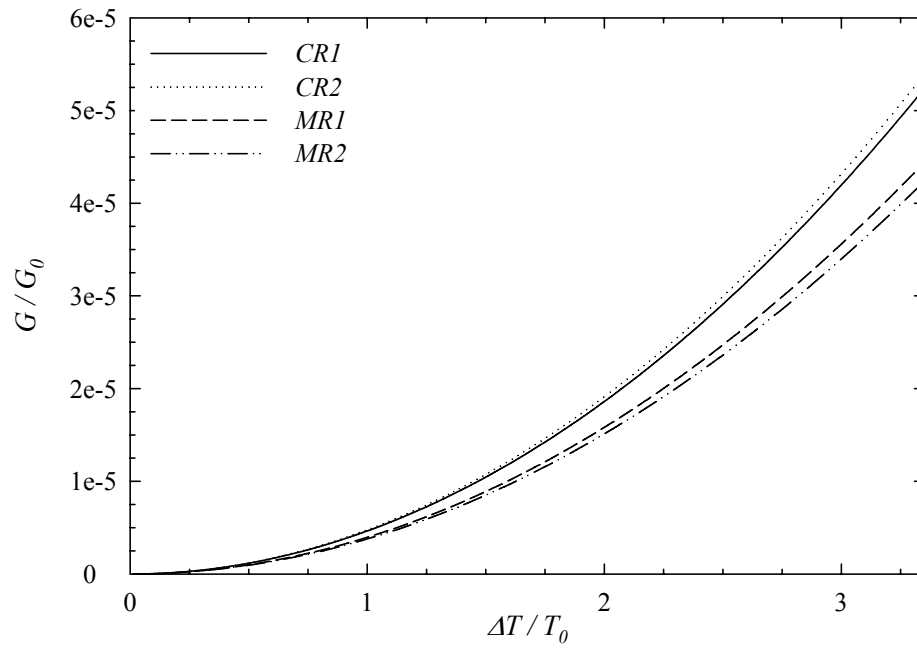


Figure 5.10 Normalized energy release rate values for crack at the bond coat – FGM interface, $a/h_I=1$

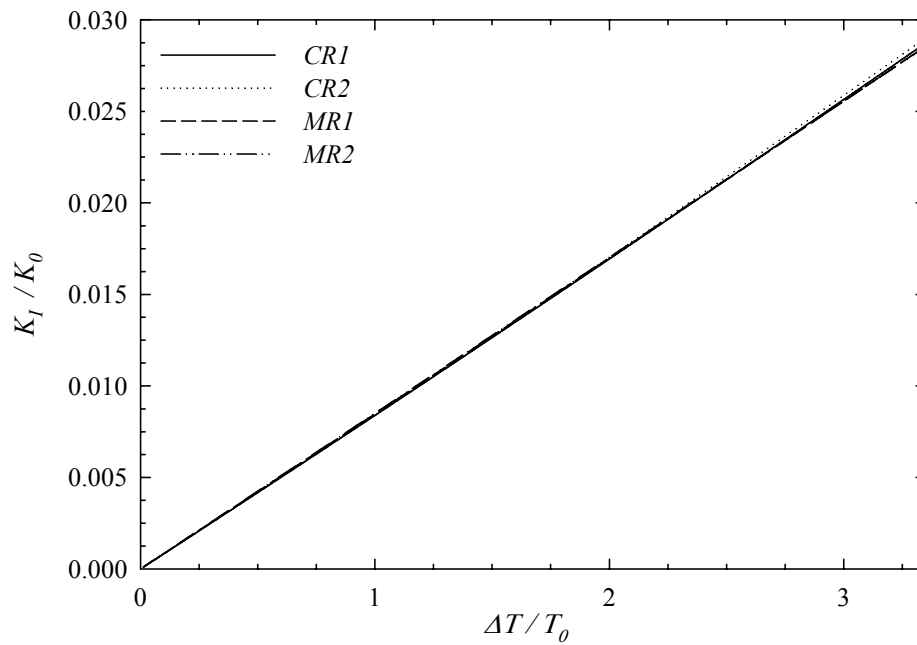


Figure 5.11 Normalized mode I stress intensity factors for crack at the bond coat – FGM interface, $a/h_I=5$

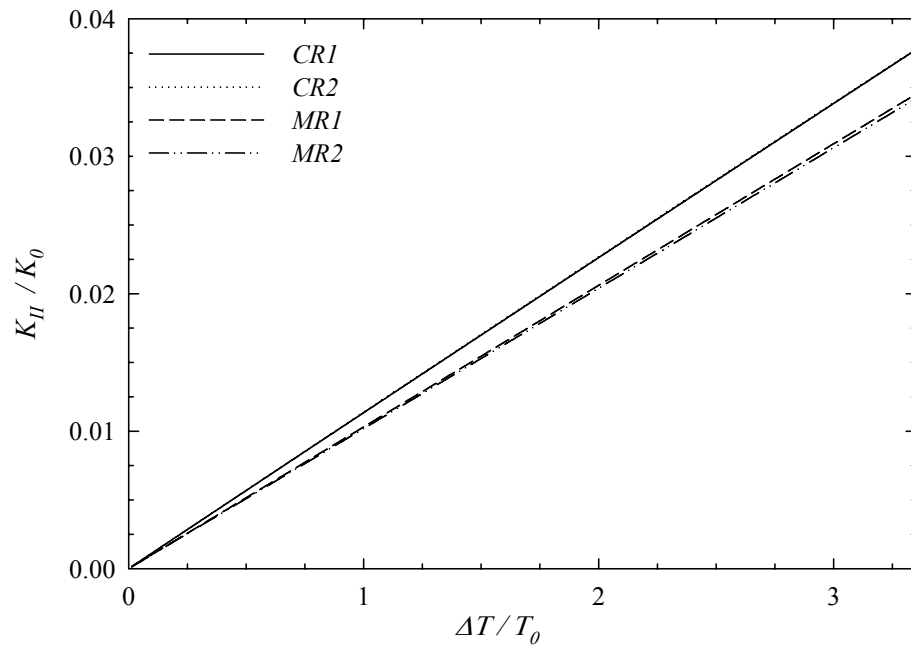


Figure 5.12 Normalized mode II stress intensity factors for crack at the bond coat – FGM interface, $a/h_I=5$

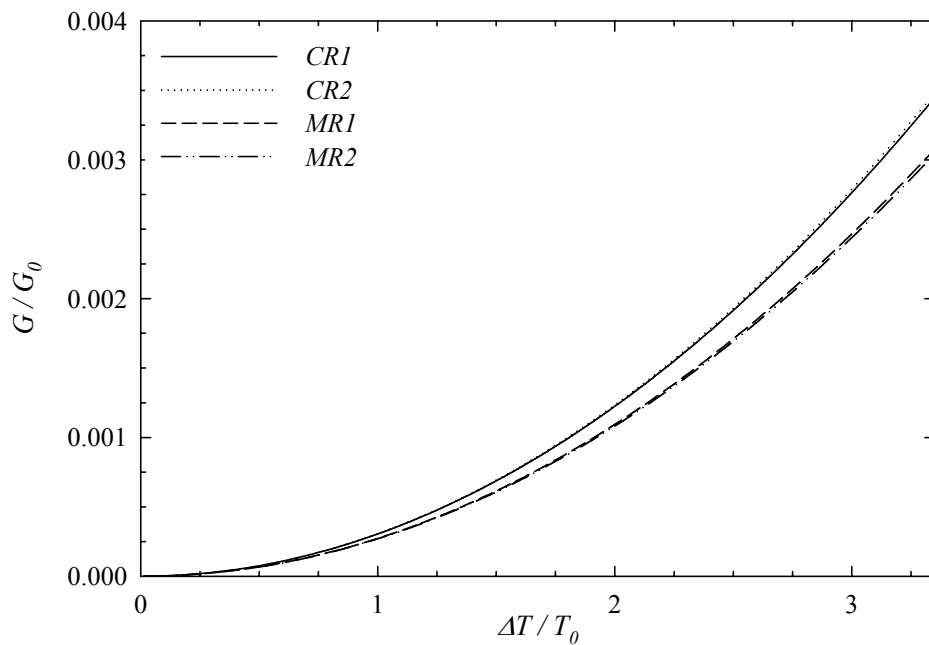


Figure 5.13 Normalized energy release rate values for crack at the bond coat – FGM interface, $a/h_I=5$

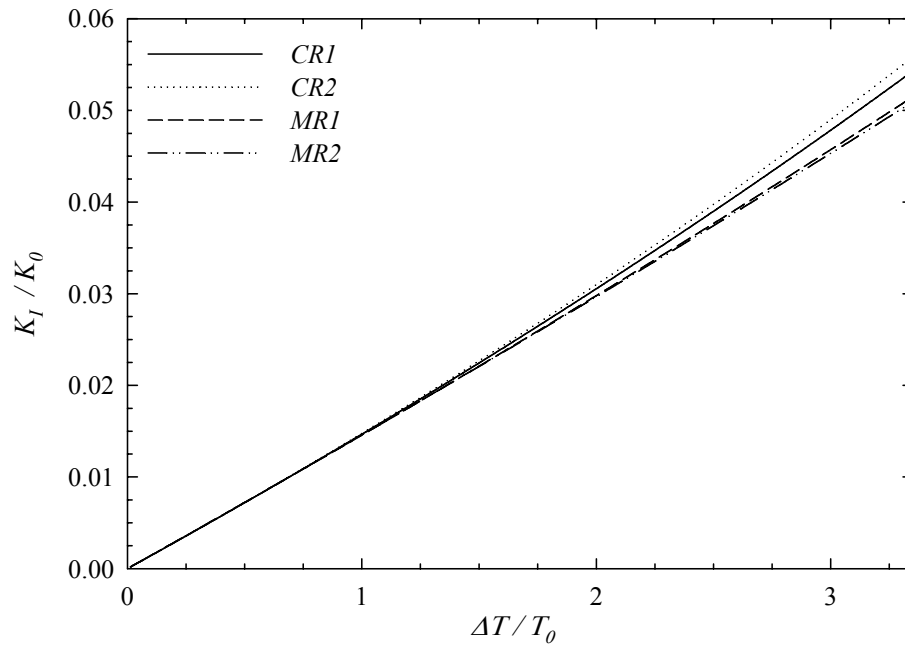


Figure 5.14 Normalized mode I stress intensity factors for crack at the bond coat – FGM interface, $a/h_I=10$

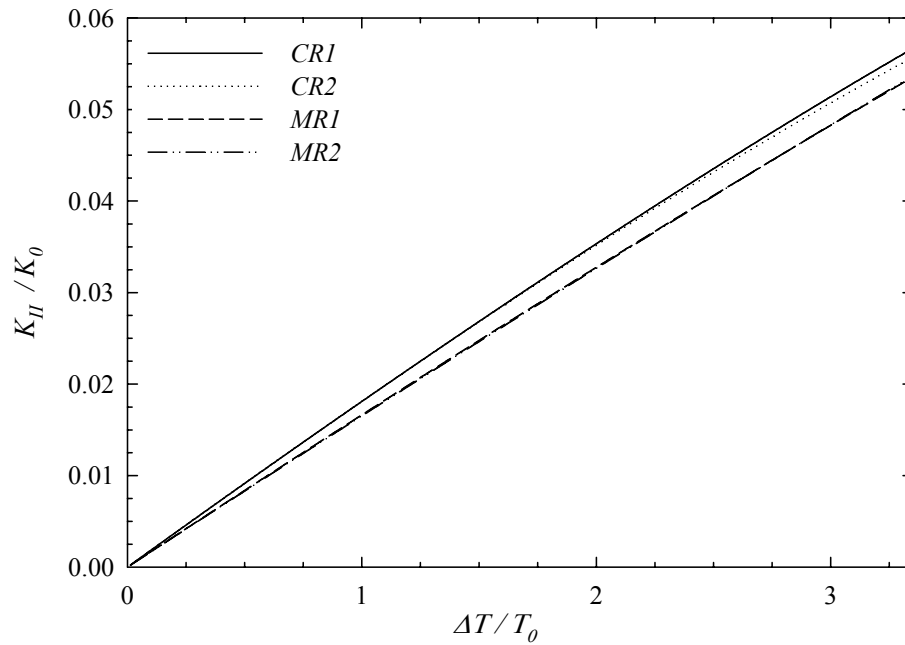


Figure 5.15 Normalized mode II stress intensity factors for crack at the bond coat – FGM interface, $a/h_I=10$

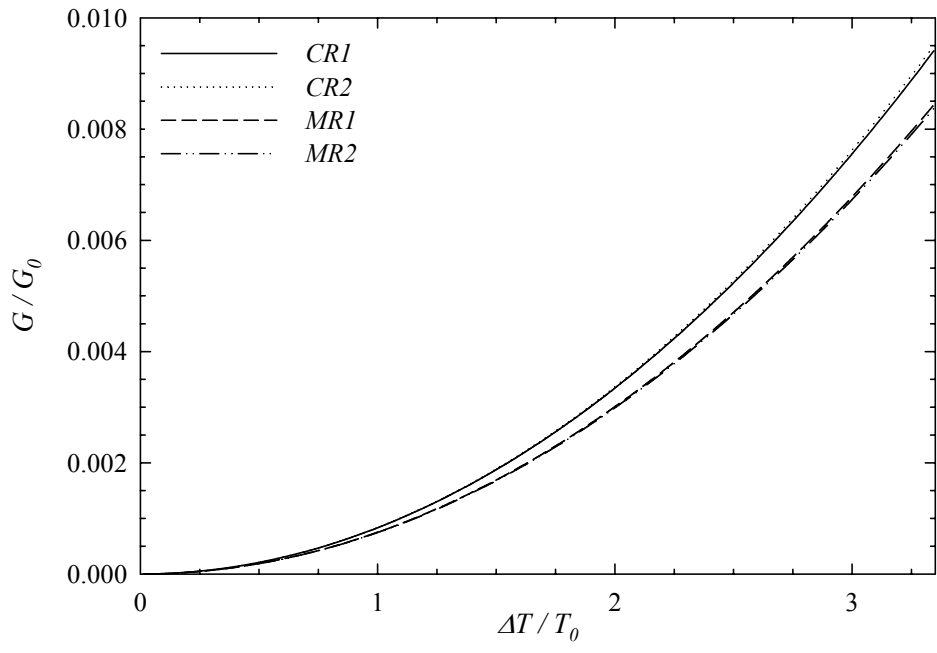


Figure 5.16 Normalized energy release rate values for crack at the bond coat – FGM interface, $a/h_I=10$

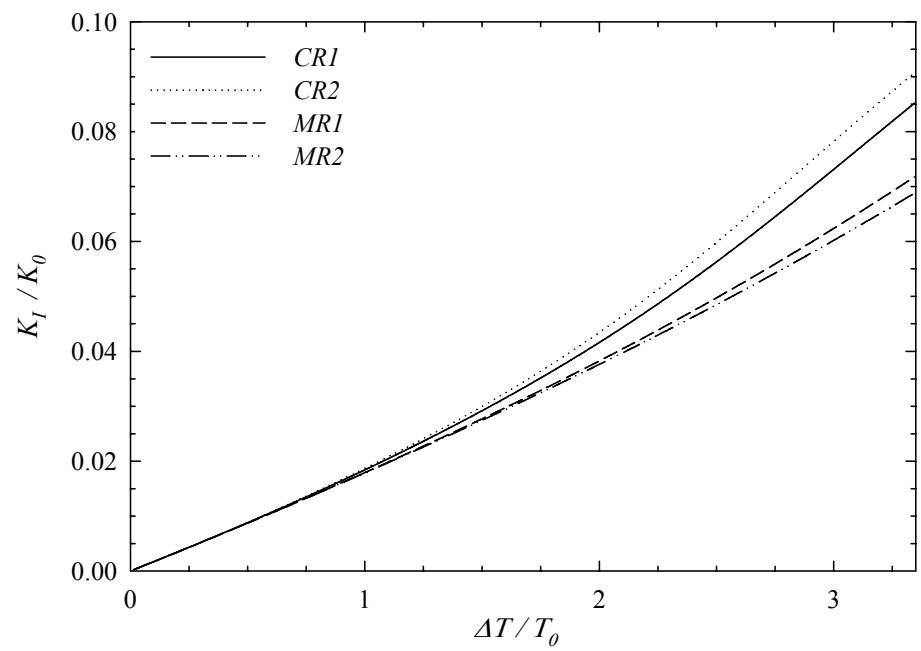


Figure 5.17 Normalized mode I stress intensity factors for crack at the bond coat – FGM interface, $a/h_I=15$

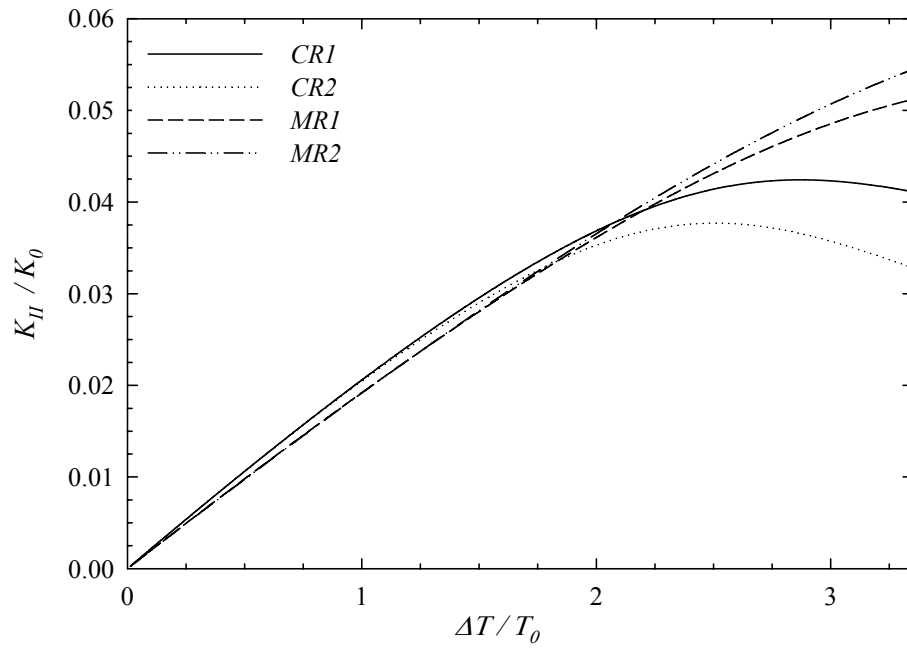


Figure 5.18 Normalized mode II stress intensity factors for crack at the bond coat – FGM interface, $a/h_f=15$

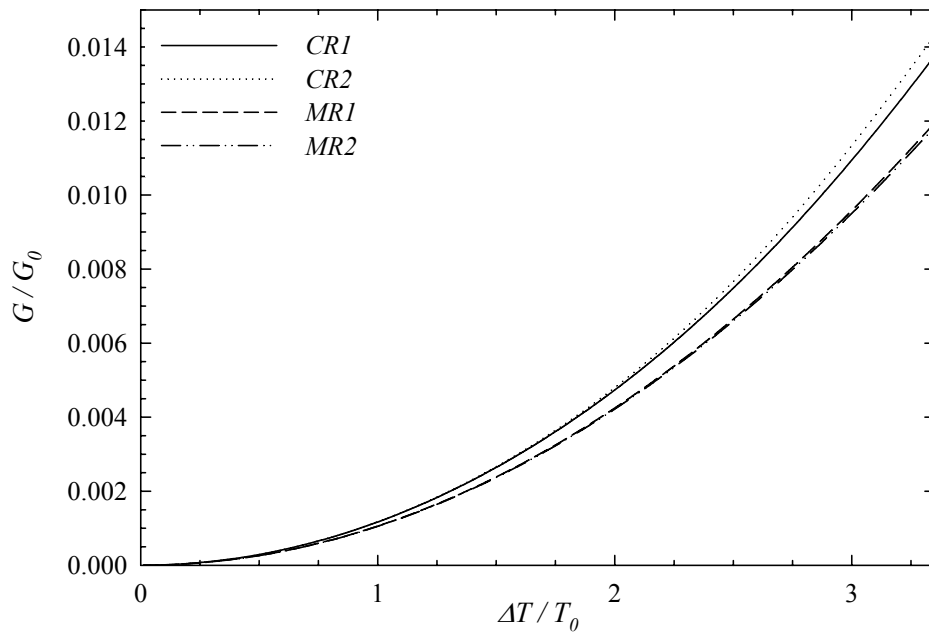


Figure 5.19 Normalized energy release rate values for crack at the bond coat – FGM interface, $a/h_f=15$

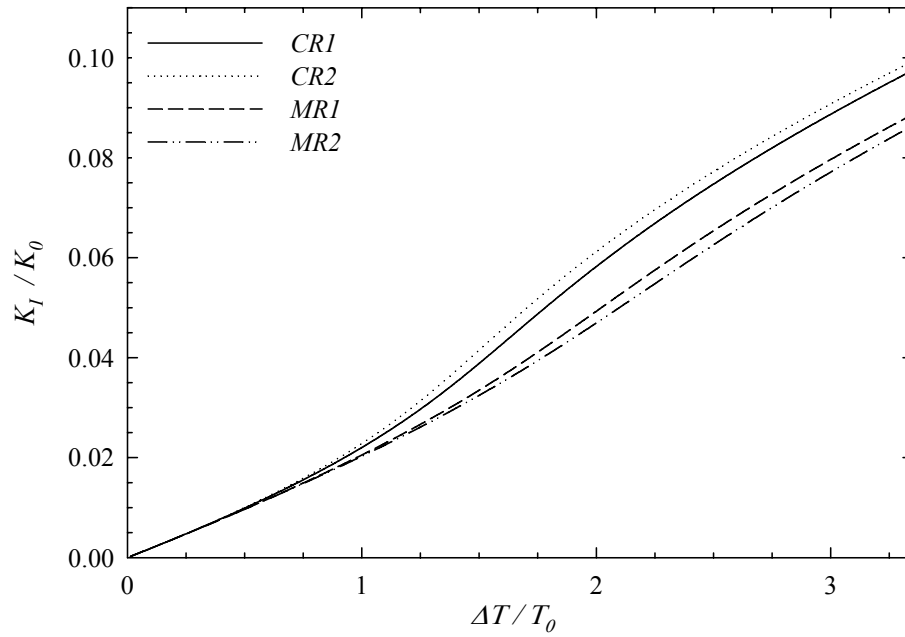


Figure 5.20 Normalized mode I stress intensity factors for crack at the bond coat – FGM interface, $a/h_I=20$

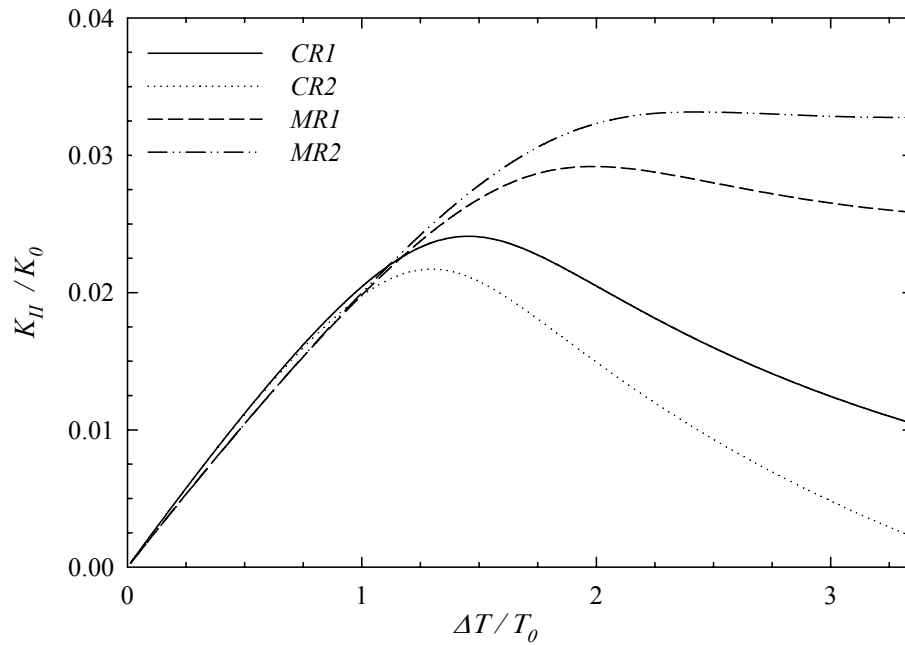


Figure 5.21 Normalized mode II stress intensity factors for crack at the bond coat – FGM interface, $a/h_I=20$

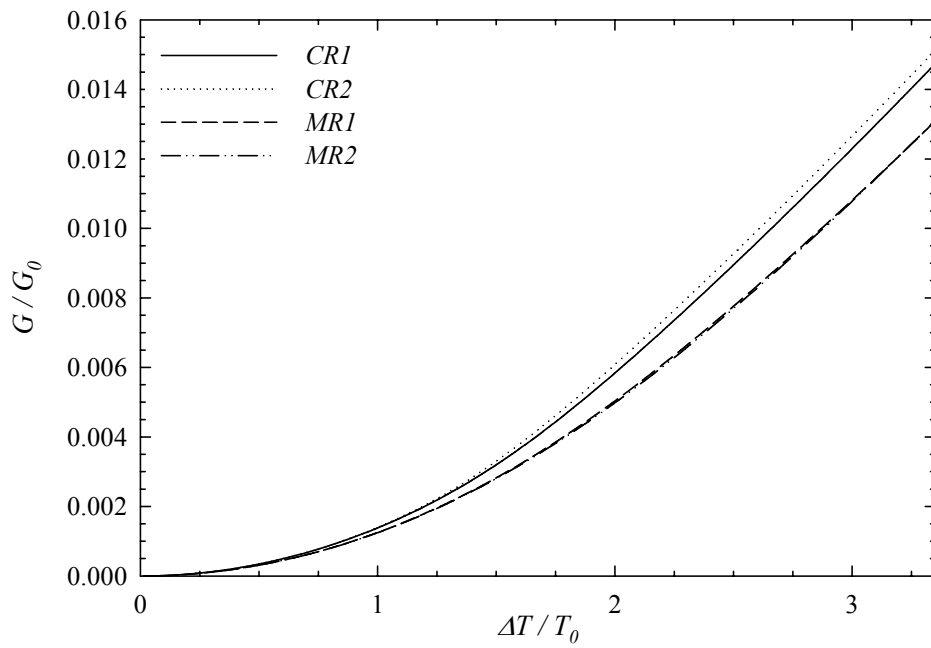


Figure 5.22 Normalized energy release rate values for crack at the bond coat – FGM interface, $a/h_I=20$

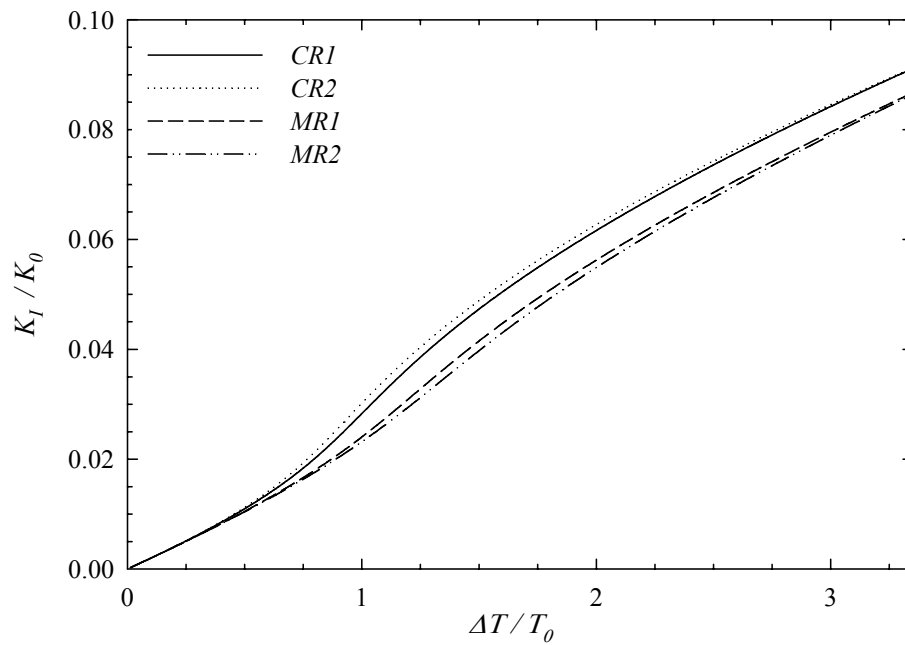


Figure 5.23 Normalized mode I stress intensity factors for crack at the bond coat – FGM interface, $a/h_I=25$

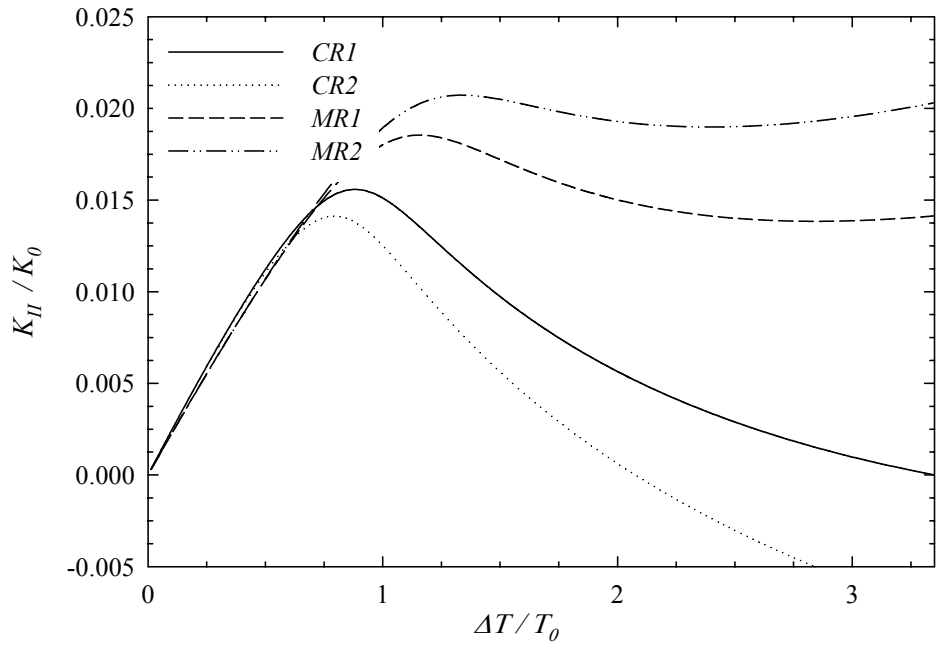


Figure 5.24 Normalized mode II stress intensity factors for crack at the bond coat – FGM interface, $a/h_I=25$

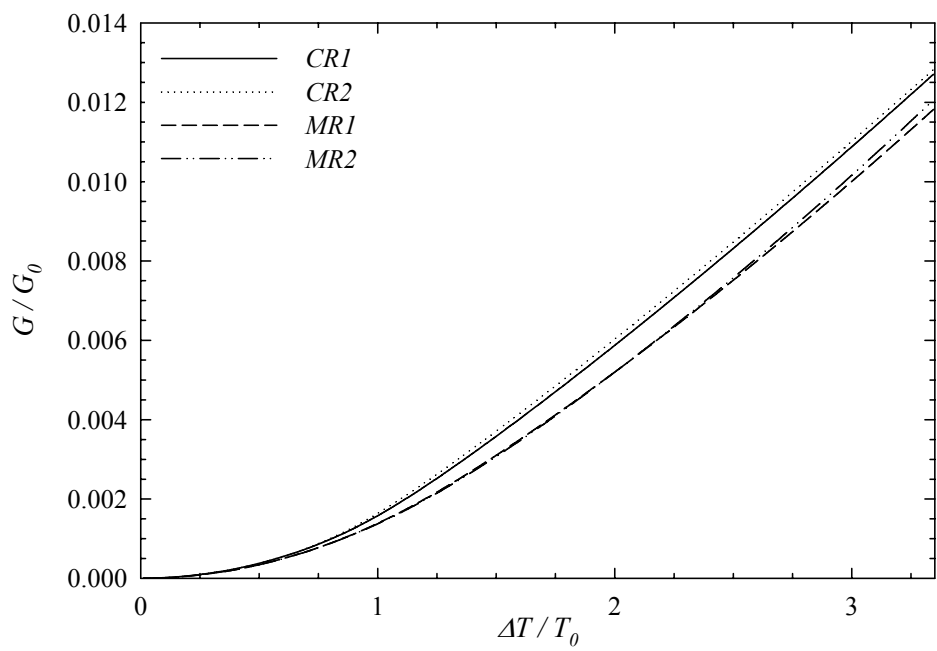


Figure 5.25 Normalized energy release rate values for crack at the bond coat – FGM interface, $a/h_I=25$

Results of mode I and mode II stress intensity factors and energy release rate will be given in Figures 5.25-5.37 for different types of material properties.

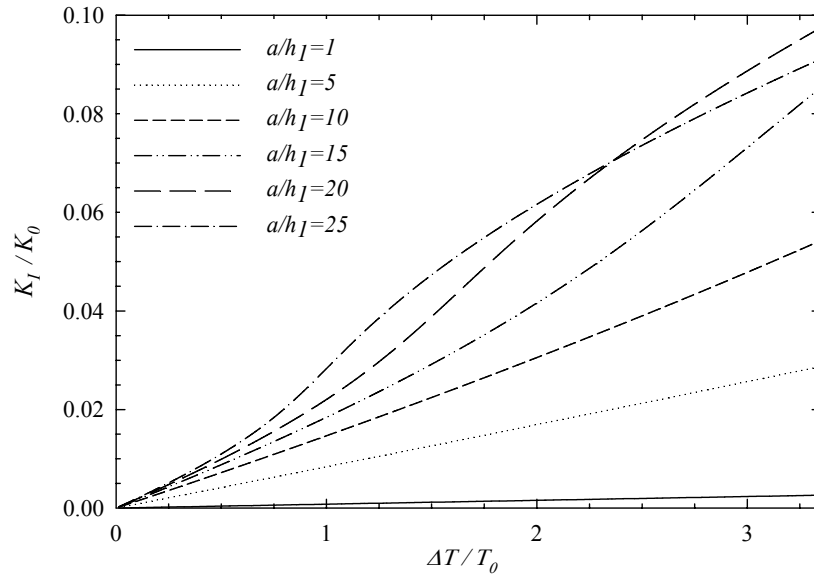


Figure 5.26 Normalized mode I stress intensity factors for crack at the bond coat – FGM interface, *CRI* material properties for FGM

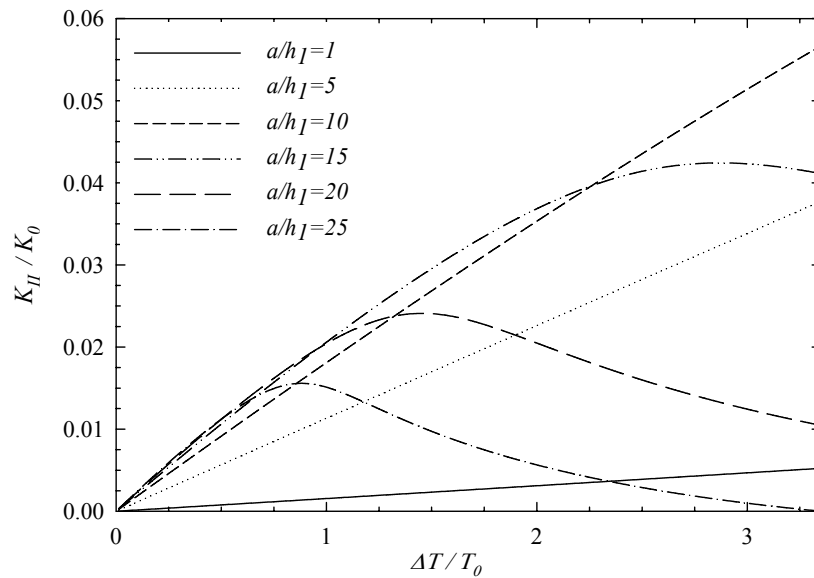


Figure 5.27 Normalized mode II stress intensity factors for crack at the bond coat – FGM interface, *CRI* material properties for FGM

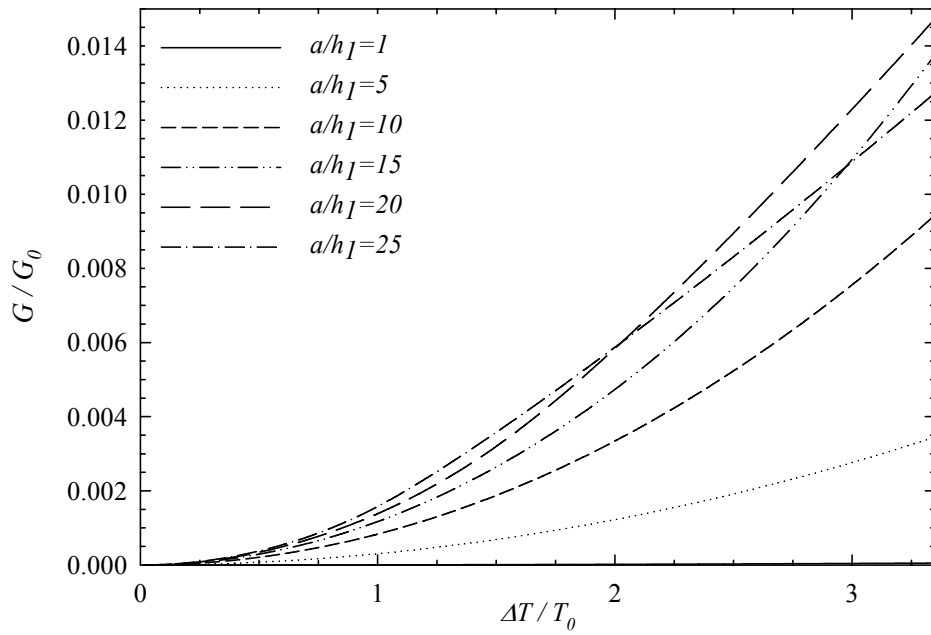


Figure 5.28 Normalized energy release rate values for crack at the bond coat – FGM interface, *CR1* material properties for FGM

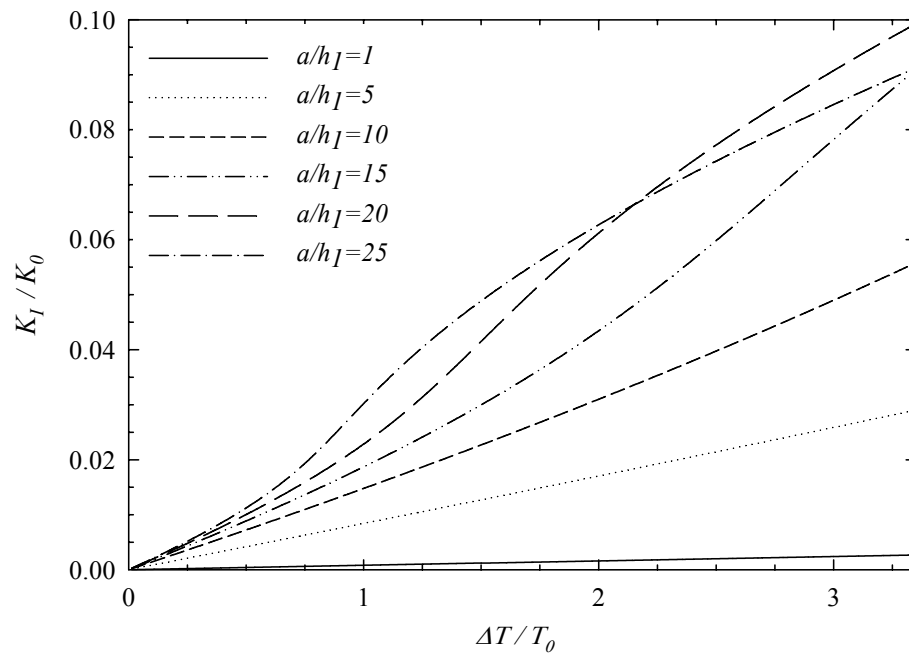


Figure 5.29 Normalized mode I stress intensity factors for crack at the bond coat – FGM interface, *CR2* material properties for FGM

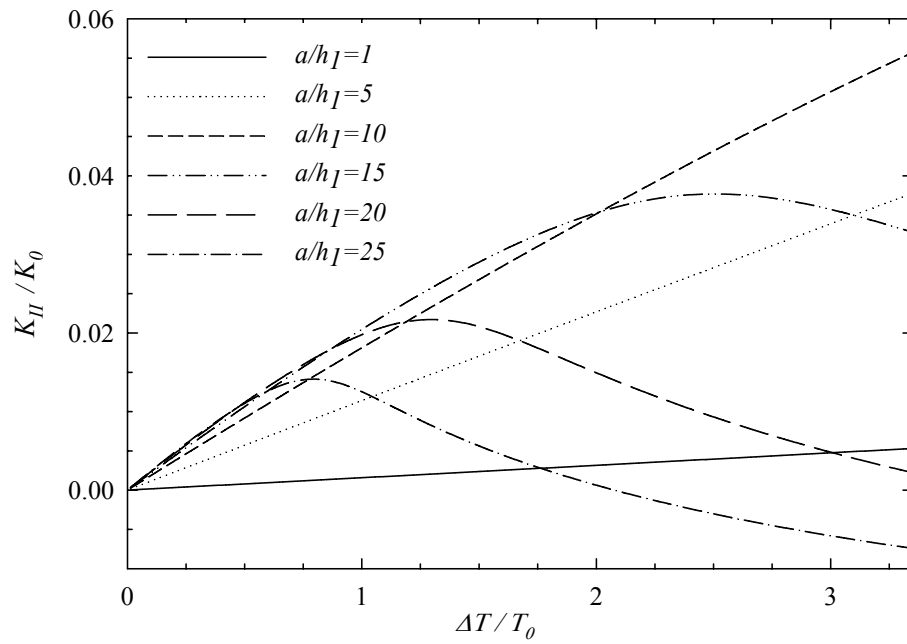


Figure 5.30 Normalized mode II stress intensity factors for crack at the bond coat – FGM interface, CR2 material properties for FGM

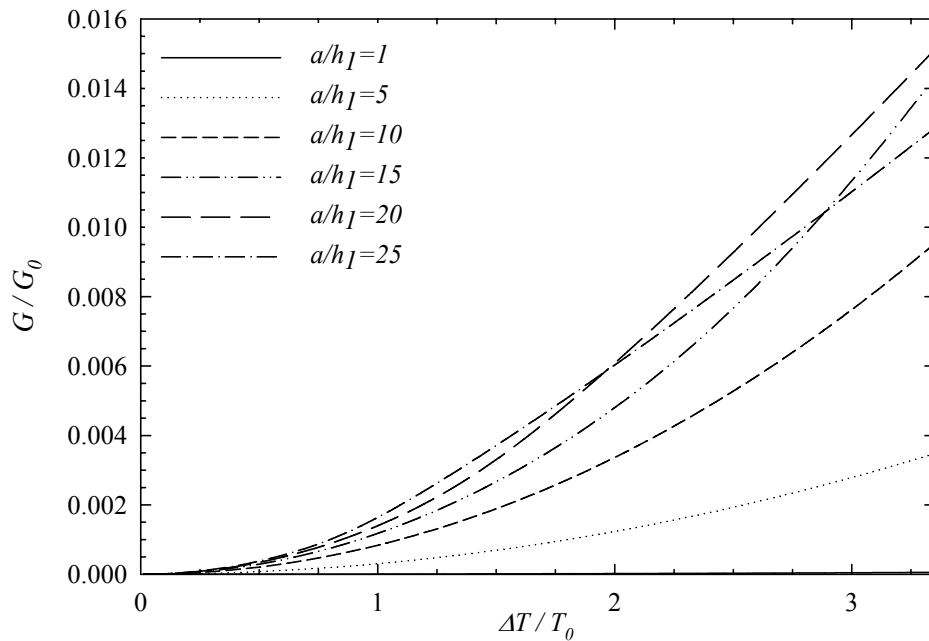


Figure 5.31 Normalized energy release rate values for crack at the bond coat – FGM interface, CR2 material properties for FGM

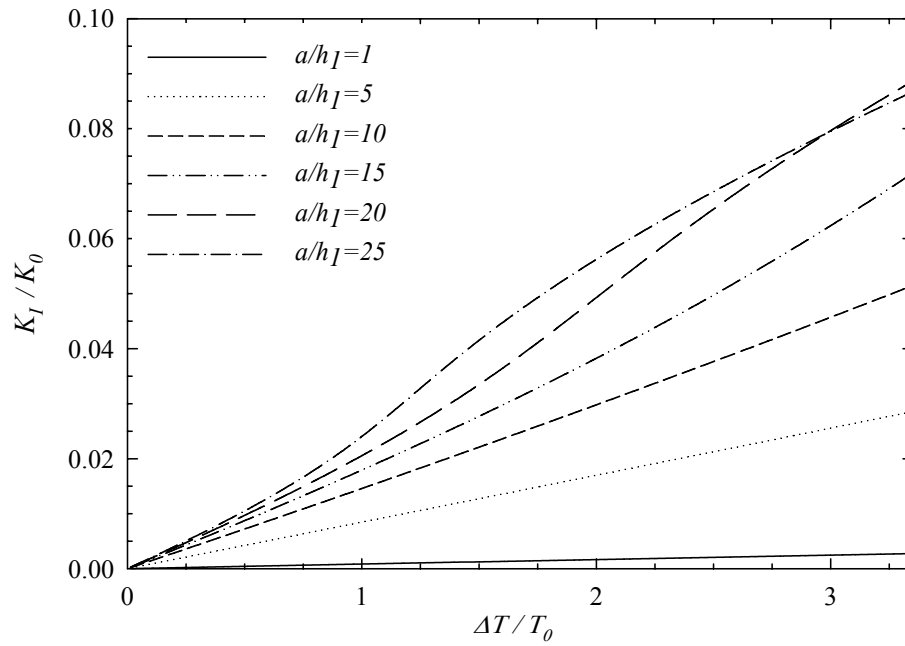


Figure 5.32 Normalized mode I stress intensity factors for crack at the bond coat – FGM interface, *MRI* material properties for FGM

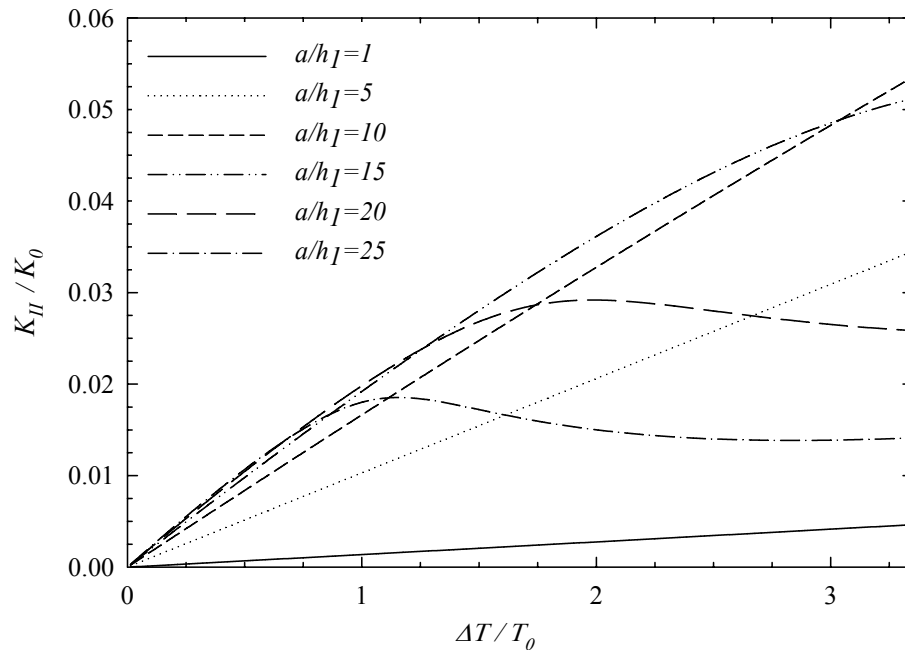


Figure 5.33 Normalized mode II stress intensity factors for crack at the bond coat – FGM interface, *MRI* material properties for FGM

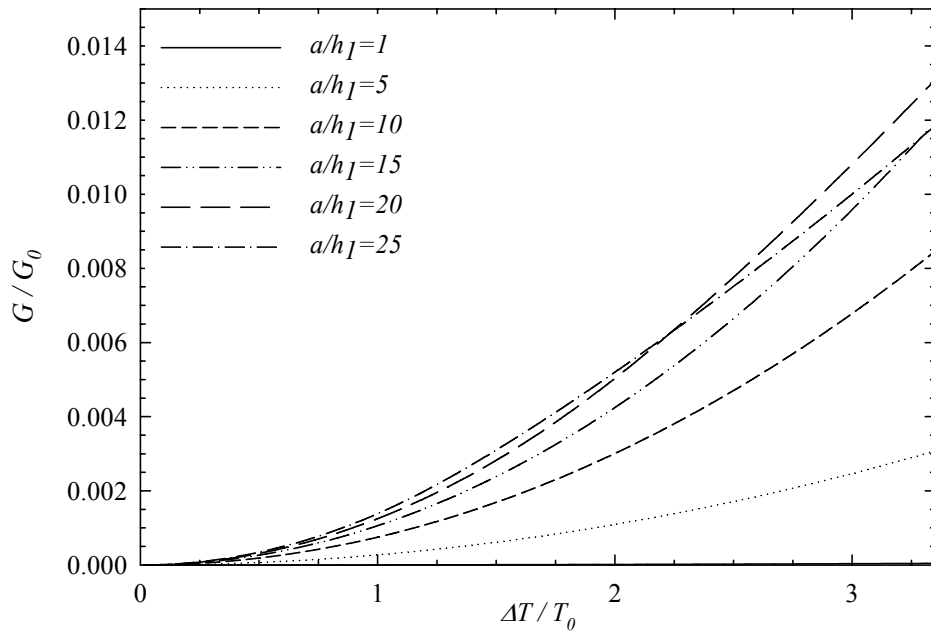


Figure 5.34 Normalized energy release rate values for crack at the bond coat – FGM interface, *MRI* material properties for FGM

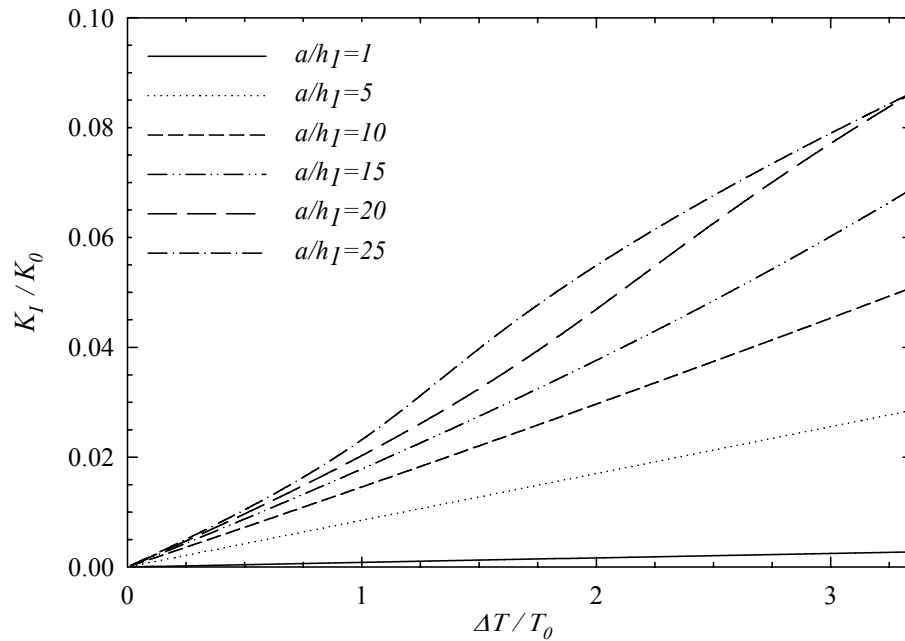


Figure 5.35 Normalized mode I stress intensity factors for crack at the bond coat – FGM interface, *MR2* material properties for FGM

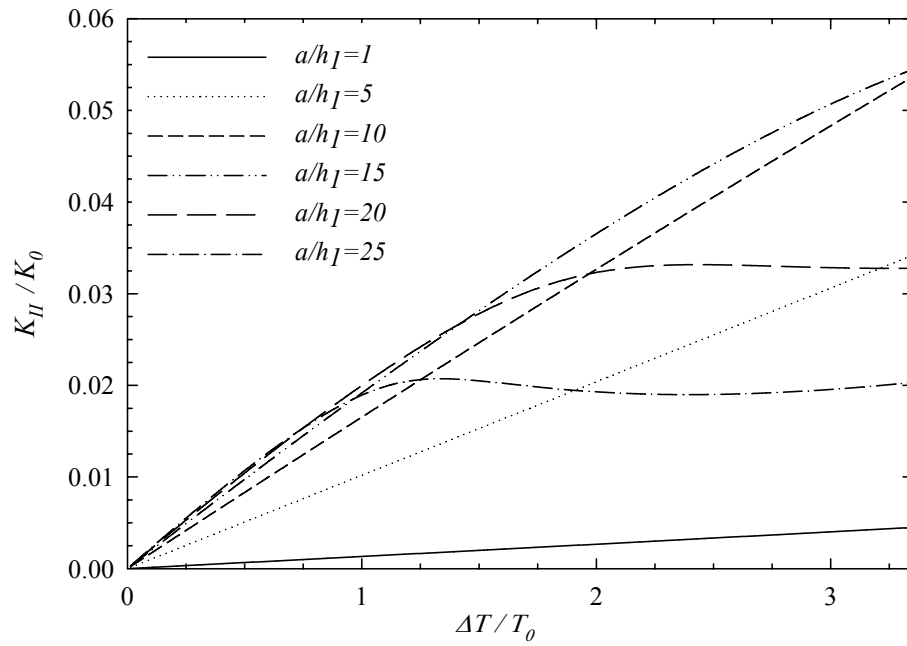


Figure 5.36 Normalized mode II stress intensity factors for crack at the bond coat – FGM interface, *MR2* material properties for FGM

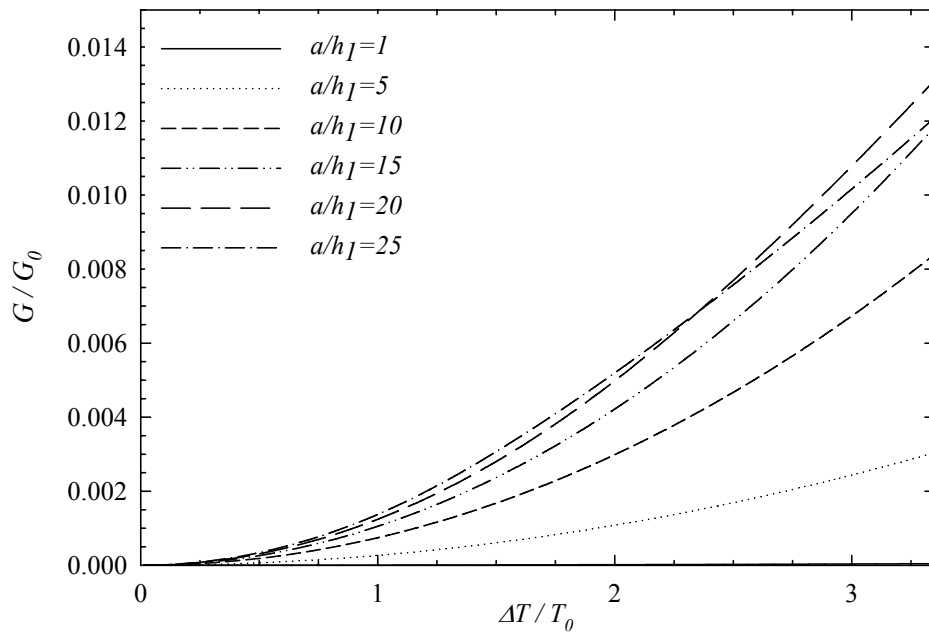


Figure 5.37 Normalized energy release rate values for crack at the bond coat – FGM interface, *MR2* material properties for FGM

Results of mode I and mode II stress intensity factors and energy release rate will be given in Figures 5.38-5.49 for different locations of crack in FGM layer.

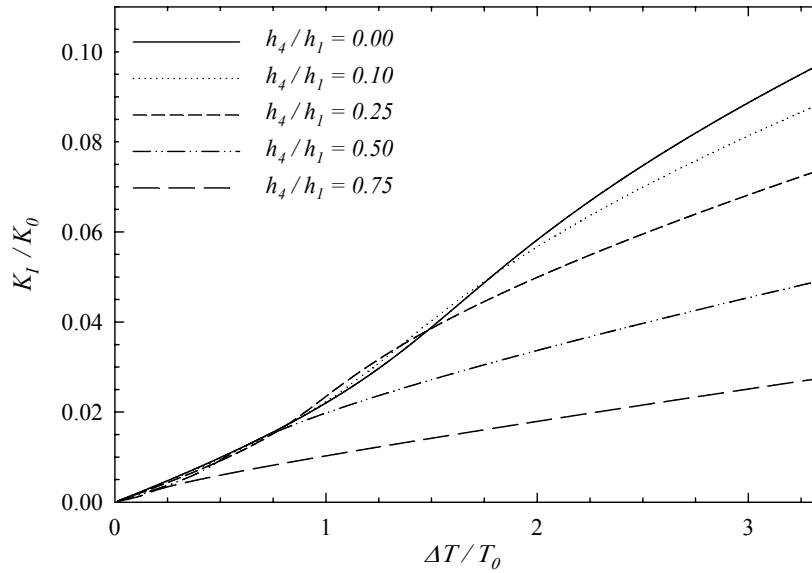


Figure 5.38 Normalized mode I stress intensity factors for changing crack heights, $a/h_1=20$ and *CRI* material properties

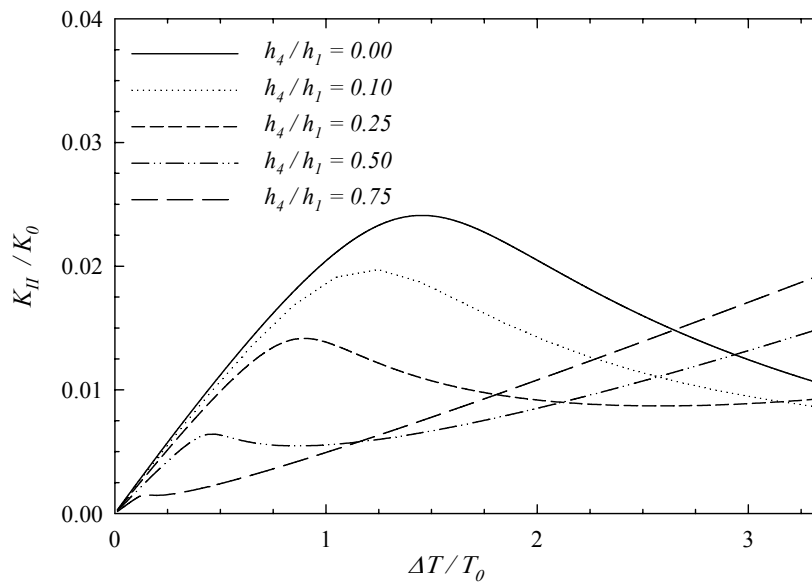


Figure 5.39 Normalized mode II stress intensity factors for changing crack heights, $a/h_1=20$ and *CRI* material properties

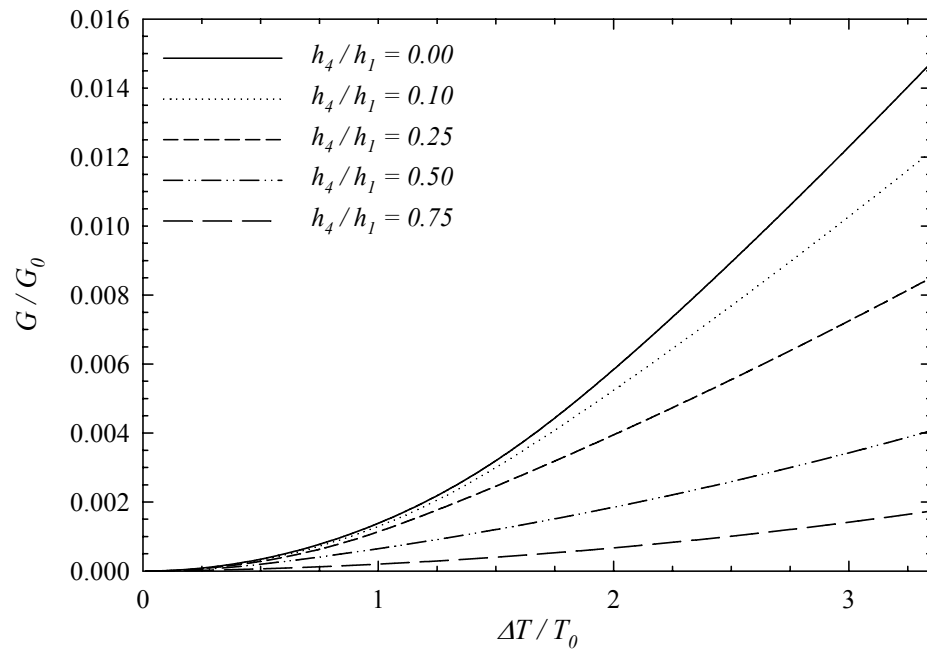


Figure 5.40 Normalized energy release rate values for changing crack heights, $a/h_1=20$ and CR1 material properties

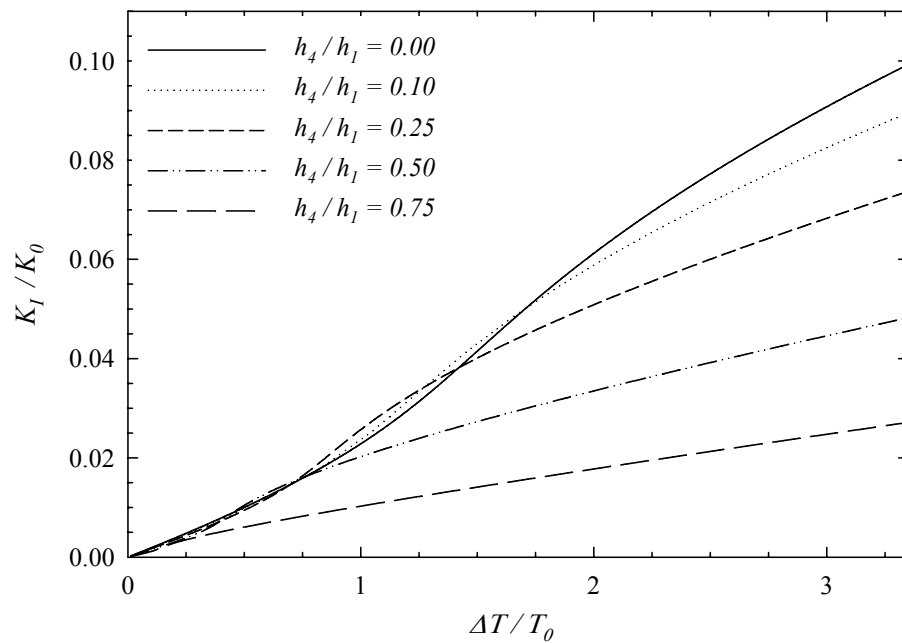


Figure 5.41 Normalized mode I stress intensity factors for changing crack heights, $a/h_1=20$ and CR2 material properties

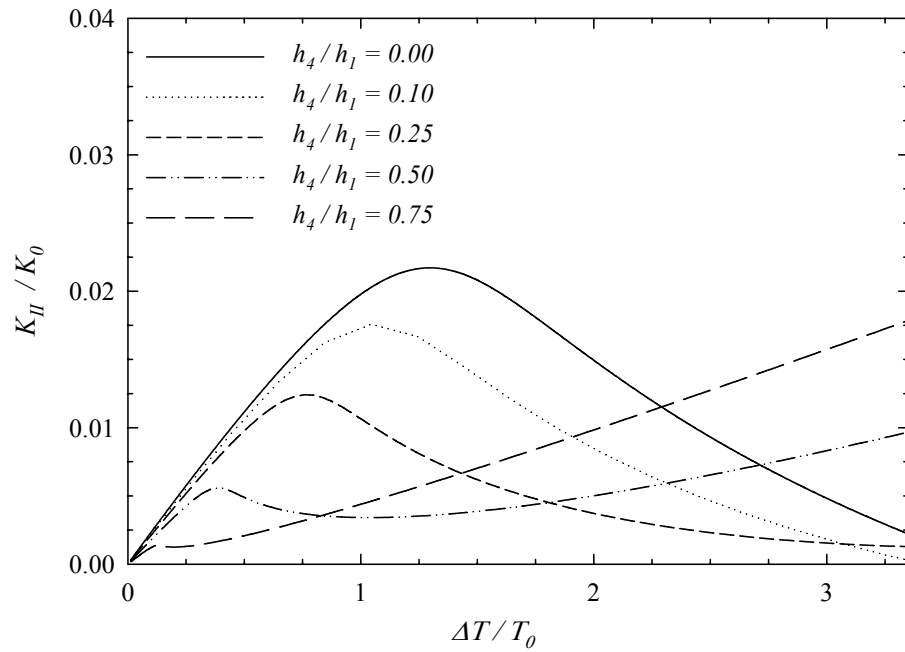


Figure 5.42 Normalized mode II stress intensity factors for changing crack heights, $a/h_1=20$ and CR2 material properties

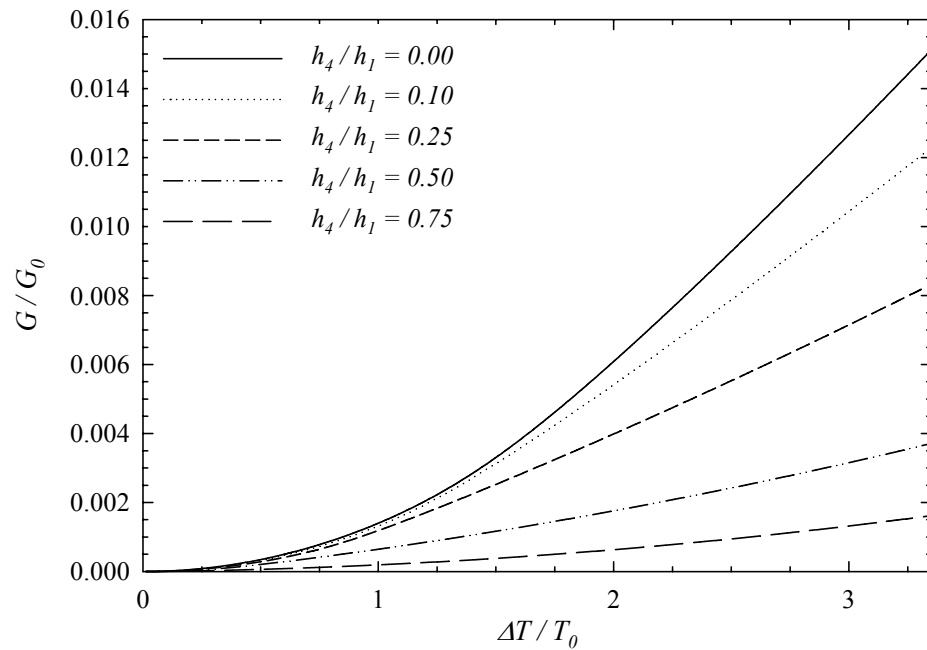


Figure 5.43 Normalized energy release rate values for changing crack heights, $a/h_1=20$ and CR2 material properties

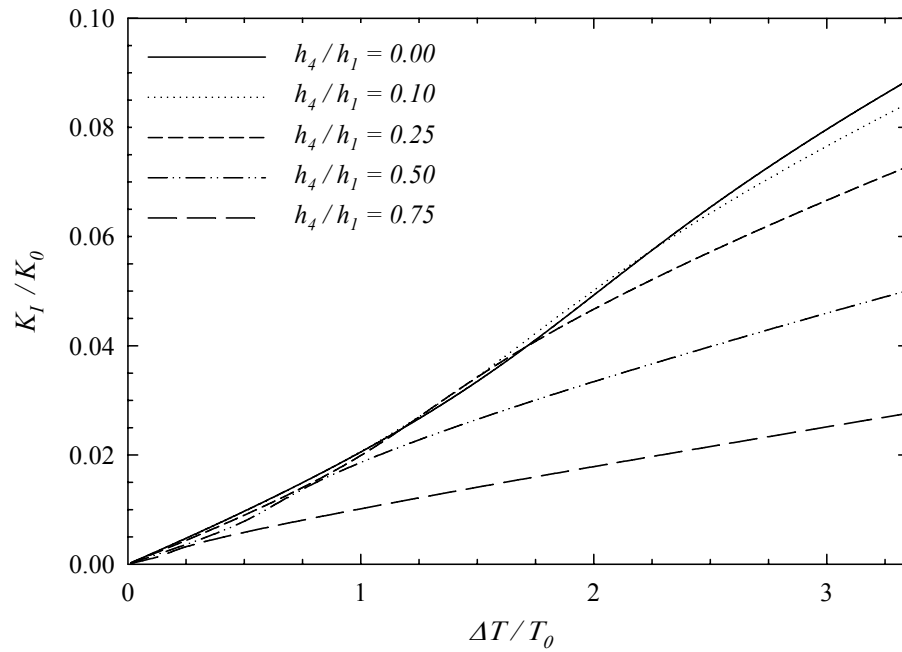


Figure 5.44 Normalized mode I stress intensity factors for changing crack heights, $a/h_1=20$ and *MRI* material properties

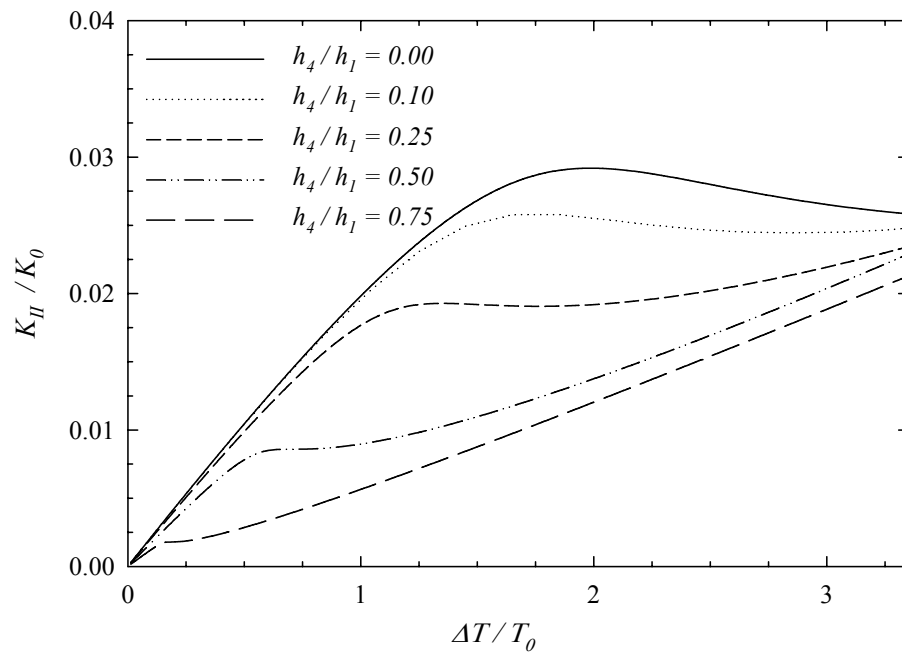


Figure 5.45 Normalized mode II stress intensity factors for changing crack heights, $a/h_1=20$ and *MRI* material properties

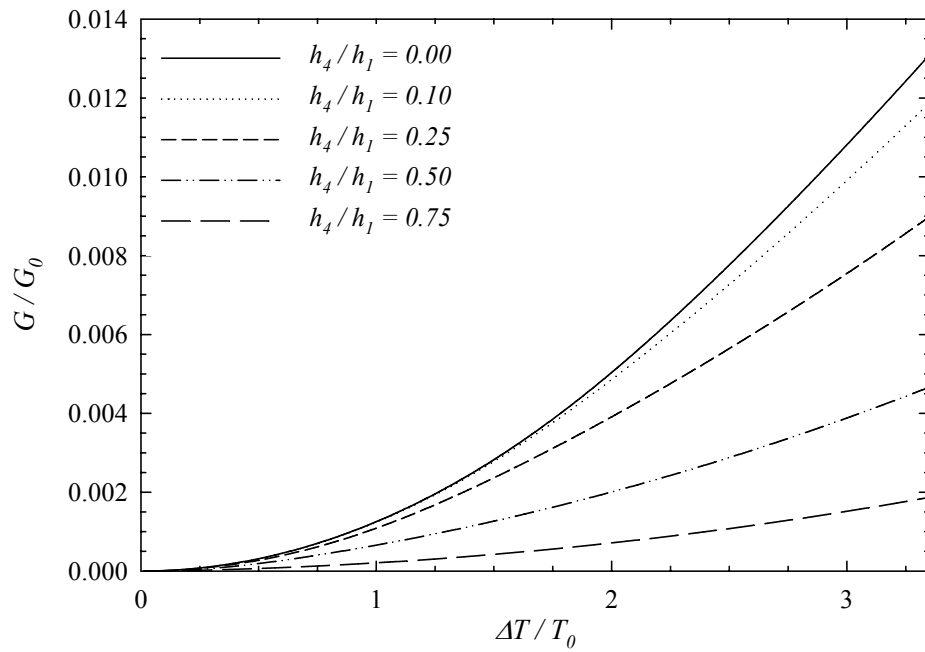


Figure 5.46 Normalized energy release rate values for changing crack heights, $a/h_1=20$ and MR1 material properties

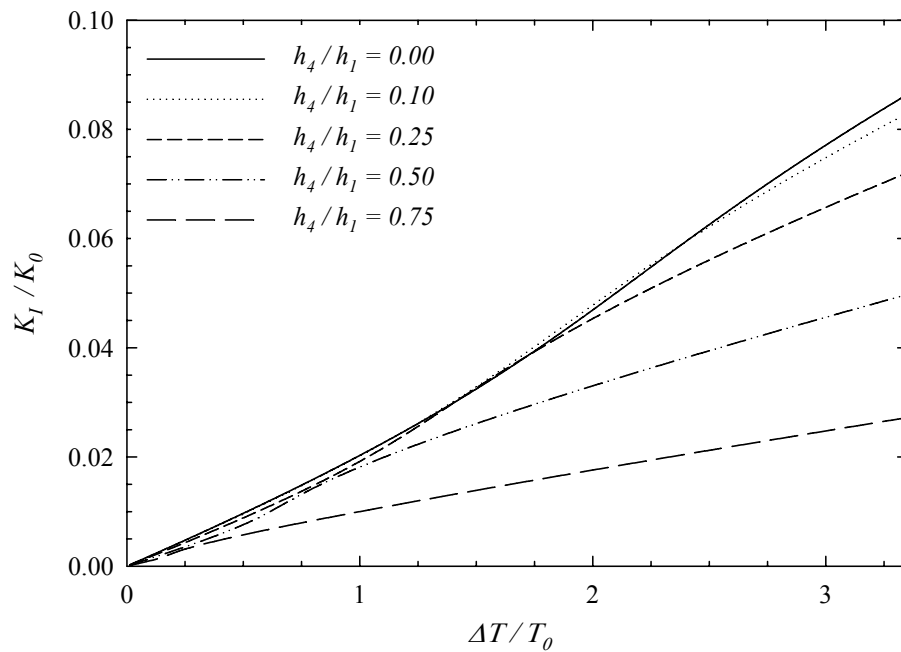


Figure 5.47 Normalized mode I stress intensity factors for changing crack heights, $a/h_1=20$ and MR2 material properties

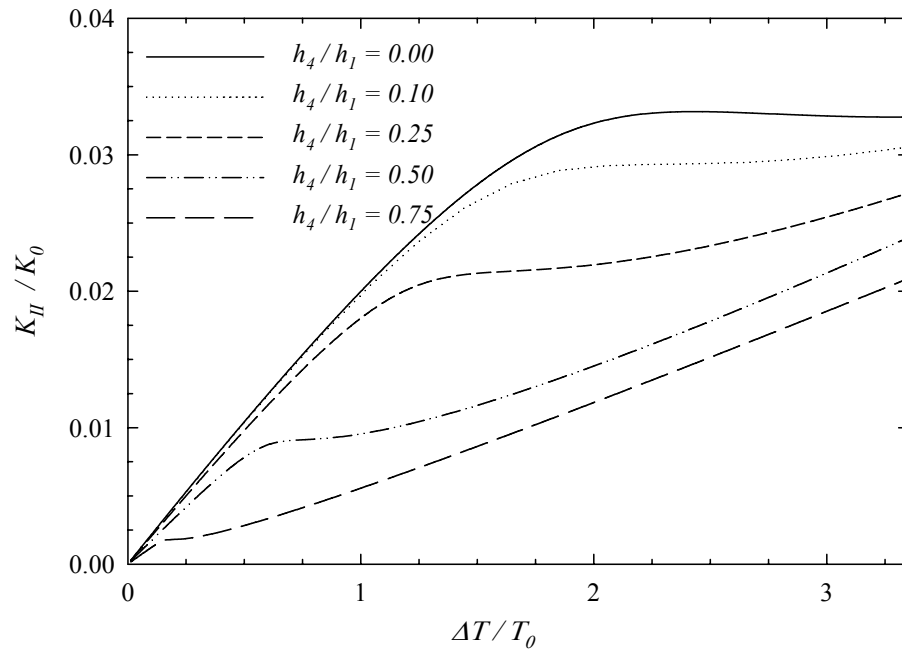


Figure 5.48 Normalized mode II stress intensity factors for changing crack heights, $a/h_1=20$ and MR2 material properties

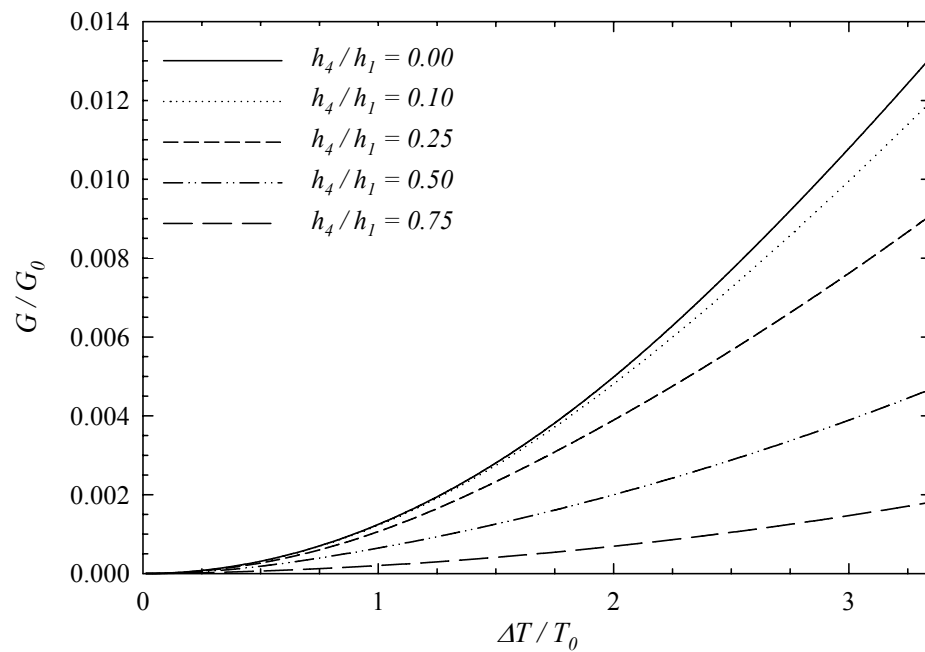


Figure 5.49 Normalized energy release rate values for changing crack heights, $a/h_1=20$ and MR2 material properties

Results of steady-state thermal analysis will be given in Figures 5.50-5.54.

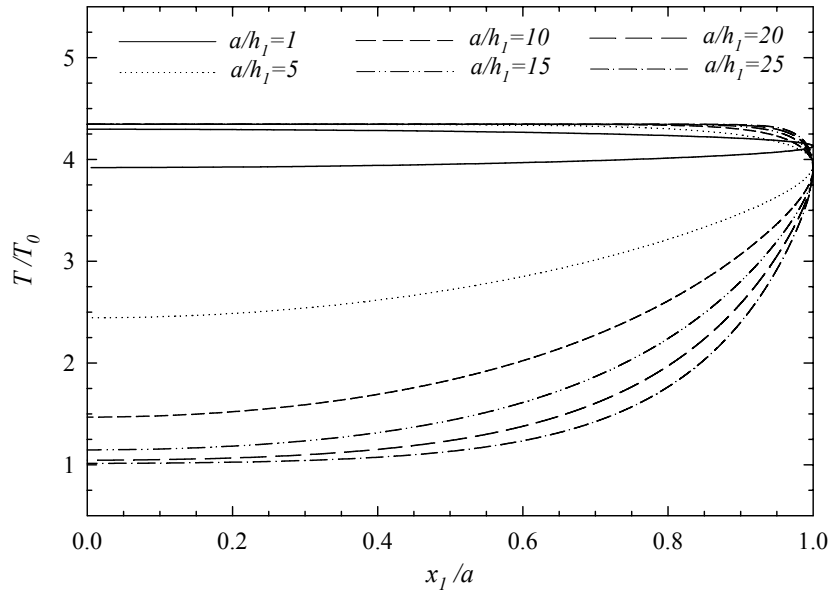


Figure 5.50 Steady-state temperature distribution on the crack surfaces for changing crack lengths, *CR1* material properties.

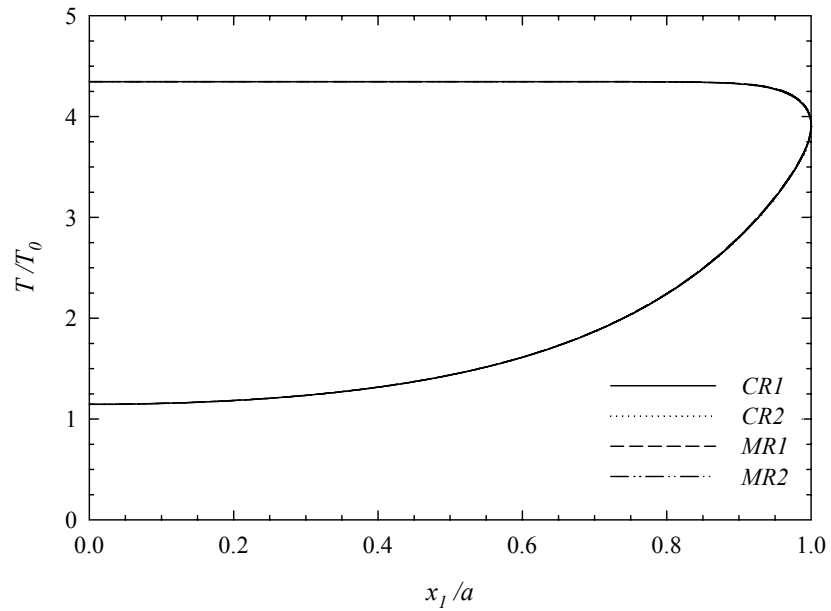


Figure 5.51 Steady-state temperature distribution on the crack surfaces for changing material properties, $a/h_1=15$

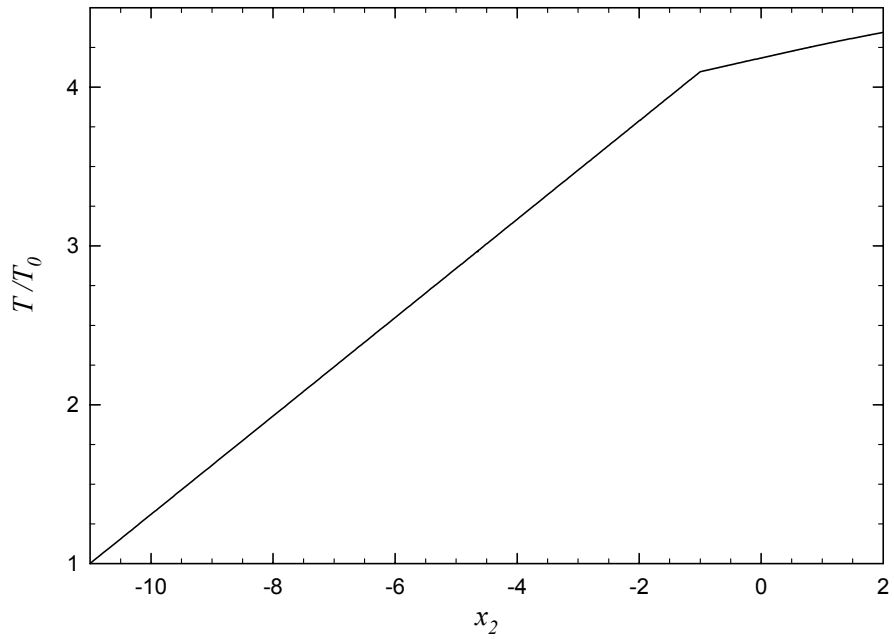


Figure 5.52 Steady-state temperature distribution on line $x_1=L$, $a/h_1=5$ and CRI material properties are chosen.

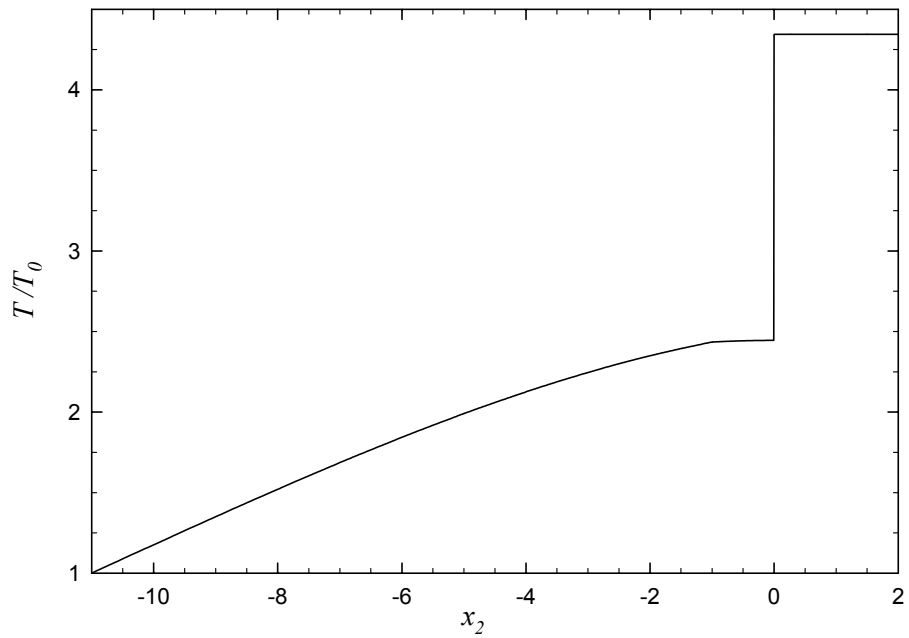


Figure 5.53 Steady-state temperature distribution on line $x_1=0$, $a/h_1=5$ and CRI material properties are chosen.

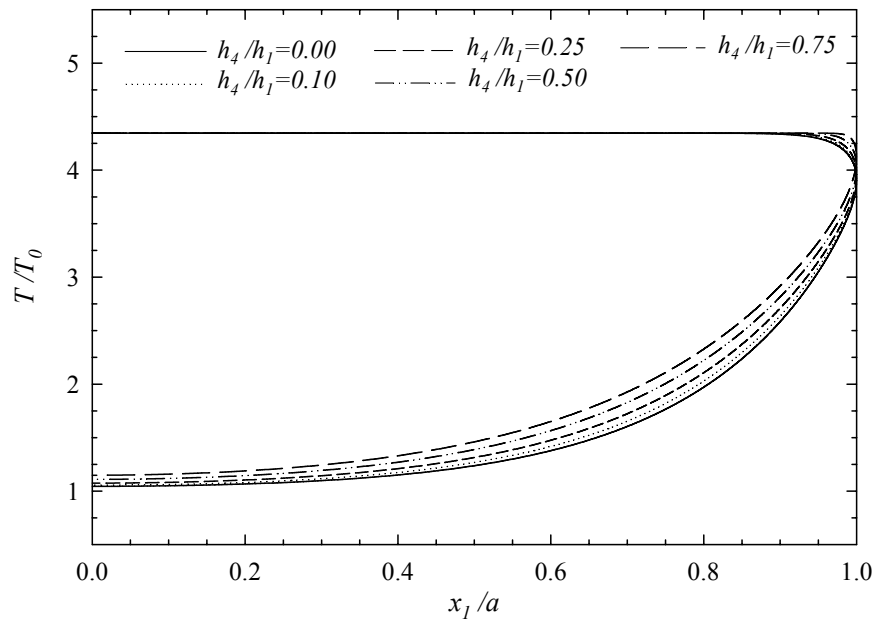


Figure 5.54 Steady-state temperature distribution by changing position of internal crack, $a/h_1=20$ and *CR1* material properties are chosen.

5.6 Discussion of Results and Conclusion

In this study, fracture mechanics parameters (stress intensity factors and energy release rate) for the buckling driven delamination problem in an orthotropic FGM coating system are calculated by developing a 2D finite element model in ANSYS finite element software. By solving the interface and internal crack problems, several case studies containing various crack lengths, crack positions and material variations are performed.

In the analyses, steady state heat conduction problem is solved and two-dimensional crack problem under thermal buckling load is investigated. In the first part of the solution, thermal analysis is done and steady state heat distribution is determined in ANSYS. Result of this thermal analysis is used as an input for the structural analysis. In this structural analysis, nonlinear large deformation problem is solved and displacement correlation technique is employed to determine mixed-mode stress intensity factors (K_I , K_{II}) and energy release rate (G). In the calculation of these results, effect of crack length, material variation and location of the crack in FGM layer is considered. The figures of K_I , K_{II} and G versus temperature change for various values of a/h_1 , material gradation and changing crack location are generated. Also plots of steady-state temperature distribution profiles on the upper and lower crack surfaces for $CR1$, $CR2$, $MR1$ and $MR2$ coatings considering $a/h_1 = 25, 20, 10, 5, 1$ cases are done.

The basic trends observed in the plots can be summarized as follows. For all of coating types of FGM layers, it observed that normalized mode I stress intensity factor increases as $\Delta T/T$ increases. K_I curves for different ceramic and metal rich coatings appear to be grouped together and in fact, the differences between the SIFs of metal rich and ceramic rich cases are not very large. If the effect of material variations are considered, from Figures 5.14-5.23 it can be said that mode I stress intensity factor and energy release rate values are bigger for ceramic rich materials at a given temperature change. However mode II stress intensity factors are lower for ceramic rich material variations.

Considering both the order of magnitude of mode I and mode II stress intensity factors for changing crack length and material variations, for lower temperature differences mode II SIFs are larger than mode I SIFs. However it is observed from mode I and II stress intensity factor plots, after a critical temperature difference mode II SIF values start to decrease and changes sign. As a result, under large deformation case (buckling) mode I stress intensity factor becomes dominant which means in case of buckling crack surfaces starts to move directly apart. Figure 5.55 shows change in order of magnitude of stress intensity factors for changing crack lengths. If the difference between mode I and mode II stress intensity factor is less than 15%, they are assumed to be nearly equal.

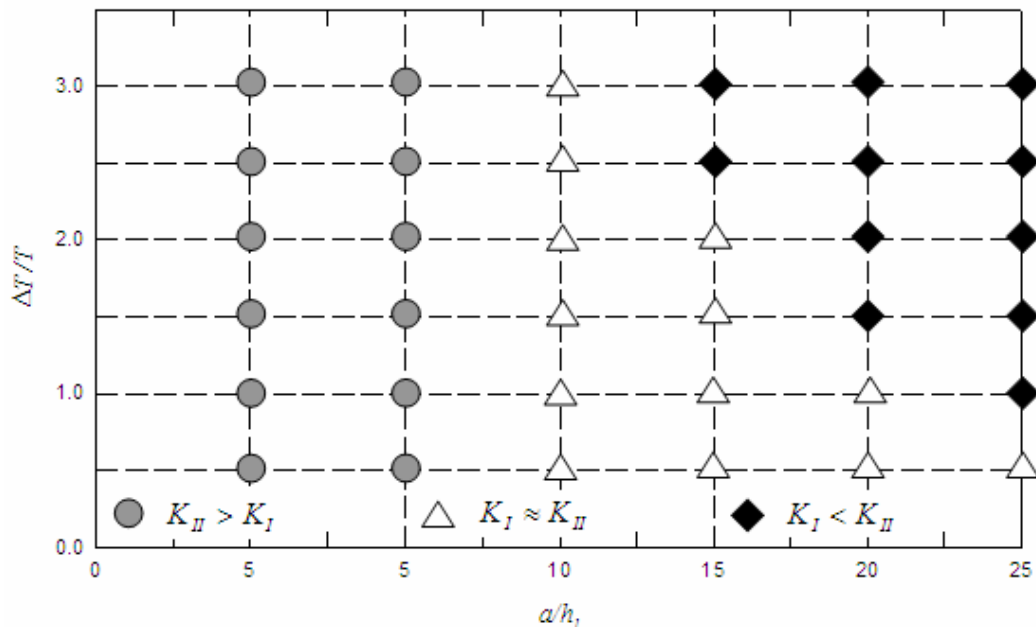


Figure 5.55 Comparison of mode I and mode II stress intensity factors for changing crack lengths, *CR1* material properties.

From the results of finite element solution, it is seen that change in crack length affects the critical buckling point of the system. Normalized mode I stress intensity factors and energy release rates are increasing as length of the crack increases. However, it interesting to note that, mode II stress intensity curve first increases and

then at a temperature it starts to decrease. Even for ceramic-rich FGM coatings mode II stress intensity factor is negative at the end of maximum temperature change.

For changing crack locations, it is observed that as the crack gets closer to the upper surface of the FGM coating, the stress intensity factors and energy release rates are decreasing. The reason of this can be due to change in temperature distribution around the crack surfaces. That can be seen from mode I and mode II stress intensity factors and energy release rate plots, as the position of the crack gets closer to the upper surface of the coating (h_4/h_1 increases), buckling occurs at a lower temperature change.

An extension to the present study can be the solution of the interface crack problem for different mechanical loads as well as thermal loads. The stress intensity factors and energy release rates can be calculated for FGM coatings and substrate systems subjected to bending, uniform tension or three point bending. The problem investigated in this study is a 2D symmetric problem. Another extension can be solution of same problem for axisymmetric case or a 3D model can be prepared in ANSYS finite element software. Different from mechanical and thermal loading conditions, the effect of multiple periodic buckling can also be considered also.

REFERENCES

- Araújo, T.D., Bittencourt, T.N., Roehl, D. and Martha, L.F. (2000). Numerical estimation of fracture parameters in elastic and elastic-plastic analysis. *European Congress on Computational Methods in Applied Sciences and Engineering, ECCOMAS 2000, Barcelona*.
- Atluri, S.N., Kobayashi, A.S. and Nakagaki, M. (1975). A Finite-Element Program for Fracture Mechanics Analysis of Composite Material. *Fracture Mechanics of Composites, ASTM-STP 593. American Society for Testing and Materials*, 86-98.
- Banks-Sills, L., Hershkovitz, I., Wawrzynek, P.A., Eliasi, R. and Ingraffea, A.R. (2005). Methods for calculating stress intensity factors in anisotropic materials: Part I- $z=0$ is symmetric plane. *Engineering Fracture Mechanics*, 72, 2328-2358.
- Chan, Y.F and Erdoğan, F.(1990). The Interface Crack Problem in Nonhomogeneous Bonded Materials of Finite Thickness. Semiconductor Research Corporation, Technical Report, Contract No:89-MP-071.
- Chiu, T.-C. (1999). Buckling of Graded Coatings – A Continuum Model. Mechanical Engineering and Mechanics, Lehigh University, Bethlehem, Pennsylvania, USA.
- Dağ, S., Yıldırım, B., and Erdoğan, F. (2004). Interface crack problems in graded orthotropic media: Analytical and computational approaches. *International Journal of Fracture*, 130, 471-496.
- Dağ, S., Kadioğlu, S. and Yahsi, O.S. (1999). Circumferential crack problem for an FGM cylinder under thermal stresses. *Journal of Thermal Stresses*, 22, 659-687.

- Gray, L.J., Phan, A.-V., Paulino, G.H. and Kaplan T. (2003). Improved quarter-point crack tip element. *Engineering Fracture Mechanics*, 70, 269-283.
- Gu, P. and Asaro, R.J. (1996). Crack in functionally graded materials. *International Journal of Solid Structures*, 34, 1-17.
- Javaheri, R. and Eslami, M.R. (2002a). Thermal buckling of functionally graded plates. *AIAA Journal*, 40, 162-169.
- Javaheri, R. and Eslami, M.R. (2002b). Thermal buckling of functionally graded plates based on higher order theory. *Journal of Thermal Stresses*, 25, 603-625.
- Kaya, A.C. and Nied, H.F. (1993). Interface Fracture Analysis of Bonded Ceramic Layers using Enriched Finite Elements. *Ceramic Coatings, ASME*, 44, 47-71.
- Kim, J.H. and Paulino, G.H. (2002). Mixed-mode fracture of orthotropic functionally graded materials using finite elements and the modified crack closure method. *Engineering Fracture of Mechanics*, 69, 157-1586.
- Krenk, S. (1979). On the elastic constants of plane orthotropic elasticity. *Journal of Composite Materials*, 13, 108-116.
- Lanhe, W. (2004). Thermal buckling of a simply supported moderately thick rectangular FGM plate. *Composite Structures*, 64, 211-218.
- Lekhnitskii, S.G. (1968) *Anisotropic Plates*. New York: Gordon and Breach Science Publishers.
- Ma, L.S. and Wang, T.J. (2003). Nonlinear bending and postbuckling of functionally graded circular plate under mechanical and thermal loadings. *International Journal of Solids and Structures*, 40, 3311-3330.

Milne, I., Ritchie, R.O. and Karihaloo, B. (2003). *Comprehensive Structural Integrity*. Hardbound, ISBN, ELSEVIER.

Na, K.S. and Kim, J.H. (2004). Three-dimensional thermal buckling analysis of functionally graded materials. *Composites, Part B*, 35, 429-437.

Najafizadeh, M.M. and Eslami, M.R. (2002). First-order-theory-based thermoelastic stability of functionally graded material circular plates. *AIAA Journal*, 40, 1444-1450.

Ochoa, O.O. and Reddy, J.N. (1992). *Finite Element Analysis of Composite Laminates*. Dordrecht: Kluwer Academic Publishers.

Ozturk, M. and Erdoğan, F. (1997). Mode I crack problem in an inhomogeneous orthotropic medium. *International Journal of Engineering Science*, 35, 869-883.

Su, K.-S. and Kim, J.-H. (2004). Three dimensional thermal buckling analysis of functionally graded materials. *Composites, Part B*, 35, 429-437.

Turvey, G.J. and Marshall, I.H. (1995). *Buckling and Postbuckling of Composite Plates*. London: Chapman and Hall.

Yıldırım, B. and Erdoğan, F. (2004). Edge crack problems in homogeneous and functionally graded material thermal barrier coatings under uniform thermal loading. *Journal of Thermal Stresses*, 27, 311-329.

Yıldırım, B., Dağ, S. and Erdoğan, F. (2005). Three dimensional fracture analysis of FGM coatings under thermomechanical loading. *International Journal of Fracture*, 132, 369-395.

Yıldırım, B., Dağ, S. and Erdoğan, F. (2005). Steady State Heat Conduction in Orthotropic Functionally Graded Materials Containin Cracks: Analytical and

Computational Techniques. *The Sixth International Congress on Thermal Stresses.*
517-520.

APPENDIX A

SAMPLE APDL CODE

```
!!! INTERFACE CRACK PROBLEM
!!! a/h1=15 AND CR1 MATERIAL COMPOSITION
!!! ANSYS PARAMETRIC DESIGN LANGUAGE(APDL)--SOURCE CODE
```

```
FINISH
/CLEAR,START
/PREP7
```

```
!!!!DEFINE CONSTANST USED IN PROBLEM
```

```
H2=1
H1=2*H2
H3=10*H2
AOH1=15
A=AOH1*H1
L=8*A
TZERO=293
```

```
!MATERIAL PROPERTIES OF CERAMIC
```

```
ECR1=90.43e9          !MODULUS OF ELASTICITY
ECR2=116.36e9
GCR12=38.21e9        !SHEAR MOULUS
PRCR21=0.28          !POISSON'S RATIO
PRCR23=0.27
PRCR32=0.21
PRCR31=0.14
KCR1=21.25           !THERMAL CONDUCTIVITY
```

KCR2=29.82

TECCR1=8E-6 !THERMAL EXPANSION COEFFICIENT

TECCR2=7.5E-6

TECCR3=9E-6

!MATERIAL PROPERTIES OF BOND COAT

EBC=137.9e9

PRBC=0.27

GBC=EBC/(2*(1+PRBC))

TECBC=15.16E-6

KBC=25

!MATERIAL PROPERTIES OF SUBSTRATE

ES=175.8e9

PRS=0.25

GS=ES/(2*(1+PRS))

TECS=13.91E-6

KS=7

!CONSTANTS OF MATERIAL VARIATION

GAM1=2.5

GAM2=2.5

GAM12=2.5

BE21=2

BE23=2

BE32=2

BE31=2

DE1=1.5

DE2=1.5

DE3=1.5

OM1=1.5

OM2=1.5

R=A/200 !RADIUS OF CRACK TIP ELEMENT

!!!!MODEL THE GEOMETRY

! CREATE KEYPOINTS

K,1,0,-(H2+H3),,

K,2,L,-(H2+H3),,

K,3,L,-H2,,

K,4,L,0,,

K,5,L,H1,,

K,6,0,H1,,

K,7,0,0,,

K,8,0,-H2,,

K,9,A,0,,

K,10,0,0,,

K,11,A,H1,,

K,12,A,-H2,,

K,13,A,-(H2+H3),,

!CREATE LINES

LSTR, 1, 13 !L1

LSTR, 2, 13 !L2

LSTR, 2, 3 !L3

LSTR, 4, 3 !L4

LSTR, 4, 5 !L5

LSTR, 11, 5 !L6

LSTR, 6, 11 !L7

LSTR, 4, 9 !L8

LSTR, 7, 9 !L9

LSTR, 6, 7 !L10

LSTR, 10, 9 !L11

LSTR, 12, 3 !L12

LSTR, 8, 12 !L13
LSTR, 9, 11 !L14
LSTR, 9, 12 !L15
LSTR, 13, 12 !L16
LSTR, 8, 10 !L17
LSTR, 8, 1 !L18

! SPECIFY THE DIVISIONS FOR THE LINES

LESIZE,1,, ,2*A/5, , , ,0
LESIZE,2,, ,2*(L-A)/5, , , ,0
LESIZE,3,, ,H3,.25 , , , ,0
LESIZE,4,, ,4, , , , ,0
LESIZE,5,, ,8,2 , , , ,0
LESIZE,6,, ,2*(L-A),2, , , ,0
LESIZE,7,, ,2*A, , , , ,0
LESIZE,8,, ,2*(L-A), , , , ,0
LESIZE,9,, ,3*A, , , , ,0
LESIZE,10,, ,8, .5, , , ,0
LESIZE,11,, ,2.5*A, , , , ,0
LESIZE,12,, ,2*(L-A), , , , ,0
LESIZE,13,, ,5*A, , , , ,0
LESIZE,14,, ,8, 2, , , , ,0
LESIZE,15,, ,4, , , , ,0
LESIZE,16,, ,H3,.25 , , , ,0
LESIZE,17,, ,4, , , , ,0
LESIZE,18,, ,H3,4 , , , ,0

! CREATE AREAS

AL,7,10,9,14
AL,17,13,15,11
AL,6,14,8,5
AL,8,15,12,4

AL,13,18,1,16

AL,2,3,12,16

! DEFINE THE PROPERTIES OF THE MESH NEAR THE CRACK TIP

KSCON, 9, R, 1,12 , 1 !SINGULAR ELEMENTS DEFINED

!GLUE AREAS

AGLUE,1,3

AGLUE,2,4

AGLUE,3,4

AGLUE,5,6

AGLUE,4,6

! SPECIFY THE ELEMENT TYPE THAT WILL BE

! USED IN THE THERMAL ANALYSIS

ET,1,PLANE35

!MESH AREAS

ASEL, ALL

AMESH, ALL

!!!!DEFINE MATERIAL PROPERTIES

!GET MAXIMUM AND MINIMUM ELEMENT NUMBERS

MPTEMP,0,0

*GET,N1EL,ELEM,0,NUM,MIND

*GET,N2EL,ELEM,0,NUM,MAXD

NMAT=0

*DO,IKP,N1EL,N2EL

*GET,XCEL,ELEM,IKP,CENT,X

*GET,YCEL,ELEM,IKP,CENT,Y

NMAT=NMAT+1

!DEFINE MATERIAL PROPERTIES OF FGM COATING

*IF, YCEL,GT,0,THEN

K11=KBC+(KCR1-KBC)*((YCEL/H1)**OM1)

K22=KBC+(KCR2-KBC)*((YCEL/H1)**OM2)

K33=K11

E11=EBC+(ECR1-EBC)*((YCEL/H1)**GAM1)

E22=EBC+(ECR2-EBC)*((YCEL/H1)**GAM2)

PR21=PRBC+(PRCR21-PRBC)*((YCEL/H1)**BE21)

PR23=PRBC+(PRCR23-PRBC)*((YCEL/H1)**BE23)

PR32=PRBC+(PRCR32-PRBC)*((YCEL/H1)**BE32)

PR31=PRBC+(PRCR31-PRBC)*((YCEL/H1)**BE31)

PR12=(PR21*E11)/E22

E33=(PR32*E22)/PR23

PR13=(PR31*E11)/E33

G12=GBC+(GCR12-GBC)*((YCEL/H1)**GAM12)

G23=G12

G13=G12

TEC11=TECBC+(TECCR1-TECBC)*((YCEL/H1)**DE1)

TEC22=TECBC+(TECCR2-TECBC)*((YCEL/H1)**DE2)

TEC33=TECBC+(TECCR3-TECBC)*((YCEL/H1)**DE3)

!DEFINE MATERIAL PROPERTIES OF BOND COAT

*ELSEIF, YCEL,GT,-H2,AND, YCEL,LT,0,THEN

K11=KBC

K22=KBC

K33=KBC

E11=EBC

E22=EBC

E33=EBC

PR12=PRBC

PR23=PRBC

PR13=PRBC

G12=GBC
G23=GBC
G13=GBC
TEC11=TECBC
TEC22=TECBC
TEC33=TECBC

!DEFINE MATERIAL PROPERTIES OF SUBSTRATE

*ELSE,

K11=KS

K22=KS

K33=KS

E11=ES

E22=ES

E33=ES

PR12=PRS

PR23=PRS

PR13=PRS

G12=GS

G23=GS

G13=GS

TEC11=TECS

TEC22=TECS

TEC33=TECS

*ENDIF

MPDATA,KXX,NMAT,,K11

MPDATA,KYY,NMAT,,K22

MPDATA,KZZ,NMAT,,K33

MPDATA,EX,NMAT,,E11

MPDATA,EY,NMAT,,E22

MPDATA,EZ,NMAT,,E33

!MATERIAL PROPERTIES OF

!SELECTED ELEMENT IS DEFINED

```

MPDATA,PRXY,NMAT,,PR12
MPDATA,PRYZ,NMAT,,PR23
MPDATA,PRXZ,NMAT,,PR13
MPDATA,GXY,NMAT,,G12
MPDATA,GYZ,NMAT,,G23
MPDATA,GXZ,NMAT,,G13
MPDATA,ALPX,NMAT,,TEC11
MPDATA,ALPY,NMAT,,TEC22
MPDATA,ALPZ,NMAT,,TEC33
MPCHG,NMAT,IKP
*ENDDO

```

!!!!THERMAL SOLUTION

FINISH

/SOL

FLST,2,2,4,ORDE,2

FITEM,2,1

FITEM,2,-2

/GO

DL,P51X, ,ALL,293,0 ! T_2 IS DEFINED

FLST,2,2,4,ORDE,2

FITEM,2,6

FITEM,2,-7

/GO

DL,P51X, ,ALL,1273,0 ! T_1 IS DEFINED

SOLVE

FINISH

!!!!STRUCTURAL SOLUTION

/PREP7

ETCHG,TTS !ELEMENT TYPE IS CHANGED FROM

KEYOPT,1,3,2 !THERMAL TO STRUCTURAL

```

KEYOPT,1,5,0
KEYOPT,1,6,0          !PLANE STRAIN CONDITION
FINISH
/SOL
ANTYPE,0
NLGEOM,1
DELTIM,1,1,3          !MAX AND MIN TIME INCREMENTS
OUTRES,ERASE
OUTRES,ALL,ALL
TIME,500              !NUMBER OF TIME STEPS
FLST,2,3,4,ORDE,3
FITEM,2,10            !DEFINE BOUNDARY CONDITIONS
FITEM,2,17
FITEM,2,-18
/GO
DL,P51X, ,UX,
FLST,2,1,3,ORDE,1
FITEM,2,1
/GO
DK,P51X, , , ,0,UY, , , , ,
TREF,293,
LDREAD,TEMP,,, , , 'file','rth',''  !READ THERMAL RESULT
SOLVE
FINISH

!!!!CALCULTION OF FRACTURE MECHANICS PARAMETERS
/POST1
N1=122                !NODES USED IN DCT EQUATIONS
NU2=397
NU3=396
NL2=3509
NL3=3508

```

DA=R

R22=DA/4

R23=DA

! MATERIAL PROPERTIES AT THE CARACK TIP!

YTIP=0

EXS1=(EBC+(ECR1-EBC)*((YTIP/H1)**GAM1))

EXS2=(EBC+(ECR2-EBC)*((YTIP/H1)**GAM2))

EXS12=(GBC+(GCR12-GBC)*((YTIP/H1)**GAM12))

S11=1/EXS1

S12=((PR21*E11)/E22)/EXS1

S22=1/EXS2

S66=1/EXS12

!COORDINATE SYSTEM IS DEFINED AT THE CRACK TIP

LOCAL,11,0,A,0,0,0, , ,1,1,

RSYS,11

!CONSTANTS AND NORMALIZATION FACTORS

AVPRIN,0,0

PI=4.*ATAN(1.)

D0=SQRT((2.*SQRT(S11*S22))+2.*S12)+S66)

K0_=ES*TECS*TZERO*(PI*H3)**0.5

G0=(1-PRS**2)*K0_**2/ES

RO=(2*S12+S66)/(2*(S11*S22)**0.5)

N=((1+RO)/2)**0.5

LAM=(S11/S22)

H11=N*LAM**0.25*(S11*S22)**0.5

H22=N*LAM**(-.25)*(S11*S22)**.5

!CALCULATE SIFs AND ERR FOR EACH TIME STEP

*DO,ITIME,1,250,1

SET, , ,1, ,ITIME, ,

DT=((1273-293)/293)/250*ITIME

!NODAL DISPLACEMENTS USED IN DCT EQUATION

UXU2=(UX(NU2))

UXL2=(UX(NL2))

UXU3=(UX(NU3))

UXL3=(UX(NL3))

UYU2=(UY(NU2))

UYL2=(UY(NL2))

UYU3=(UY(NU3))

UYL3=(UY(NL3))

UX2=UXU2-UXL2

UX3=UXU3-UXL3

UY2=UYU2-UYL2

UY3=UYU3-UYL3

!NORMALIZED MODE1 AND MODE2 STRESS INTENSITY

!FACTORS AND ENERGY RELEASE RATE RESULTS

KI_=(SQRT(2*PI/(9*DA))*(8*UY2-UY3)/(4*(SQRT(S22))*D0))/SQRT(PI)

KII_=(SQRT(2*PI/(9*DA))*(8*UX2-UX3)/(4*(SQRT(S11))*D0))/SQRT(PI)

G=H22*KI_**2+H11*KII_**2

!WRITE OUTPUT FILE FOR EACH TIME STEP

/OUT,K_A15_CR1,DAT,,APPEND

*VWRITE,DT,KI_/K0_,KII_/K0_,G/G0

(4(2X,F20.10))

/OUT

*ENDDO